Cruise Report: EKAMSAT Pilot Cruise

8–26 June 2023, Mormugao to Mormugao, R/V *Roger Revelle*

Craig Lee, Selina Bolella, Devmi Gamage, Joaquim Ignacio Goes, Jossia Joseph, Ankitha Kannad, Siddhant Kerhalkar, Alexander Brown Kinsella, Griffin Michael Modjeski, K.B.R.R. Hari Prasad, Asish Soni, Janet Sprintall, Amit Tandon, Maria Laura Zoffoli, Harsa Bardhan Dalabehera, Charles William Kovach, Melanie Faire McCoy, Rohan Armando Jordan Carneiro Menezes, R. Chandra Sekhar Naik, Justine Damaris Parks, Emma Renee Robertson, Anupama Sahoo, Debarshi Sarkar, and Pawan Soyam

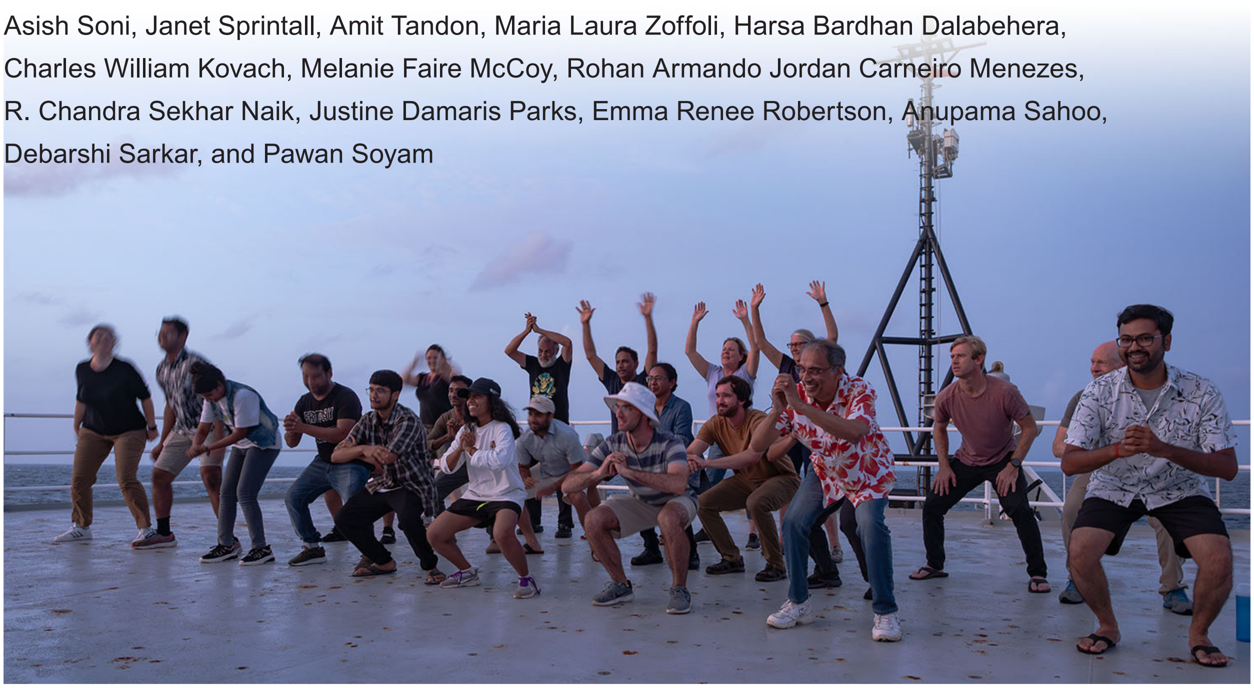

Technical Report

APL-UW TR 2403

July 2024

Applied Physics Laboratory **University of Washington**
1013 NE 40th Street Seattle, Washington 98105-6698

ONR Grants N00014-23-1-2085, N00014-23-1-2054, N00014-23-1-2053, N00014-23-1-2091, and N00014-24-1-2274

ACKNOWLEDGMENTS

We thank Captain Desjardins, resident technicians Mason Schettig and Howell Johnson, and the crew of R/V *Roger Revelle* for their professionalism, excellent support, and good humor. Special thanks to cooks Richard Buck and Lydia Phillips for creating a welcoming environment for our Indian researchers by providing both western and Indian meals. The EKAMSAT team also thanks Dr. M. Ravichandran, Dr. Srinivas Kumar, Dr. Pattabhi Rama Rao, and Dr. Anil Kumar for their unflagging support.

This work was supported by ONR grants N00014-23-1-2085, N00014-23-1-2054, N00014-23-1-2053, N00014-23-1-2091, and N00014-24-1-2274.

ABSTRACT

A team of researchers from the U.S. and India conducted a pilot cruise for the collaborative Ministry of Earth Sciences/Office of Naval Research Enhancing Knowledge of the Arabian sea Marine environment through Science and Advanced Training (EKAMSAT) program. Science focused on understanding the evolution of the ocean and atmospheric boundary layer in the southeastern Arabian Sea during the onset of the summer monsoon, sampling in the southeastern Arabian Sea 8 – 26 June 2023 from R/V *Roger Revelle*. The passage of Cyclone Biparjoy marked the start of the cruise, which produced a phytoplankton bloom in the restratifying suface layer left in its wake. Biparjoy also left dry atmospheric conditions, modulating cloud formation and the onset of the southwest monsoon. Sampling included underway vertical profiling of temperature, salinity and microstructure, extensive ship-based atmospheric measurements, radiosonde launches, black carbon and a suite of chemical and biogeochemical parameters. Autonomous surface drifters and long-endurance gliders were used to augment ship-based sampling.

TABLE OF CONTENTS

1. BACKGROUND AND OBJECTIVES

The Ministry of Earth Sciences/Office of Naval Research Enhancing Knowledge of the Arabian sea Marine environment through Science and Advanced Training (EKAMSAT) program focuses on understanding upper ocean and lower atmosphere processes in the eastern Arabian Sea. Primary research interests include lateral stirring processes, vertical mixing, atmospheric boundary layer structure, and feedback between the atmosphere and ocean with the aim of improved monsoon prediction. EKAMSAT is the latest in a decade-long (2013 to present) sequence of Indo–U.S. collaborative programs designed to improve predictive monsoon models through study of air-sea fluxes and upper ocean processes. All programs involve exchange visits, scientific training, and capacity building.

The central objective — improved forecasting of the monsoon — requires an improved understanding of the interaction between the waters of the Arabian Sea and the overlying atmosphere. These interactions are in turn influenced by freshwater input from the Bay of Bengal, which supports the formation of a shallow, highly stratified surface layer during the winter monsoon and the subsequent transition period between the winter and summer monsoons. This thin seasonal surface layer warms more intensely than surrounding waters, creating a region of anomalously warm sea surface temperature in the eastern Arabian Sea. A central theme of this investigation is understanding the evolution and fate of the Arabian Sea Warm Pool and its impact on the summer monsoon.

All climate models exhibit a cool SST bias that results in a too dry atmosphere in the Arabian Sea and hence the models are unable to adequately predict the strength and timing of the monsoon onset. Regional stratification, including the distribution and thickness of barrier layers (BL) and temperature inversions (TI) that have the potential to warm the mixed layer, is not reproduced satisfactorily in the models and so provides a likely source of the cool bias. Similarly, the source of dry bias likely lies in the atmospheric BL processes, implicating the coupling at the atmosphere–ocean interface. Ultimately, the observations and proposed analyses that result from EKAMSAT will provide a testbed for the evaluation, veracity, and refinement of these numerical models and their predictions.

Primary objectives for the EKAMSAT 2023 pilot cruise:

- Quantify evolution of the ocean and atmospheric boundary layer in the southeastern Arabian Sea during the onset of the summer monsoon, including the evolution and eventual destruction of the thin, warm surface layer (the Arabian Sea Warm Pool)
    - Observe the synoptic features of the BL and TI distribution in the southeast Arabian Sea and their relationship to the salinity front
    - Understand the dynamical mechanisms responsible for formation of the regional salinity stratification
    - Assess the influence of BLs and TIs on SST and the subsequent local coupled air-sea interaction over the salinity front and the warm pool region

- Develop approaches for conducting research expeditions using vessels from the U.S. Academic Research Fleet (ARF) operating from Goa

Secondary objectives for the pilot:

- Characterize upper ocean bio-optical variability in the northeastern Arabian Sea during the summer monsoon onset
- Sample aerosols in the northern Arabian Sea

2. OPERATIONS SUMMARY

Overview

EKAMSAT pilot sampling focused on characterizing the evolution of the oceanic and atmospheric boundary layers near the National Institute of Ocean Technology (NIOT) surface mooring AD08. Although the science plan called for sampling across the monsoon onset, to capture transition to the active phase of the summer monsoon, vessel availability placed the sampling period after the climatological monsoon onset date. Despite this, the EKAMSAT pilot experienced only dry, pre-monsoon atmospheric conditions, likely because Cyclone Biparjoy removed atmospheric moisture over the eastern Arabian Sea, delaying monsoon onset.

Cyclone Biparjoy passed to the west of the EKAMSAT sampling region as R/V *Roger Revelle* was departing Mormugao, producing rough seas (3–5 m significant wave height, worsening offshore) and challenging working conditions. The cold wake left by Biparjoy's passage created a region of elevated productivity and strong upper ocean gradients that, although outside EKAMSAT's primary science focus, warranted exploration.

Measurements included heat, salinity, and density of the upper ocean, the currents and turbulence of the upper ocean, ocean optics, surface wind speed and direction, rainfall, solar radiation, and temperature, winds and moisture content in the lower atmosphere.

Underway sampling was used to survey spatial variability around the S1-C flux time series site and the Biparjoy cold wake filament, and to collect oceanic and atmospheric boundary layer observations for the two S1-C flux time series. Measurements included:

- Ship-based sensors collecting measurements while underway, including Doppler velocity profilers, ship- and science-supplied meteorological sensors, flow-through analyses of water from the *Revelle* science seawater system
- Profiles of upper ocean temperature and salinity collected underway using an Ocean Sciences Underway CTD (UCTD) system. The UCTD is a small, tethered free-falling probe that samples the upper ocean while the ship is underway.
- Profiles of upper ocean turbulence, temperature, and salinity using a Rockland Scientific Vertical Microstructure Profiler (VMP). The VMP is a tethered free-falling probe that was used to collect rapidly repeated profiles for periods of several hours at a time. The VMP required additional time to assemble and test, and was not used for routine sampling until the second flux time series.
- Near-surface ocean temperature measured with the towed Sea Snake thermistor chain

- Profiles of the atmospheric boundary layer using balloon-launched radiosondes
- A Seabird 911+ CTD system equipped with a 24-place, 10-l rosette was used to collect:
  - Deep profiles to anchor the endpoints of a 'butterfly' survey
  - Daily 200-m profiles (1–2 casts, early afternoon, timed to align with satellite passes) for biological and bio-optical properties
- Autonomous instruments were deployed from *Revelle* to expand the footprint of the ship-based surveys:
  - A Seaglider long-endurance underwater glider conducted additional occupations of the 'butterfly' survey around the S1-C flux time series site
  - Fifty micro-SVPs were deployed in two 25-drfiter arrays. The first sampled the area surrounding the S1-C flux time series and the second the Biparjoy cold wake filament.
  - An experimental BO-SVP (bio-optical drifter) collected a 2-day drifting time series of surface properties in the Biparjoy cold wake filament
  - One Lagrangian float was deployed at the time series site

Ocean/Atmosphere Variability and Cyclone Biparjoy

The Indian National Center for Ocean Information Services (INCOIS) shared daily telemetered data from the AD moorings (maintained by NIOT) outside the Indian EEZ. Moorings reported surface and sub-surface (1, 5, 10, 20, 30, 50, 75, 100, 200, and 500 m) variables at 3-hr intervals (Table 1, Fig. 1). The three AD moorings reveal the large-scale differences in air-sea interaction and hydrography within the Arabian Sea along with the propagating pattern of Cyclone Biparjoy, which made landfall in Gujarat on 15 June 2023. The upper-ocean response to the cyclone and the monsoon onset is evident. Meteorological conditions during the pre-cruise period featured clear skies, O(5 m/s) southwesterly winds and clear diurnal cycles in both air and sea surface temperature (SST) at all the moorings (Fig. 1). Surface salinity at AD08 was fresher than at AD07 and AD06 by 1–1.5 g/kg (Fig. 1e). Cyclone effects are visible on 5 June at AD08, with a decrease in SST, peak shortwave radiation, and wind speeds accelerating to 10 m/s. Higher winds were accompanied by upper-ocean mixing and mixed layer deepening that drove an increase in sea surface salinity (SSS) by 1 g/kg (Fig. 2e and f). AD07 observed Biparjoy around 7 June, with wind speeds of 15 m/s. At AD06, winds peak at 22 m/s, with fluctuating direction, on 11 June. Deepening mixed layers were accompanied by decreases of roughly 2°C in air temperature and 4°C in SST at AD07 and AD06 (Figs. 2a, b).

Cold wakes are also evident in the AMSR-2 microwave remote sensing dataset on 16 June (Fig. 1a). Biparjoy likely disrupted AD06 telemetry 16–22 June. Atmospheric conditions and sea state relaxed after the cyclone's passage, with southwesterly winds of

5–10 m/s at the three moorings. The post-Biparjoy period was also marked by decreased sea surface salinity gradients, clear skies, and diurnal cycles in air temperature. Diurnal cycles in SST were muted in contrast to the pre-cyclone period, likely due to the increased winds and wave state. However, strong temperature-driven stratification began to build at AD06, with mixed layers shoaling to roughly 15 m by the end of the cruise period.

Summary of Science Sampling

Heavy seas associated with the passage of Biparjoy forced a retargeting of the pilot cruise sampling region. Plans called for sampling around mooring AD07, which forecasts predicted would have significant wave heights of 5–7 m on our planned 10 June arrival date, dropping to a more workable 3–4 m on 15–16 June. We thus shifted the focus south, to mooring AD08; wave heights were predicted to drop to 3 m by 13 June. Unlike AD07, AD08 is inside the Indian EEZ. We thus targeted our initial surveys and time series site to be as close to the mooring as possible while also remaining outside the EEZ.

The first task was to determine whether the AD08 site was sufficiently one-dimensional to support the planned evaluation of mixed layer models. Heavy seas slowed the transit, resulting in a 11 June arrival at S1-W (Tables 2 and 3; Fig. 3). Conditions on 11 June were too rough to begin UCTD operations, so initial efforts used underway (intake, ADCP, and meteorological) systems to sample a 50-km 'Zonal-1' section centered on the S1-C time series site (Fig. 3). Deep (2000 m) CTD casts anchor the ends and center. A second, smaller 'Time Series Survey' mapped 2D lateral variability while also deploying the first 25-element SVP drifter array (Table 4). Sea state subsided enough to allow UCTD operations late on 12 June, and the next day was spent occupying the 'Butterfly' survey with the UCTD. The initial set of surveys found no strong lateral gradients, suggesting that the site would serve well.

The next phase focused on collecting 'Flux Series 1' (Fig. 3), a four-day, quasi-1D time series of profiles through the atmospheric and oceanic boundary layers. This was accomplished by positioning at S1-C, pointing *Revelle* into the wind (to maximize the quality of atmospheric measurements collected by instruments mounted to the bow mast) and easing forward at the slowest possible speed that allowed continuous profiling with the UCTD. Radiosonde were launched at regular intervals, and a 200-m CTD profile was collected to support biological and bio-optical efforts. When the distance from S1-C exceeded 5 nm, the ship repositioned back to S1-C and sampling continued. This first time series ran 14–17 June, with Seaglider SG530 deployed on 14 June and the first VMP profiling added to the time series beginning 16 June. Dry, break phase conditions, with strong wind forcing, prevailed through the entire 'Flux Time series 1' period. SG530 was tasked to sample the 'Butterfly' survey, to provide an ongoing assessment of the potential role of lateral advection.

Table 1. *Variables measured at AD moorings. Salinity was computed for each depth using conductivity, temperature, and depth variables as inputs in the GSW function.*

	Variable Name		Variable Name
1	'Latitude [DD]',	34	'Water Temperature @ 075m [Deg C]',
2	'Longitude [DD]',	35	'Water Temperature @ 100m [Deg C]',
3	'Relative Humidity [%]',	36	'Water Temperature @ 200m [Deg C]',
4	'Sea Level Pressure [hPa]',	37	'Water Temperature @ 500m [Deg C]',
5	'Air Temperature [Deg C]',	38	'Conductivity @ 001m [mmho]',
6	'Wind Direction [Deg]',	39	'Conductivity @ 005m [mmho]',
7	'Wind Speed [m/s]',	40	'Conductivity @ 010m [mmho]',
8	'Wind Gust [m/s]',	41	'Conductivity @ 015m [mmho]',
9	'Precipitation [mm]',	42	'Conductivity @ 020m [mmho]',
10	'Pressure @ 500m [bar]',	43	'Conductivity @ 030m [mmho]',
11	'Current Speed @ 1.25m [cm/s]',	44	'Conductivity @ 050m [mmho]',
12	'Current Speed @ 015m [cm/s]',	45	'Conductivity @ 075m [mmho]',
13	'Current Speed @ 025m [cm/s]',	46	'Conductivity @ 100m [mmho]',
14	'Current Speed @ 035m [cm/s]',	47	'Conductivity @ 200m [mmho]',
15	'Current Speed @ 050m [cm/s]',	48	'Conductivity @ 500m [mmho]',
16	'Current Speed @ 075m [cm/s]',	49	'Significant Wave Height (hm0) [m]',
17	'Current Speed @ 100m [cm/s]',	50	'Significant height due to swell (hm0a) [m]',
18	'Current Direction @ 1.25m [Deg]',	51	'Significant height due to the sea wind (hm0b) [m]',
19	'Current Direction @ 015m [Deg]',	52	'Maximum Wave Height (hmax) [m]',
20	'Current Direction @ 025m [Deg]',	53	'Average direction (mdir) [Deg]',
21	'Current Direction @ 035m [Deg]',	54	'Average direction of the swell (mdira)[Deg]',
22	'Current Direction @ 050m [Deg]',	55	'Average direction of the sea wind (mdirb)[Deg]',
23	'Current Direction @ 075m [Deg]',	56	'Average period (tm02) [s]',
24	'Current Direction @ 100m [Deg]',	57	'Average period of the swell (tm02a)[s]',
25	'Short Wave Radiation [w/m^2]',	58	'Average period of the sea wind (tm02b)[s]',
26	'Long Wave Radiation [w/m^2]',	59	'Mean wave period (tm10)[s]',
27	'Water Temperature @ 001m [Deg C]',	60	'Peak wave period (tp)[s]',
28	'Water Temperature @ 005m [Deg C]',	61	'Zero crossing wave period(tz)[s]',
29	'Water Temperature @ 010m [Deg C]',	62	'High frequency mean wave direction (thhf)[Deg]',
30	'Water Temperature @ 015m [Deg C]',	63	'Period of the highest wave (thmax) [s]',
31	'Water Temperature @ 020m [Deg C]',	64	'Direction associated with the peak period (thtp) (Deg)',
32	'Water Temperature @ 030m [Deg C]',	65	'Wave spreading at spectral peak period (sprtp) [Deg]',
33	'Water Temperature @ 050m [Deg C]',	66	'UI',

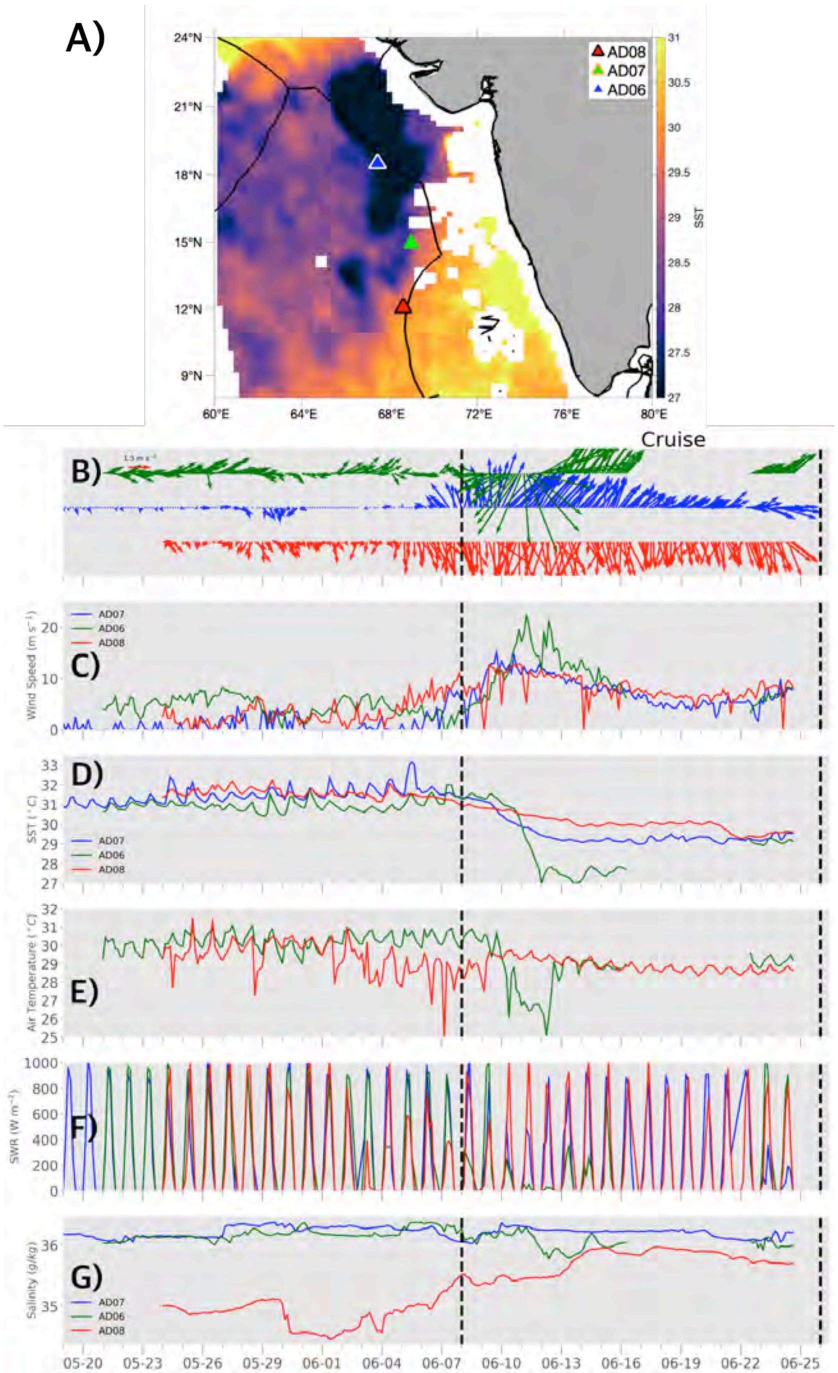

Figure 1. *A) 3-day averaged microwave-SST from AMSR-2 for 16 June 2023 with the locations of NIOT moorings AD06 (67.45°E,18.50°N), AD07 (68.98°E,14.93°N), and AD08 (68.63°E,12.07°N). Buoy colors are consistent across plots. B) Wind speed direction, C) Wind speed magnitude, D) Shortwave radiation, E) Salinity (10-m depth), F) Sea surface temperature (1-m depth), and G) Air temperature from the NIOT moorings 19 May – 26 June 2023. The cruise duration is indicated by the period between the dashed vertical lines.* ***NOTE:*** *It appears that the wind direction is reported falsely at AD08 because the wind direction has an offset of 180 degrees to other moorings (even after the onset of monsoons). AD06 also did not telemeter any data 16–22 June.*

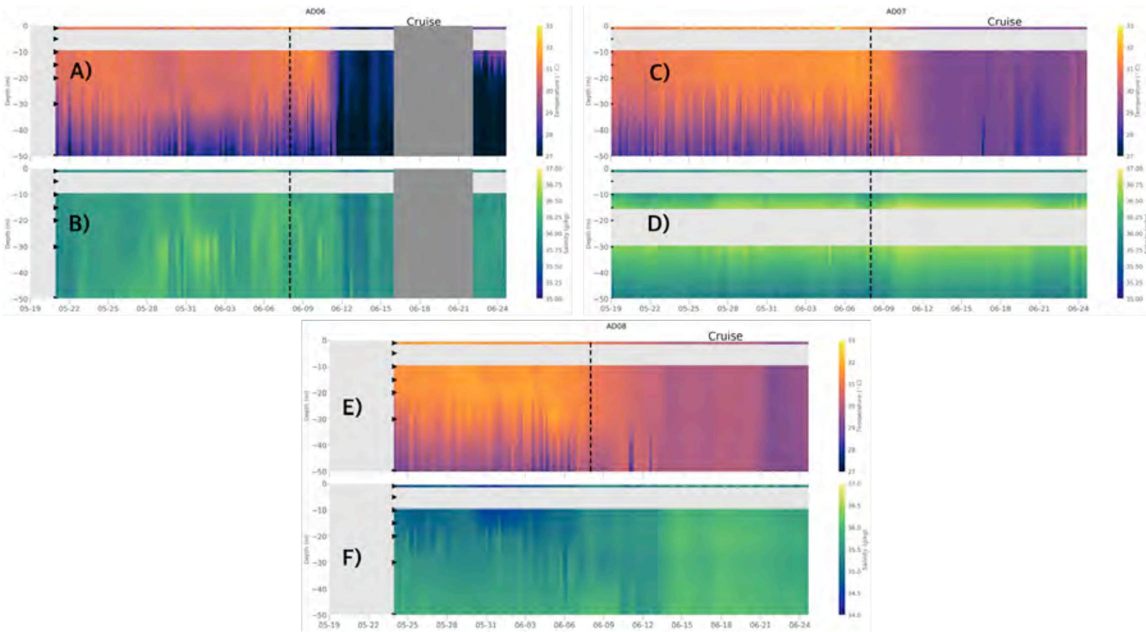

Figure 2. *Profiles of A) Temperature and B) Salinity over the top 50 m from NIOT moorings AD06 (67.45°E,18.50°N). C), D) and E), F) are the same as A) and B) but for AD07 (68.98°E,14.93°N) and AD08 (68.63°E,12.07°N), respectively, 19 May – 26 June 2023. The cruise duration is indicated by the period between the dashed vertical lines. AD06 did not telemeter any data 16–22 June.*

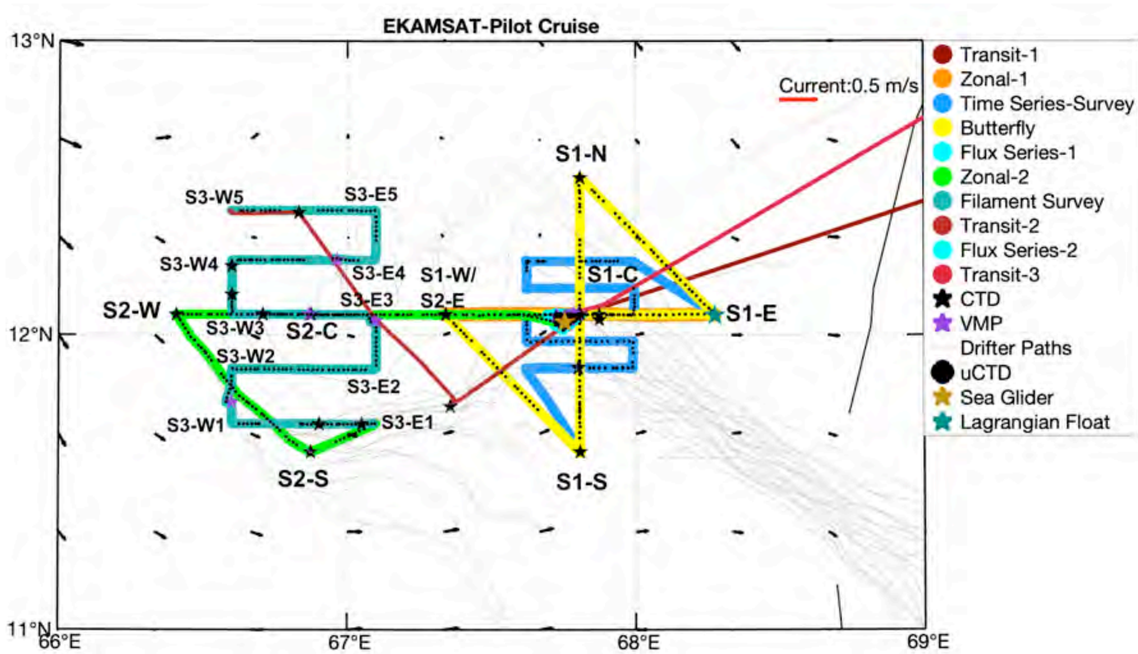

Figure 3. *Map of the Arabian Sea showing different assets and ship sections used to sample during the EKAMSAT pilot cruise on R/V* Roger Revelle *during June 2023. The background arrows are the currents averaged over a 5-day period 17–22 June 2023 as derived from OSCAR current product.*

Table 2. *Timeline of events*

Date (2023)	Event	Notes
9 June	Depart Mormugao	
11 June	Begin science ops, CTD at S1-W	
11 June	CTD at S1-C	
11 June	Deploy MLF	
11 June	CTD at S1-E	
11-12 June	Deploy SVP Array 1	
12 June	CTD at S1-S	
12 June	UCTD 'Butterfly' survey	S1-S – S1-W – S1-E – S1-N – S1-S
13 June	CTD at S1-N	
13 June	Deploy BGC float	
14-17 June	Flux time series 1 at S1-C	UCTD and noon/afternoon optics/CTD
14 June	Deploy SG530	
16 June	Begin using VMP with UCTD	
17 June	Biparjoy wake UCTD section	Initial wake section
18-20 June	'Filament' survey	
18-19 June	SVP Array 2	Deploy along transit path of 'Filament' survey
18 June	Deploy SVP-BO drifter	NE of S2-S
20 June	Recover SVP-BO drifter	
20-24 June	Flux time series 2 at S1-C	UCTD with VMP 04:00-07:00 and 17:00-20:00 and noon/afternoon optics/CTD
24 June	End science ops	
26 June	Arrive Mormugao	

Table 3. *UCTD survey waypoints*

	Latitude (°N)	Longitude (°E)
S1-C	12 04.20	67 48.40
S1-N	12 32.20	67 48.40
S1-S	11 36.20	67 48.40
S1-E	12 04.20	68 16.40
S1-W	12 04.20	67 20.40

Table 4. *SVP Array 1*

Name	Lat (°N)	Lon (°E)
SVP01	12 15.05	067 59.42
SVP02	12 15.05	067 53.91
SVP03	12 15.05	067 48.40
SVP04	12 15.05	067 42.89
SVP05	12 15.05	067 37.38
SVP06	12 09.62	067 37.38
SVP07	12 09.62	067 42.89
SVP08	12 09.62	067 48.40
SVP09	12 09.62	067 53.91
SVP10	12 09.62	067 59.42
SVP11	12 04.20	067 59.42
SVP12	12 04.20	067 53.91
SVP13	12 04.20	067 48.40
SVP14	12 04.20	067 42.89
SVP15	12 04.20	067 37.38
SVP16	11 58.78	067 37.38
SVP17	11 58.78	067 42.89
SVP18	11 58.78	067 48.40
SVP19	11 58.78	067 53.91
SVP20	11 58.78	067 59.42
SVP21	11 53.35	067 59.42
SVP22	11 53.35	067 53.91
SVP23	11 53.35	067 48.40
SVP24	11 53.35	067 42.89
SVP25	11 53.35	067 37.38

Given predictions for continued dry conditions for days to come, we elected to break the time series on 17 June to sample the phytoplankton bloom associated with Biparjoy's wake. This was easily accomplished by sliding our focus area west. An initial 'Zonal-2' section used underway systems and UCTD to resolve cross-filament structure, followed by a radiator pattern 'Filament Survey'. The second SVP drifter array (Table 5) was deployed to map circulation along the southern half of the 'Filament Survey', along with sampling by multiple CTD casts. The experimental SVP-BO drifter was also deployed for a 2-day drift during this period.

With forecasts predicting a possible active phase transition near the end of the cruise, we returned to S1-C to collect a final 'Flux Series 2'. Sampling followed the approach used for 'Flux Series 1', but substituting VMP sampling for UCTD profiling twice per day, from 04:00–07:00 local, to capture maximum surface cooling and convections, and 17:00–20:00, after the period of maximum net surface warming. Although the transition to active conditions did not occur until after *Revelle* had returned to Goa, 'Flux Series 2' provides contrast to 'Flux Series 1' by sampling the dry phase boundary layers in weak, rather than strong, wind forcing.

Table 5. *SVP Array 2*

Name	Lat (N)	Lon (E)
SVP2_01	12 04.2	67 20.4
SVP2_02	12 04.2	67 14.8
SVP2_03	12 04.2	67 09.2
SVP2_04	12 04.2	67 03.6
SVP2_05	12 04.2	66 57.9
SVP2_06	12 04.2	66 52.4
SVP2_07	12 04.2	66 46.8
SVP2_08	12 04.2	66 41.2
SVP2_09	12 04.2	66 35.6
SVP2_10	12 04.2	66 30.0
SVP2_11	12 04.2	66 24.4
SVP2_12	11 59.9	66 27.3
SVP2_13	11 56.4	66 30.5
SVP2_14	11 52.0	66 34.0
SVP2_15	11 48.0	66 37.3
SVP2_16	11 44.9	66 41.2
SVP2_17	11 41.8	66 44.8
SVP2_18	11 38.6	66 48.1
SVP2_19	11 36.2	66 52.4
SVP2_20	11 39.0	66 59.0
SVP2_21	11 42.0	67 06.0
SVP2_22	11 42.0	66 59.0
SVP2_23	11 42.0	66 51.0
SVP2_24	11 42.0	66 44.0
SVP2_25	11 42.0	66 36.0

Underway Systems

Ship-mounted meteorological sensors and a flow-through thermosalinograph (TSG) were used to characterize air-sea fluxes and background gradients in surface ocean properties. Atmospheric and ocean surface properties (Fig. 4; Table 6) were sampled at 1 Hz, with wind speed, relative humidity, and air temperature measured roughly 17 m above the water. A WaMoS/MWaMoS radar-based wave and surface current monitoring system measured wave properties, including significant wave height and period, at roughly 1-min intervals (Fig. 5). Bulk air-sea fluxes (Fig. 6; Table 7) were estimated using the COARE 3.6 algorithm applied to 15-min averaged wave and meteorological measurements.

The *Revelle* bow TSG system collected measurements at a nominal depth of 5 m to provide maps of near-surface spatial variability (Figs. 7–9). Near-surface measurements and SVP drifter tracks collected during ‘Zonal-2’ and ‘Filament Survey’ sampling reveal a sharply-turning surface flow, perhaps a meandering filament of cooler, saltier water, created due to asymmetry in the wake of Cyclone Biparjoy (Figs. 10 and11). Buoyancy gradients were strongly positive in the eastern half of the section and negative in the western half.

Near-term tasks include cross-calibration of TSG, Sea Snake, and UCTD systems, as well as the *Revelle* standard meteorological package with the NOAA sensors installed for EKAMSAT.

Underway CTD (UCTD)

An Ocean Sciences Underway CTD (UCTD) was used to collect profiles of temperature and salinity to 250 m depth (Fig. 12). This system uses a small, tethered, free-falling CTD probe to sample the upper ocean while the ship is underway at speeds 0.5–8 knots. This enabled the collection of both high-spatial resolution surveys (Figs. 13, 14) and time series (Figs. 15, 16). In total, 189 individual UCTD deployments were completed, each typically lasting one hour, with 5–7 casts per deployment (Table 8).

<u>UCTD Issues</u>:

- Initially we only obtained 1 cast per deployment. In uCast preferences, need to check “change stop seconds to 0” then select “update” and wait to cast update to refresh and show next seconds.
- Because of the number of novices on board and the rough conditions of swell and waves and winds, we had quite a few probe hits against the stern. We retired many of the probes but then after all 6 probes had been hit we started to test out those that had received bumps through comparison of profiles with subsequent and past probes. Eventually this lead to only one probe (0366) being retired once we occupied the first SC-1 time series, as it became obvious that it was saltier compared to other probes.
- Several probes did not collect casts. It was eventually determined that this was likely due to false starts brought on when the magnetic plug was not cleanly removed on deployment. If the magnetic plug is not completely removed then the probe will not record properly. The procedure would be to return the probe to the lab and replace, and set up the replacement probe.

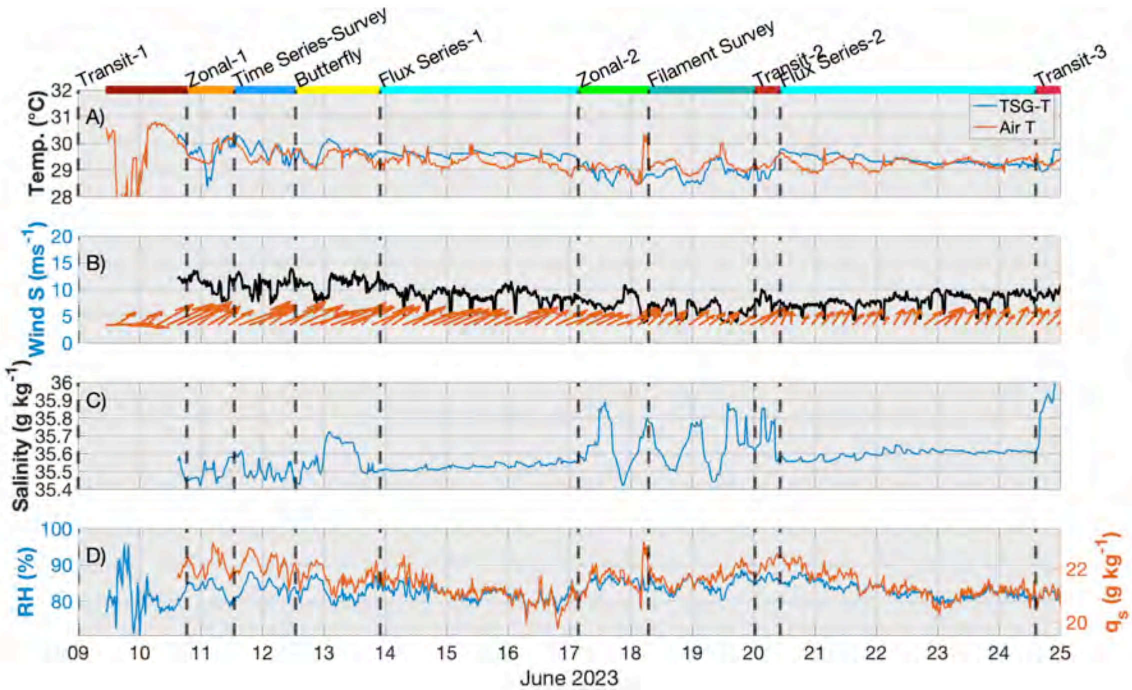

Figure 4. *Time series of A) through-flow temperature (blue) and air temperature (top, red), B) wind speed magnitude (black) and direction (red), C) salinity from through-flow, D) relative humidity (blue) and specific humidity (red) from the ship measurements during EKAMSAT pilot cruise in June 2023 on R/V* Roger Revelle. *The time series was divided based on sections shown in Fig. 3.*

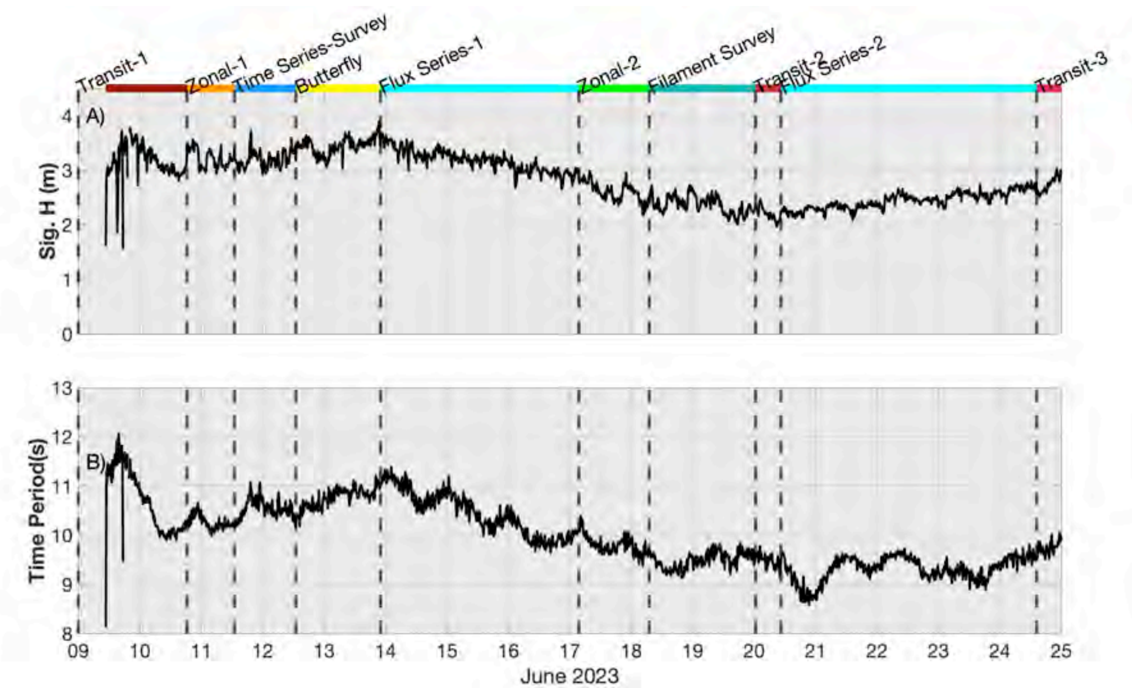

Figure 5. *Time series of A) significant wave height and B) time period of the wave from the ship measurements during EKAMSAT pilot cruise in June 2023 on R/V* Roger Revelle. *The time series was divided based on sections shown in Fig. 3.*

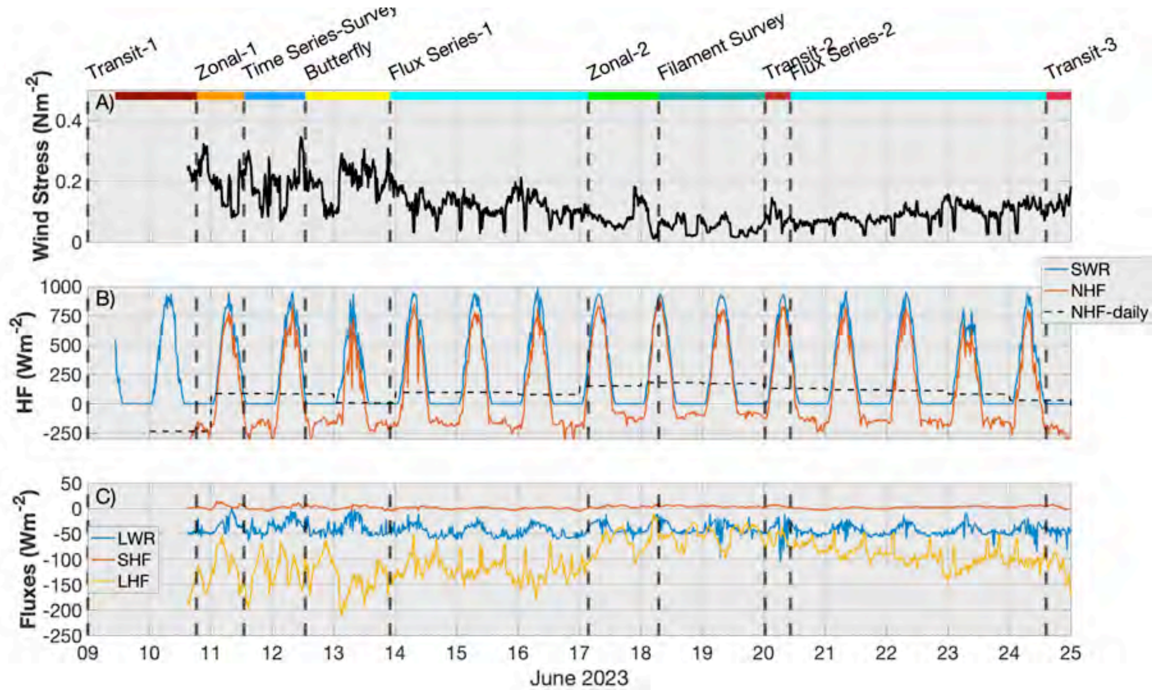

Figure 6. *Time series of A) wind stress, B) shortwave (blue), net heat (red), and daily averaged heat fluxes (broken line, center), C) longwave (blue), sensible (red), and latent heat flux (yellow) derived using COARE 3.6 (including wave parameters) from the ship measurements during EKAMSAT pilot cruise in June 2023 on R/V* Roger Revelle*. The time series was divided based on sections shown in Fig. 3.*

Table 6. *MET and TSG variables*

Item	Type	Description	Associated Parameters (Appendix)
1	TMP	Air Temperature	AT, AF, WC, WF
2	HRH	Relative Humidity, Temperature	RH, RT, DP, RF, DF, WB, WF
3	BPR	Barometric Pressure, [Compensation Temp]	BP, BC
4	PRC	Precipitation	PR, PT
5	WND	Wind Speed, Wind Direction	WS, WD, WK,TK, TW,Tl
6	SWR	Short Wave Radiation	SW
7	LWR	Long Wave Radiation Dome Temperature, Body Temperature, Thermopile voltage	LW, LD, LB, LT
8	FLW	Flowmeter	FM, Fl
9	SST	Surface Seawater Temperature	ST, SF
10	SSC	Surface Seawater Conductivity	sc
11	VLT	A/D Volts	VT
12	FLU	Fluorometer	FL, TB
13	XMS	Transmissometer	TR, BA
14	OXY	Oxygen	OC, OT, OS, OX, OG
15	TSG	Thermosalinograph	TT, TF, TC, SA, SD, SV
16	USP	Unspecified (user defined)	XX
17	PAR	Surface PAR	PA
18	AWT	Auxiliary Water Temperature	WT
19	AXT	Auxiliary air Temperature	AX
20	IST	Instrumentation	IP, IT, IS, IA, IV, IX
21	PRS	Pressure	PS
22	PDR	Water Depth	BT
23	NME	NMEA messages	LA, LO, GT, CR, SP, ZD,GA,GS
24	GYR	Gyro	GY
25	ASH	Ashtech Heading, Pitch, Roll	SH, SM, SR
26	TSV	Time Server	TS
27	WCH	Winch Wire Out, Wire Speed, Tension	ZO, ZS, ZT
28	ALK	Alkalinity (pH)	PH
29	VRU	Vertical Reference Unit (Pitch, Roll, Heave)	VP, VR, VH, VY, VX
30	SOW	Ship’s Speed Log (Speed over water)	SL
31	UCW	Uncontaminated Seawater Pump(s) status	PZ
32	MBD	Multibeam (Center beam Depth)	MB
33	PCT	pCO_2	PC
34	SND	Depth Sounder	BT, LF, HF
35	MAG	Magnetometer	MG, MD, MS, MG
36	GRV	Gravimeter	GC

Table 7. *Flux parameters from COARE 3.6 algorithm*

1	friction velocity that includes gustiness (m/s), u*
2	wind stress that includes gustiness (N/m^2)
3	sensible heat flux (W/m^2). Positive for $T_{air} < T_{skin}$
4	latent heat flux (W/m^2). Positive for $q_{air} < q_s$
5	atmospheric buoyany flux (W/m^2). Positive when hlb and hsb heat the atmosphere
6	atmospheric buoyancy flux from sonic. Same as above, computed with sonic anemometer T
7	Webb factor to be added to hl covariance and ID latent heat fluxes
8	temperature scaling parameter (K), t*
9	specific humidity scaling parameter (kg/kg), q*
10	momentum roughness length (m)
11	thermal roughness length (m)
12	moisture roughness length (m)
13	wind stress transfer (drag) coefficient at height z_u (unitless)
14	sensible heat transfer coefficient (Stanton number) at height z_u (unitless)
15	latent heat transfer coefficient (Dalton number) at height z_u (unitless)
16	Monin–Obukhov length scale (m)
17	Monin–Obukhov stability parameter z_u/L (dimensionless)
18	cool-skin temperature depression (degC), positive value means skin is cooler than subskin
19	cool-skin humidity depression (g/kg)
20	cool-skin thickness (m)
21	wind speed at reference height (user can select height at input)
22	air temperature at reference height
23	air specific humidity at reference height
24	air relative humidity at reference height
25	neutral value of wind speed at reference height
26	neutral value of air temp at reference height
27	neutral value of air specific humidity at reference height
28	Net IR radiation computed by COARE (W/m^2). Positive heating ocean
29	Net solar radiation computed by COARE (W/m^2). Positive heating ocean
30	latent heat of vaporization (J/K)
31	density of air at input parameter height z_t, typically same as z_q (kg/m^3)
32	neutral value of wind speed at z_u (m/s)
33	wind speed adjusted to 10 m (m/s)
34	neutral value of wind speed at 10m (m/s)
35	neutral value of drag coefficient at 10m (unitless)
36	neutral value of Stanton number at 10m (unitless)
37	neutral value of Dalton number at 10m (unitless)
38	rain heat flux (W/m^2). Positive cooling ocean
39	sea surface specific humidity, i.e. assuming saturation (g/kg)
40	evaporation rate (mm/h)
41	air temperature at 10m (deg C)
42	air specific humidity at 10m (g/kg)
43	air relative humidity at 10m (%)
44	air pressure at 10m (mb)
45	air density at 10m (kg/m^3)
46	gustiness velocity (m/s)
47	whitecap fraction (ratio)
48	energy dissipated by wave breaking (W/m^2)

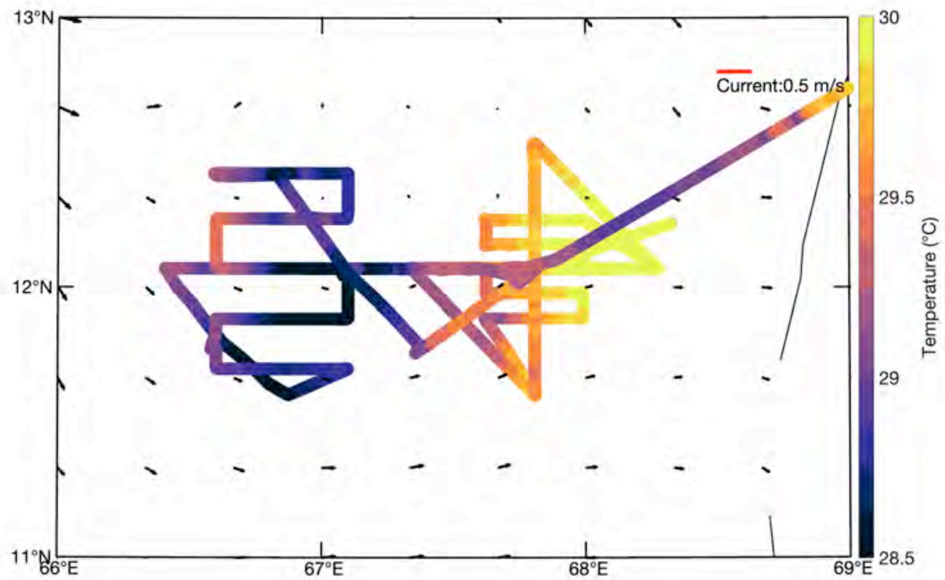

Figure 7. *Map of the Arabian Sea showing the through-flow temperature (~4–5 m depth) from R/V* Roger Revelle *during the EKAMSAT pilot cruise in June 2023. The background arrows are the currents averaged over the period 17–22 June 2023 as derived from OSCAR current product.*

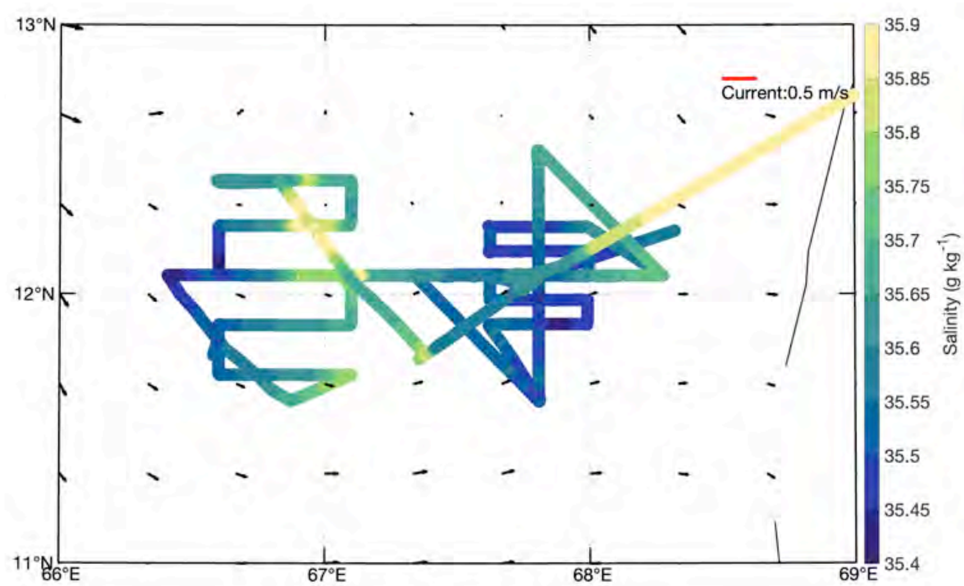

Figure 8. *Map of the Arabian Sea showing the through-flow salinity (~4–5 m depth) from R/V* Roger Revelle *during the EKAMSAT pilot cruise in June 2023. The background arrows are the currents averaged over the period 17–22 June 2023 as derived from OSCAR current product.*

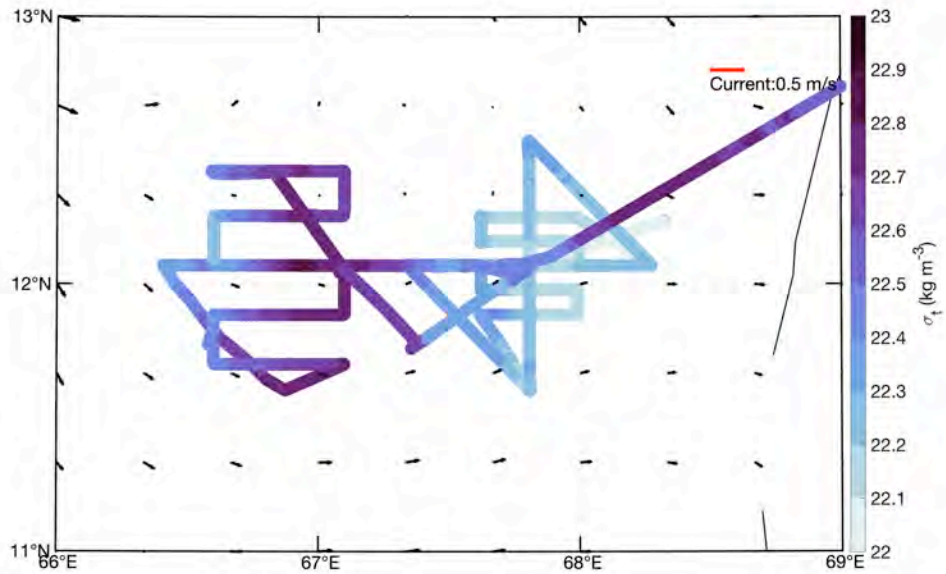

Figure 9. *Map of the Arabian Sea showing the through-flow density (s_t ~4–5 m depth) from R/V* Roger Revelle *during the EKAMSAT pilot cruise in June 2023. The background arrows are the currents averaged over the period 17–22 June 2023 as derived from OSCAR current product.*

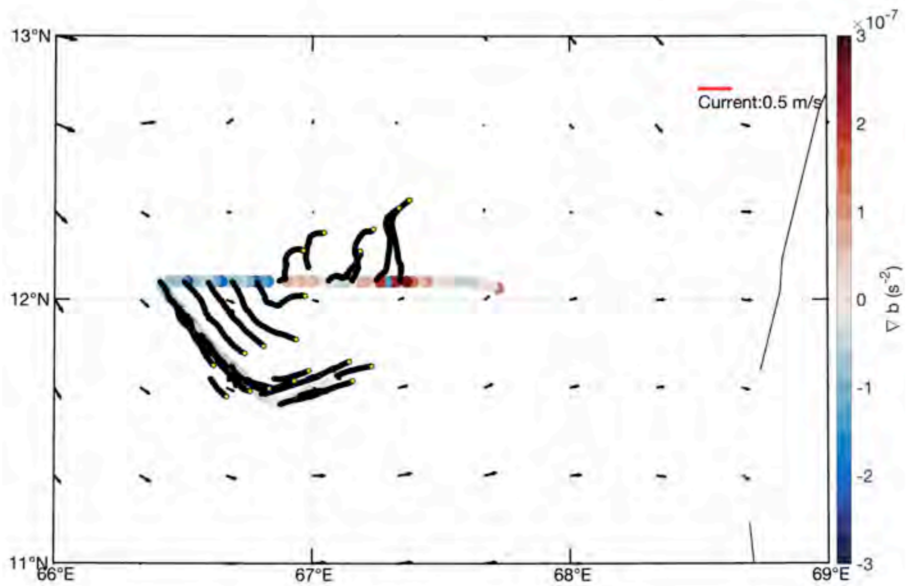

Figure 10. *The horizontal buoyancy gradient on the Zonal-2 section (Fig. 3) overlayed by the movement of drifters 17–19 June 2023. The background arrows are the currents averaged over the period 17–22 June 2023 as derived from OSCAR current product.*

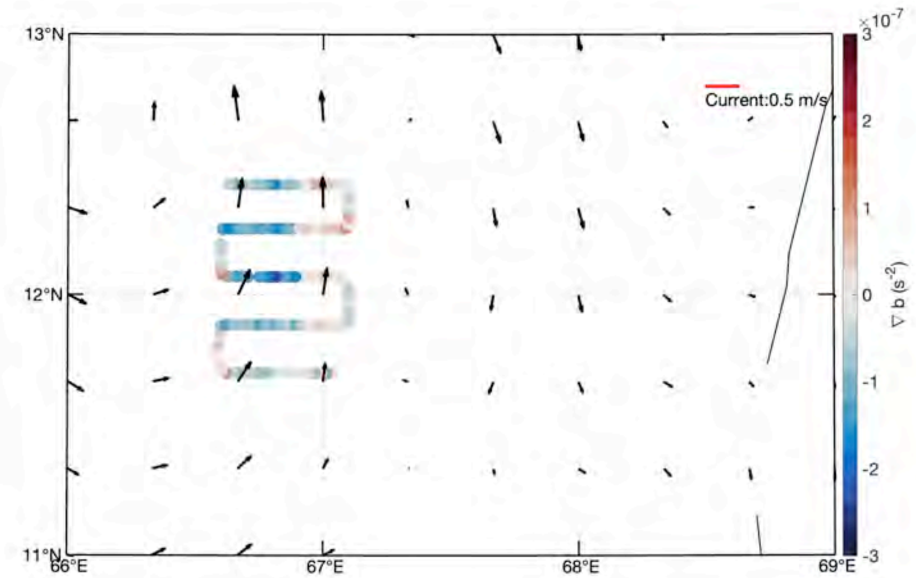

Figure 11. *The horizontal buoyancy gradient on the Filament section (Fig. 3). The background arrows are the currents averaged over the period 17–22 June 2023 as derived from OSCAR current product.*

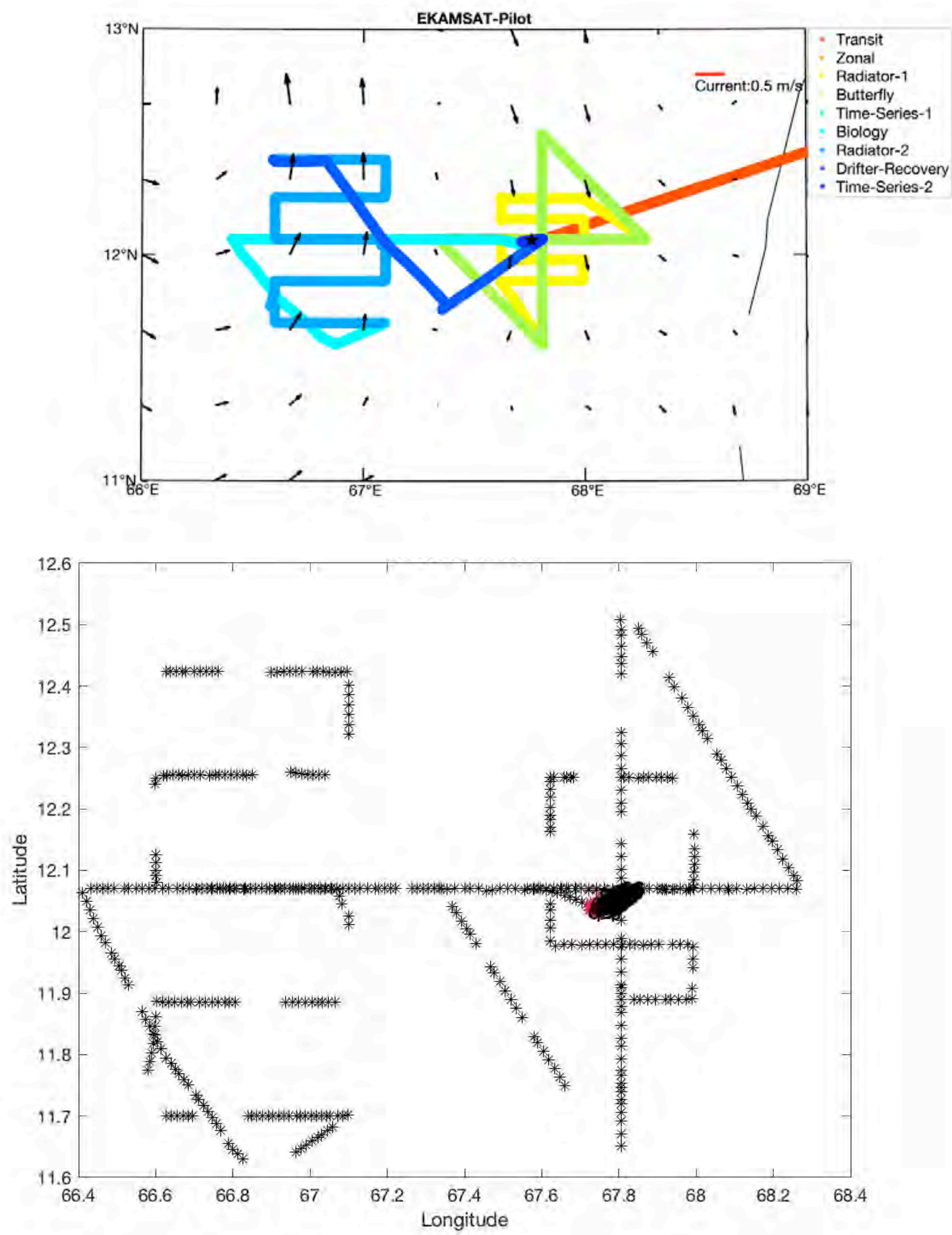

Figure 12. *(top) Complete EKAMSAT cruise map showing different sectional surveys (courtesy Siddhant Kerhalkar and Ankitha Kannad); (bottom) UCTD deployment locations along track.*

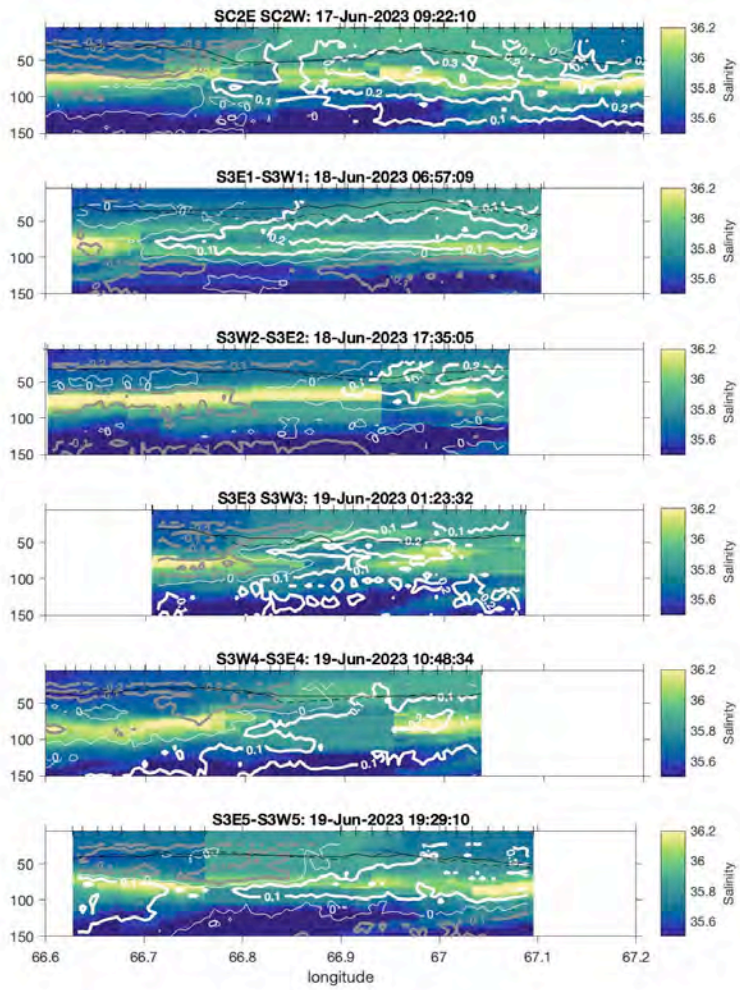

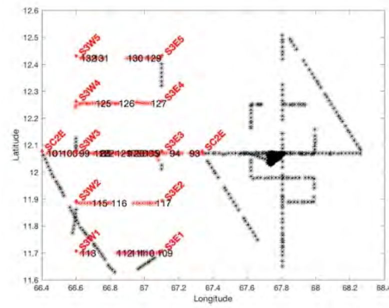

Figure 13. *Zonal salinity sections occupied as part of the Zonal-2 and Filament surveys crossing the filament associated with Cyclone Biparjoy. ADCP meridional velocity is shown in the contours (grey is southward and white is northward, contour interval 0.1 m/s). Chronological occupations are shown from top to bottom. Note strong northward jet (~0.4 m/s) associated with the front in the upper panel associated with saltier water in the near surface layer. Subsequent panels show weaker jet but confirm mixing of saltier water occurs in the central filament region. Note erosion of salinity maxima in that region. MLD (density defined) is shown by the solid black line and ILD (T(z=4 m) – 0.5°C) shown by dashed black line. Note barrier layers present (~15–20 m thick) in central filament region in two southern sections (S3E1–S3W1; S3W2–S3E2).*

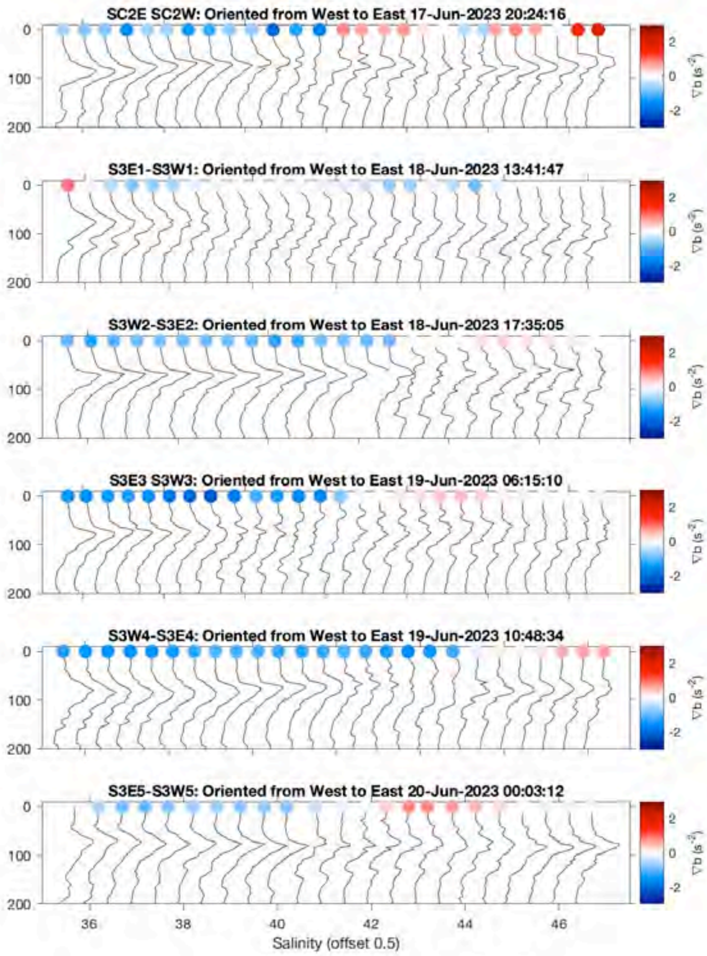

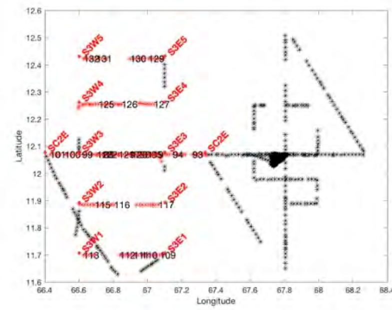

Figure 14. *As in Fig. 13 but showing each individual salinity profile for the Filament survey with the horizontal gradient in buoyancy for each profile (interpolated from the underway TSG data) shown at the top of each profile. Note changes in the salinity maximum shape and magnitude relative to position across the filament and the change in buoyancy experienced on either side of the jet, with more interleaving and shallower MLD found to the east. Sections shown chronologically (top to bottom) and all sections oriented from west to east (i.e., showing longitude).*

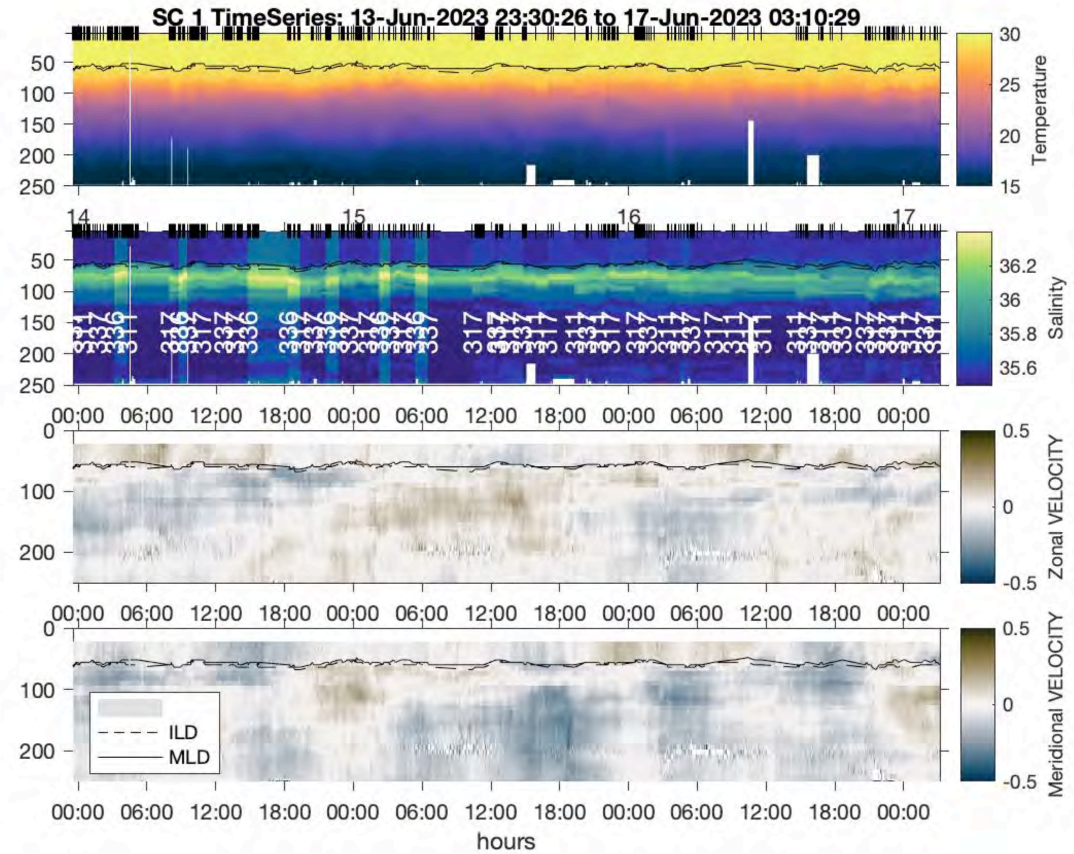

Figure 15. *Four-day flux time series at SC-1 showing from top to bottom: temperature, salinity, zonal velocity, meridional velocity. Dashed line shows the ILD (T(z=4 m) – 0.5) and MLD (density defined). Probe deployments noted by dashes along top axis and probe serial number indicated in second panel. Note the unvarying MLD and the presence of the salinity maximum waters at 70–100 m just below the MLD that likely arise from the higher salinity waters from the Persian Gulf and Red Sea that then subduct below the fresh surface waters from the Bay of Bengal.*

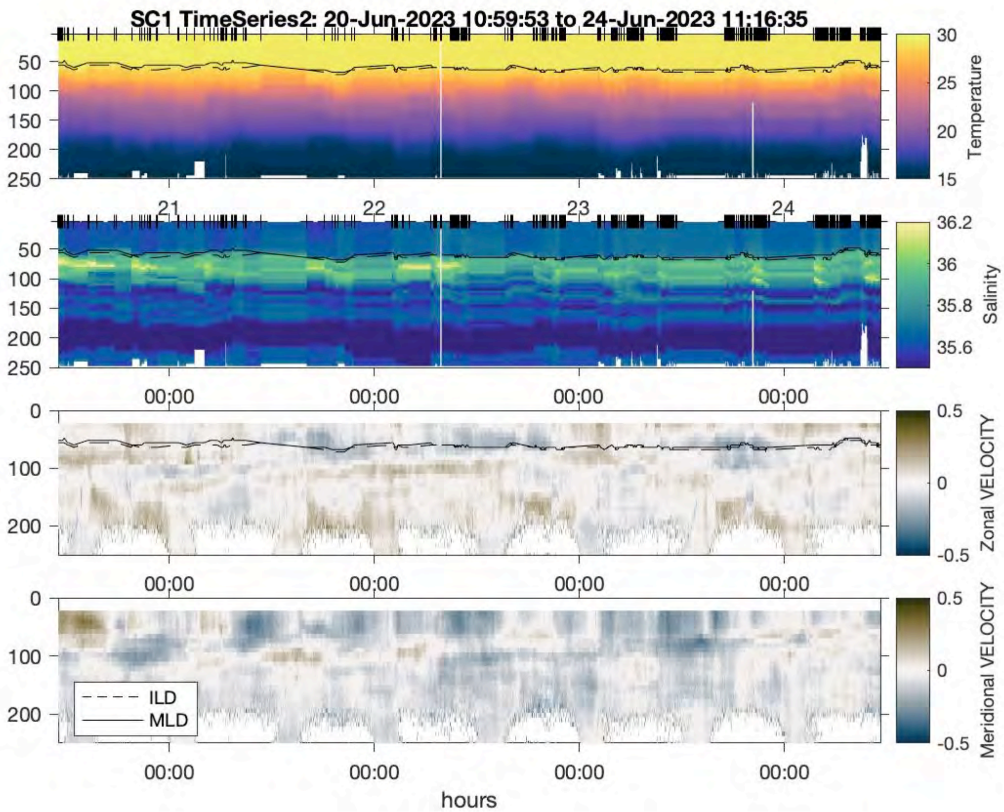

Figure 16. *Flux series 2. Mixed layers of ~50 m at top of S_{max} layer.*

Table 8. UCTD casts undertaken as part of EKAMSAT

Section Name	Start Date	Start Cast #	Start Cast Name	End Date	End Cast #	End Cast Name	Number Casts
Zonal	06/10/23 18:30	1	014_0337_6112023_0815	06/11/23 13:00	2	001_0296_6112023_0928	
Time Series Survey	06/11/23 13:00	3	021_0337_6112023_1623	06/12/23 13:00	13	001_0337_6122023_0619	10
Butterfly	06/12/13 00:00	14	005_0311_6122023_1612	06/13/23 22:00	34	040_0317_6132023_2017	20
Flux Series 1	06/13/23 22:00	35	003_0337_6132023_2330	06/17/23 03:30	90	001_0311_6172023_0240	55
Zonal-2	06/17/23 03:30	91	022_0317_6172023_0328	06/18/23 07:00	101	008_0317_6172023_1946	10
Filament Survey	06/18/23 07:00	102	015_0311_6172023_2120	06/20/23 00:30	132	017_0296_6192023_2330	30
Flux Series 2	06/20/23 10:30	133	001_0337_6202023_1055	06/24/23 19:00	189	018_0317_6222023_0202	56

Vertical Microstructure Profiler (VMP)

Summary: We deployed a Rockland Scientific vertical microstructure profiler (VMP) from the back deck of R/V *Roger Revelle* to measure ocean mixing and temperature–salinity profiles. The instrument was towed from a commercial fishing reel for 1–3 hr at a time in 14 deployments. Measurements were concentrated at local dawn and dusk, when the effects of mixing would be most evident. Profiles show many instances of dissipation coincident with a deepening mixed layer and/or patches of shear measured by the ship-based ADCP.

Setup: The instrument used was an RSI VMP-250-IR, serial number 092. Two attached brushes with no extra weights gave a vertical fall speed of about 0.8 m/s in the upper layers, slowing to about 0.7 m/s near the bottom of the 250-m casts.

Our rod and reel assembly was built from commercial fishing gear. We used a Lindgren–Pitman (LP) deep drop fishing rod along with an LP SV-2400 fishing reel. All guides were removed from the rod except for the last to provide a distance of more than 20 in between the level wind and the first guide to prevent excessive torque on the level wind. The same worm screw was used for the whole cruise with minimal signs of wear.

We set up our reel assembly on the starboard quarter of the back deck (see Fig. 17). A rod holder was mounted to two holes in the transom using hose clamps and left for the duration of the cruise. The rod and reel were stored in the main lab and brought out for each deployment. A nylon safety line was used to attach the reel to the transom with a bowline knot while deployed. Two 12V AGM batteries were wired in series and seated in a Pelican case as a battery box, which was secured to a capstan and eye bolt with a ratchet strap while the reel was deployed. The battery box was brought into the main lab using a small cart after about 6 hr of use for overnight charging.

There were three segments to the line: about 500 m of 500# test Spectra line on the reel, a 4-m-long 1/8-in Spectra red leader line, and a nylon tether of about 0.5 m attached to the instrument by a bowline knot (Fig. 18). To connect the reel line to the leader, an eye was spliced into the end of the 500# line around a small thimble. An eye was also spliced into both ends of the leader line around larger thimbles. The end of the reel line was attached to one end of the leader by a shackle and a swivel (two pieces of hardware were necessary to accommodate the step down in line width). On the other end, the red leader line was attached to the tether by a swivel. Small zip ties were used in all bolts to prevent backing out. The tether was detached from the swivel at the end of each deployment for storage of the reel and VMP. The 500 m on the reel was not quite enough line, as we sometimes got close to the end of the reel when casting to 250 m. See Fig. 19 for a view of the entire line setup.

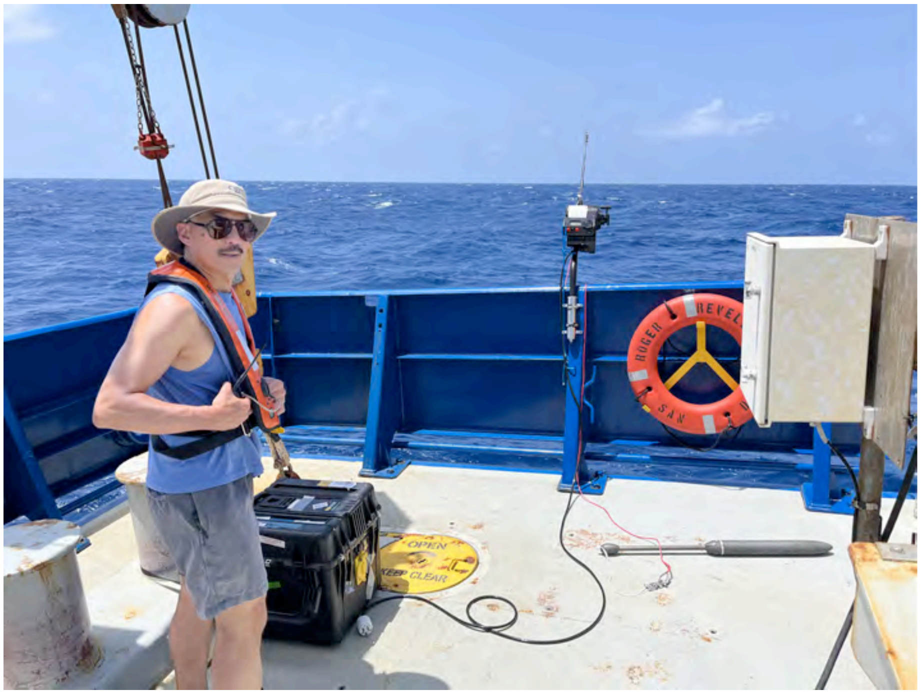

Figure 17. *The rod and reel setup for the VMP on the starboard quarter. A dummy probe is attached to the line for testing.*

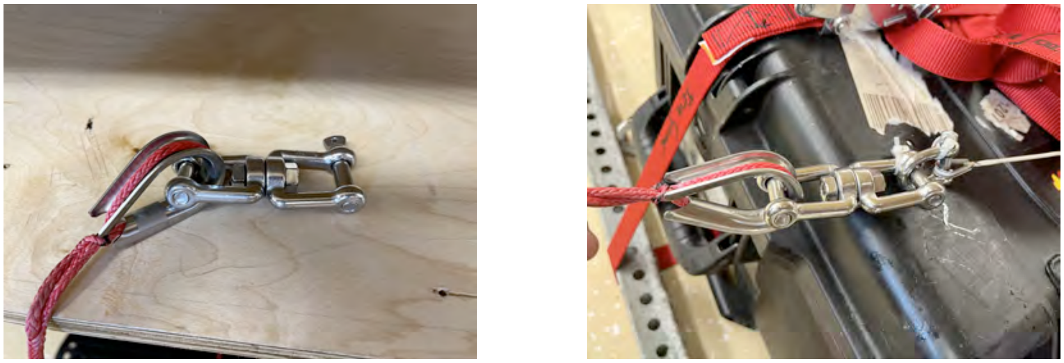

Figure 18. *The two ends of the VMP red leader line. Left panel: the near-instrument end that attaches to the nylon tether. Right panel: the near-reel end that connects to the spool of 500# Spectra line.*

Figure 19. *Recovering the VMP at the end of a deployment. All three segments of the line are visible with their connecting hardware.*

Deployments: There were 14 VMP deployments with a total of 187 casts (Table 9). Deployment 1 (D1) had a fall speed that was too fast (about 1.2 m/s). Deployments D2–D14 had good instrument fall speeds and sufficient decoupling from the ship motion (Fig. 20).

During Flux Series 2 (deployments D6–D14), we sampled twice per day in two 3-hr deployments, nominally from 04:00–07:00 and 17:00–20:00 local time. The dawn deployment was scheduled to end before significant shortwave heating began, and the dusk deployment was scheduled to bracket the time at which the net heat flux changed sign. These times were determined from the daily-mean heat fluxes computed from the ship-based met sensors.

Casts were nominally to 150 m depth for D1 and D2, to 200 m for D3–D7, and to 250 m for D8–D14. For 200-m casts, the instrument was released for 4 min, and for 250-m casts it was released for 5 min. The instrument was retrieved at reel speed setting 3 to 3.5, depending on sea state, and slowed as it neared the surface.

For deployments D1–D5, the bridge was asked to point into the waves and maintain a speed of 1 knot over water. For deployments D6–14, the ship was pointed into the wind (which generally aligned with the wave direction) to maximize the quality of the flux measurements. At times, a speed of 1 knot over water wasn't possible while maintaining heading, so the bridge drove as slowly as was possible.

Processing and Observed Features: Data were visualized using the ODAS quick_look MATLAB script along with a custom script by Pat Welch for at-sea VMP processing.

The uppermost part of the profiles was contaminated by the ship wake down to a typical depth of 10 or 15 m. Peaks in dissipation were generally seen at the base of the mixed layer as well as at the boundaries between water masses lower in the profile. The ship-based ADCP often had patches of shear coinciding with areas of dissipation. See Figs. 21 and 22 for representative dissipation profiles and spectra. See Fig. 23 for dissipation and TS profiles over a full deployment.

Issues: Deployments of the VMP generally went smoothly. The largest issue was the shear probes, which showed poor agreement on several deployments (Table 9). The same temperature probes rode for all deployments, while the shear probes were changed many times during the cruise. We used 9 of the 10 shear probes for at least one deployment.

The Valtrex 24V battery charger stopped working on 6/21. Upon connecting to the battery, all buttons would flash briefly, as normal. But subsequent connection to the A/C power source would not start charging the battery. The ship electrician repaired the visible issues with the A/C connection and checked the fuses, but we could not get the charger working again. We switched to a 24V, 10A (the maximum amperage that should be used with AGM batteries) charger that the ship had available, which worked well for the rest of the cruise.

Table 9. *VMP deployments*

D#	Deploy Date	Deploy Time (UTC)	Recovery Time (UTC)	T1	T2	S1	S2	Casts	Depth (m)	Notes
0	6/15	8:30	9:00	test	test	test	test	4	N/A	Test deployment with test probes.
1	6/16	7:45	9:00	1030	1305	1275	1038	11	150	First deployment with real probes. Drop speed was too fast (~1.2 m/s) and shear probes did not agree well with each other.
2	6/17	15:10	16:20	1030	1305	1021	1516	10	150	In bloom area after first CTD cast. Most casts only went to ~125m. During Zonal-2 Section. Good probe agreement.
3	6/18	14:45	16:15	1030	1305	1021	1516	10	200	Dusk deployment in bloom area. 1/3 during Filament Survey. Good probe agreement.
4	6/18	23:45	1:15	1030	1305	1021	1516	10	200	Dawn deployment in bloom area. 2/3 during Filament Survey. Good probe agreement. Some spikes at depth from Sh2.
5	6/19	14:40	16:00	1030	1305	1021	1264	11	200	Dusk deployment in bloom area. 3/3 during Filament Survey. Changed S2 since last deployment. Positive bias in Sh1 relative to Sh2.
6	6/20	12:55	14:05	1030	1305	1038	1264	10	200	Dusk deployment. 1/9 during Flux Series 2. Probe agreement deteriorates over deployment.
7	6/20	23:30	0:50	1030	1305	1038	1264	11	200	Dawn deployment. 2/9 during Flux Series 2. Both probes questionable. Sh1 shows anomalous regions at moderate depths. Sh2 has large positive bias in upper 50 m.
8	6/21	11:30	14:45	1030	1305	1038	1848	19	250	Dusk deployment. 3/9 during Flux Series 2. First 3-hr deployment. Sh1 has gone bad (both too positive and too negative). Process Sh2 only.
9	6/21	22:40	1:40	1030	1305	1268	1848	17	250	Dawn deployment. 4/9 during Flux Series 2. Sh2 positively biased in upper layer and Sh1 positively biased at depth.

D#	Deploy Date	Deploy Time (UTC)	Recovery Time (UTC)	T1	T2	S1	S2	Casts	Depth (m)	Notes
10	6/22	12:10	15:00	1030	1305	1196	1848	15	250	Dusk deployment. 5/9 during Flux Series 2. Sh1 probe was bad (values both unrealistically small and unrealistically large). Should be processed with Sh2 only.
11	6/22	22:35	1:50	1030	1305	1252	1848	16	250	Dawn deployment. 6/9 during Flux Series 2. Relatively good agreement between probes. Positive bias in Sh1 relative to Sh2 grows with depth.
12	6/23	11:35	14:45	1030	1305	1252	1848	17	250	Dusk deployment. 7/9 during Flux Series 2. One aborted cast due to reel issue. Relatively good agreement between probes. Positive bias in Sh1 relative to Sh2 grows with depth.
13	6/23	22:55	1:55	1030	1305	1252	1848	16	250	Dawn deployment. 8/9 during Flux Series 2. Relatively good agreement between probes. Positive bias in Sh1 relative to Sh2 grows with depth.
14	6/24	11:35	14:10	1030	1305	1252	1848	14	250	Dusk deployment. 9/9 during Flux Series 2. Relatively good agreement between probes. Positive bias in Sh1 relative to Sh2 grows with depth.

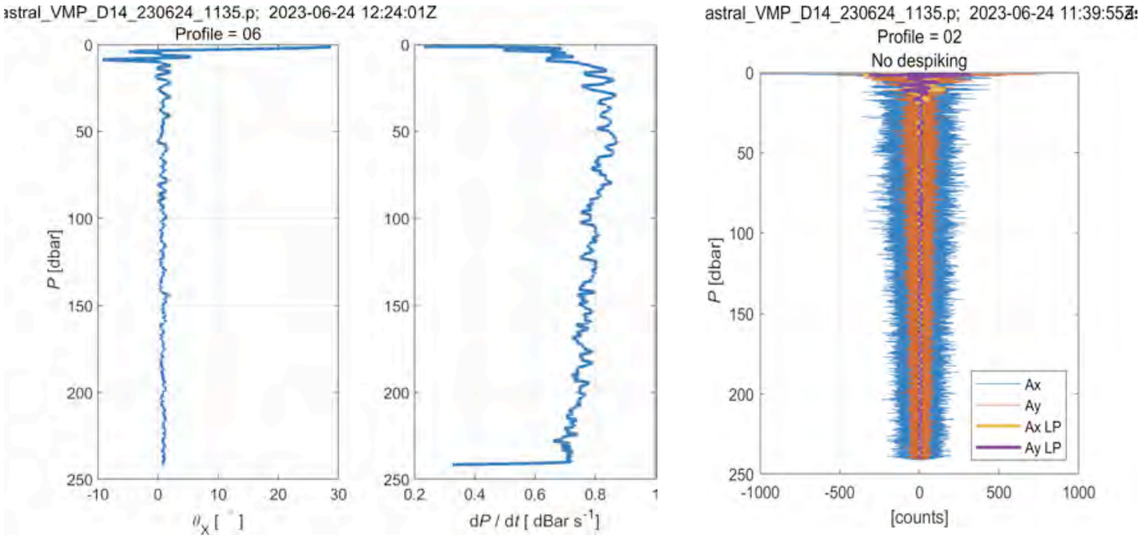

Figure 20. *Example instrument fall characteristics from casts during D14. Left panel: Instrument inclination with depth, showing <2° below the topmost layer. Center panel: Instrument fall speed of about 0.8 m/s near the surface and 0.7 m/s at depth. Right panel: Instrument vibration showing an acceptable range.*

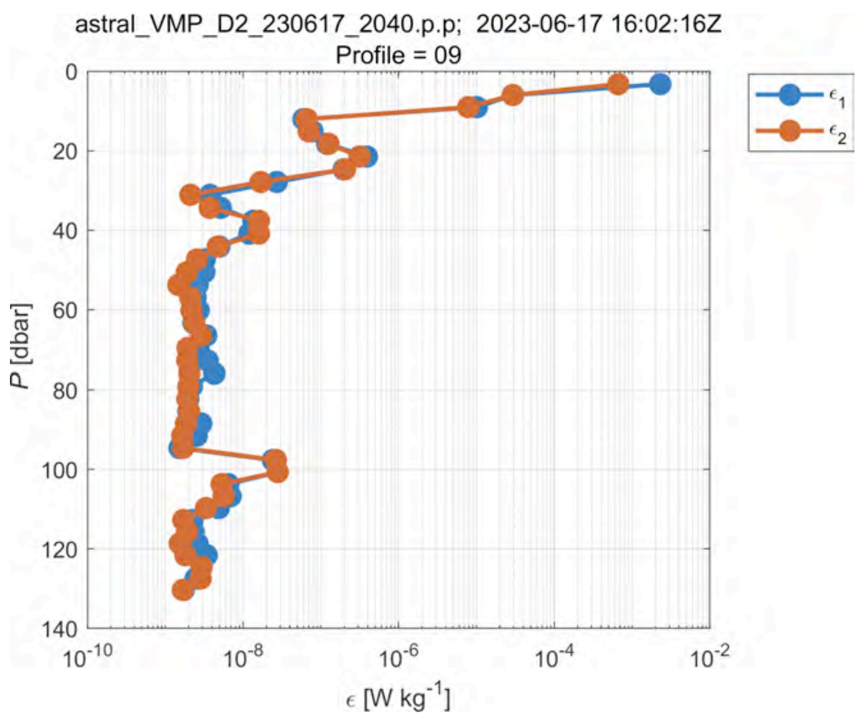

Figure 21. *A representative dissipation profile from D2, cast 9 with good agreement between the shear probes.*

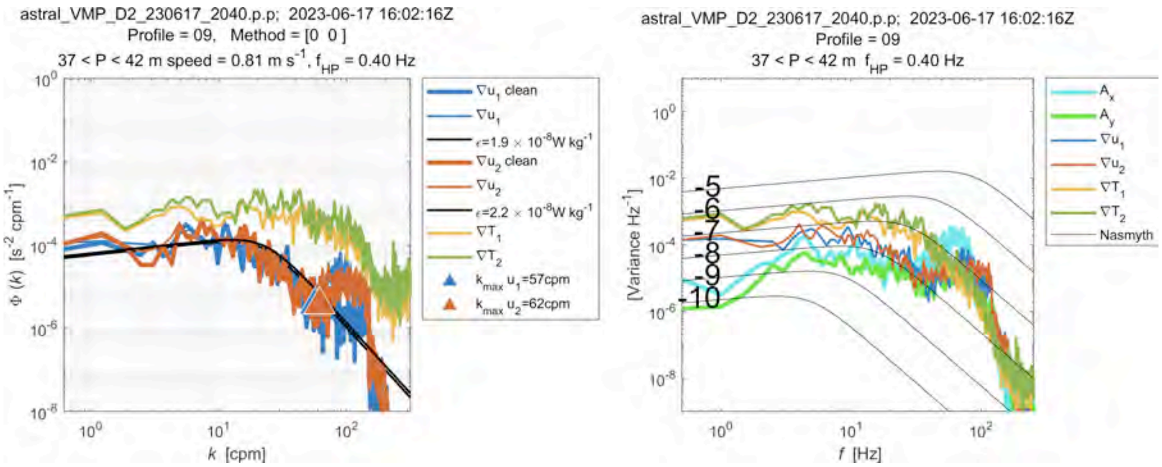

Figure 22. *A representative set of spectra from the same cast as Fig. 21 computed from the depth bin 37–42 dbars.*

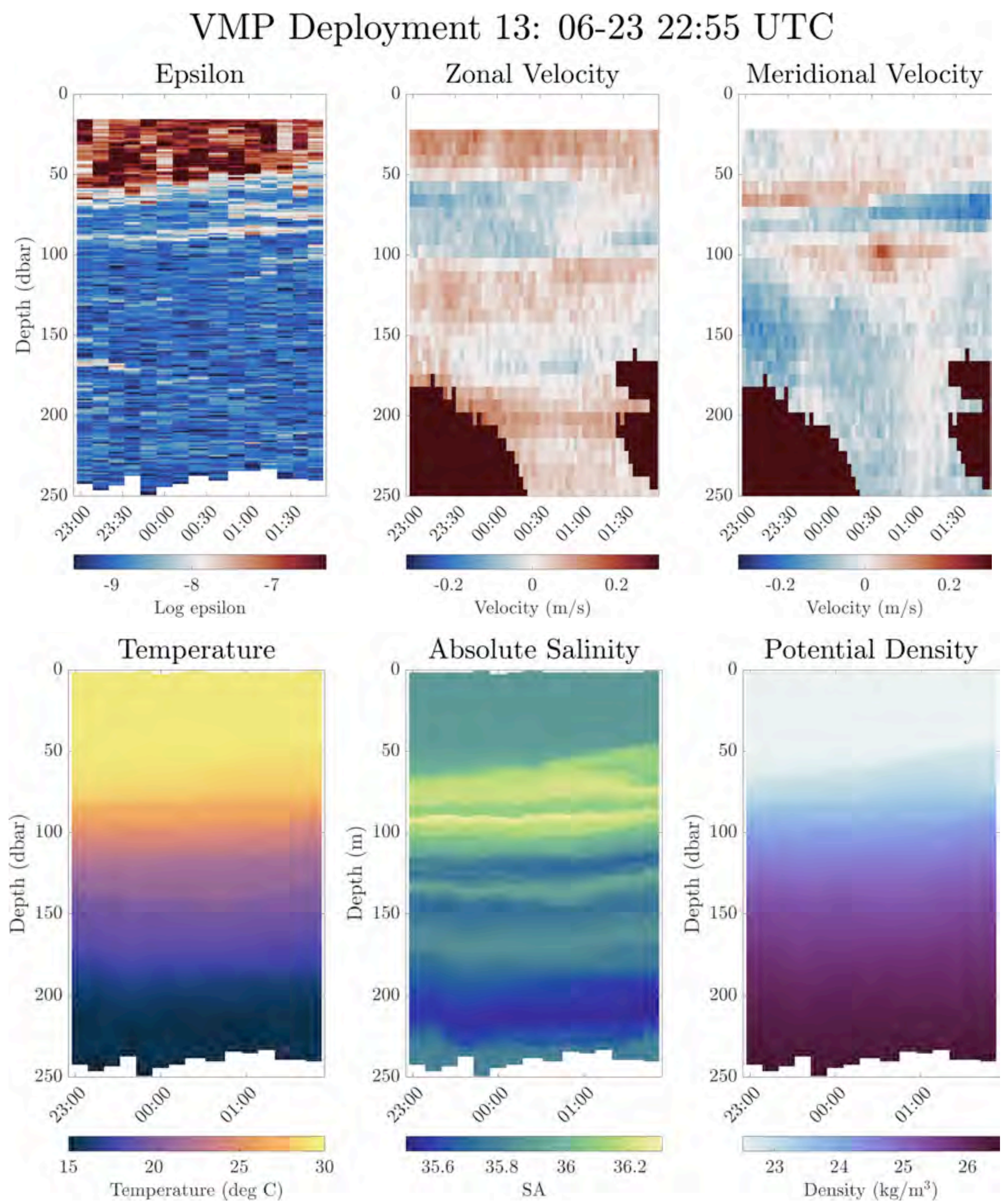

Figure 23. *An example deployment of the VMP. The top-left panel shows VMP-measured dissipation while the top-center and top-right panels show velocity from the ship-based ADCP. Bottom panels show TS data from the VMP JAC sensors.*

During one deployment, the nylon bolt holding the magnet broke during installation due to over-tightening (NB: hand tighten only!). The technician was able to remove the broken bolt with a drill attachment. We switched to the spare magnet in the VMP case.

The hose clamp attachment of the rod holder to the transom was difficult to tighten properly. Recovery of the VMP would stress the clamps so that the rod holder would inevitably end up at an angle to the vertical. On 6/24, the bottom clamp broke during installation of the reel. In future deployments, a more secure setup of the hose clamps should be considered.

The reel motor steadily increased in noisiness over the course of the cruise. It sounded as if bearings or lubricant had become worn. Our cruise was short enough so that the reel worked well throughout our deployments, but on a longer voyage it may need to be opened and serviced mid-cruise.

The ship's bow thrusters stopped working early in Flux Series 2, so we were reliant on the Z-drives for the rest of the cruise. This meant that the ship could not drive as slowly while maintaining heading. Speed over ground was typically between 1 and 1.5 knots for the remaining deployments, with more variable speed over water.

Atmospheric and Sea Surface Temperature Measurements

The University of Notre Dame and the NOAA Physical Sciences Lab (Boulder) were responsible for atmospheric and oceanic sea surface temperature (SST) measurements. Instrumentation included:

- Vaisala CL31 Ceilometer
- Vaisala Present Weather and Visibility Sensor PWD 22
- Inter Met Systems iMet-4 Radiosonde
- Water Temperature Sensor (Sea Snake; NOAA fabrication)
- Vaisala PTB220 Barometer
- Eppley Standard Precision Pyranometer
- Hemisphere Crescent VS100 Series GPS Compass
- Vaisala Humidity and Temperature Meter Series (HMT) 337
- Li-Cor Open Path CO_2/H_2O Analyzer LI-7500
- Gill WindMaster Pro Anemometer
- Systron and Donner 6 Axis Motion Detector Sensor

Instrument Preparation

To prepare the bow mast system and other NOAA instrumentation, Griffin Modjeski and Jay Orson Hyde spent a week at the NOAA headquarters in Boulder, CO with engineer Ludovic Bariteau. As NOAA conducts many concurrent experiments and did not have a bow mast system at the ready, the University of Notre Dame (UND) team built a new system, power router, and a network switch. The installation, testing, and preliminary data acquisition of the bow mast system and other NOAA-borrowed instrumentation on the ship deck was supposed to be carried out in Cape Town, South

Africa; however, due to air freight complications, the equipment cleared customs late and it could only be secured on *Revelle*. To continue this installation through to the mobilization stage, Griffin and Jay traveled to Port Louis, where *Revelle* had just concluded an experiment up the eastern coast of Africa around Madagascar. There, the UND team managed to unbox and mount the NOAA instruments and the UND ceilometer and present weather detector. By the end of installation, the data acquisition system was malfunctioning and the UND instruments required power and communication. The last of these issues were resolved during the beginning of the cruise by the UND team consisting of Griffin Modjeski, Devmi Gamage, and Selina Bolella.

Atmospheric Profile Measurements: Radiosonde Launches

The first successful radiosonde launch was on 13 June 06:19 UTC; consecutive radiosonde launches were conducted every 6 hr until 24 June 2023, 12:00 UTC, daily at 00:00, 06:00, 12:00 and 18:00 UTC (05:30, 11:30, 17:30, 23:30 Indian Standard Time, Table 11 and Fig. 24). Additional radiosonde launches, at 3-hr intervals, were made during the latter part of the cruise, guided by weather forecasts (Table 11, green highlight).

<u>Radiosonde Data Collection / Processing</u>: iMetOS-II software was used to process the radiosonde data (Table 12). Each radiosonde release has a folder with the name format EyyyymmHHMM. For example, E2023062100 indicates a release on 21 June 2023 at 00:00 UTC. Under the folder there are several files: summary (EyyyymmHHMM_SUMMARY.txt), all the above telemetry data (EyyyymmHHMM _TSPOTINT.txt) and RAOBEyyyymmHHMM.csv including the Temperature, Relative Humidity, Wind direction, Wind speed, and Geopotential altitude with latitudes and longitudes.

<u>Radiosonde Launch Checklist</u>: Biodegradable Radiosonde Dereeler, Crescent wrench (adjustable), 2 zip ties, Regulator, Radiosonde, Meteorological balloon, O-rings (we have been using 2 to further seal the regulator), Key for opening the hydrogen cylinder/tank, Radio.

<u>Radiosonde Launch Procedure</u>: Preparations started at least 15 min before the launch. First the iMetOS-II software was initialized, then the antenna communications of radiosonde was turned on followed by the filling of the balloon with helium. The radiosonde was tied to the balloon using the dereeler, the signal quality from iMetOS-II was checked and then the balloon was released (Fig. 25). The software provides Skew-T log-P diagrams, Wind Speed, and Wind Direction profiles for real time data.

Cloud Height Detection: Vaisala CL-31 Ceilometer

A Vaisala CL-31 Ceilometer (Fig. 26, left) was used to measure cloud base heights, ranging from 0 to 7.6 km (0 to 25000 ft). CL-31 employs a pulsed diode laser LIDAR technology, where short powerful laser pulses are sent out in a vertical direction or near vertical direction. The reflection of light-backscatter caused by haze, fog, mist, precipitation, and clouds is measured as the laser pulses traverse the sky. The resulting backscatter profile, that is, the signal strength versus the height, is stored and processed and the cloud bases are detected. The time delay between laser pulses and the detection of the backscatter signal can be used to retrieve the cloud base height. Data outputs were obtained using CL-View software, a Vaisala graphical user interface for ceilometers. Successful ceilometer measurements were obtained from the start to the end of the cruise period (11–24 June 2023). The data were stored in E3mmddHH.dat format.

Present Weather Conditions: Vaisala Present Weather Detector (PWD) 22

PWD 22 (Fig. 26, center) is a multi-variable sensor for automatic weather observing systems. The sensor combines the functions of a forward scatter visibility sensor and a present weather sensor. PWD 22 has visibility range 10 m to 20 km and includes seven precipitation types. It measures precipitation water content with a capacitive Vaisala RAINCAP Rain Sensor and combines this information with optical scatter and temperature measurements. The three independent measurements provide data for evaluating the prevailing visibility and weather (Vaisala PWD 22 User's Guide).

Measurements of the PWD 22 were recorded 11–24 June 2023. For the weather messages, NWS supported internal weather codes as well as WMO SYNOP codes (4680) are used in PWD 22. First, the Terraterm commands (11–13 June) and then a MATLAB script (13–24 June) were used to obtain the PWD 22 data. The data files are in the format yyyymmddTHHMMSS.txt.

Sea Snake

A Sea Snake (from Physical Science Laboratory, NOAA) (Fig. 26, right) was used for the measurement of temperature near the surface. The Sea Snake used in this case could record data when the ship's speed was slower than 6 knots (this is a limitation of the present version as it did not include the pulley, which is crucial to alleviating stress in the sea snake while being towed at higher speeds). The deployment information of Sea Snake is given in Table 13. Sea Snake data were a part of the bow mast data. The SST data are being processed by Dr. Elizabeth Thompson of NOAA.

Bow Mast

Other major NOAA instrumentation includes those of the bow mast: Vaisala PTB220 Barometer, Eppley Standard Precision Pyranometer, Hemisphere Crescent VS100 Series GPS Compass and the bow mast system with Vaisala Humidity and Temperature Meter Series (HMT) 337, Li-COR Open Path CO_2/H_2O Analyzer LI-7500, Gill WindMaster Pro Anemometer, and a Systron and Donner 6 Axis Motion Detector Sensor. The manual cleaning of instrumentation was carried out regularly (Table 14).

Meteorological Weather Forecast

UND also provided weather briefings. The collected daily weather briefings and forecasts are found in an Appendix.

Table 11. *Radiosonde launch information. Orange shading marks failed launches, green marks periods of increased launch rate, one sonde every 3 hr.*

Date 2023/06	Local Time	UTC	SUCCESS	FOLDER NAME: E	Latitude	Longitude
11	11:30	06:00	No: software failure	2023061106		
12	13:00	07:30	No : telemetry short circuit	2023061206		
12	17:30	12:00	No : telemetry short circuit	2023061212		
13	11:49	06:19	Yes	2023061306	12°24'21.3"N	067°56'15.0"E
13	17:50	12:20	Yes (antenna skimmed water)	2023061312	12°28'55.5"N	067°48'21.4"E
13	23:30	18:00	No	2023061318		
14	05:30	00:00	Yes	2023061400	12°04'05.3"N	067°48'11.8"E
14	12:23	05:53	Yes	2023061406	12°02'40.4"N	067°45'16.5"E
14	17:32	12:02	Yes	2023061412	12°03'01.1"N	067°46'03.5"E
14	23:30	18:00	NO?? No data	2023061418		
15	05:32	00.02	Yes	2023061500	12°02'23.6"N	067°44'05.1"E
15	11:30	06:00	Yes	2023061506	12°03'18.3"N	067°46'20.9"E
15	17:30	12:00	Yes	2023061512	12°03'48.9"N	067°47'37.6"E
15	23:30	18:00	Yes	2023061518	12°02'29.8"N	067°43'21.8"E
16	05:30	00:00	Yes	2023061600	12°02'32.2"N	067°45'40.0"E
16	11:32	06:00	Yes	2023061606	12°03'26.4"N	067°46'58.7"E
16	17:30	12:00	Yes: radiosonde hit A frame	2023061612	12°02'14.7"N	067°44'29.1"E
16	23:30	18:00	Yes	2023061618	12°03'27.2"N	067°45'29.8"E
17	05:29	00:00	Yes	2023061700	12°03'25.2"N	067°47'08.1"E
17	11:28	06:00	Yes: sonde skimmed water	2023061706	12°04'11.5"N	067°31'05.0"E
17	17:30	12:00	Yes	2023061712	12°04'12.0"N	067°07'52.0"E
17	23:30	18:00	Yes	2023061718	12°04'11.5"N	066°42'48.9"E
18	05:30	00:00	Yes	2023061800	11°51'50.1"N	066°34'08.9"E
18	11:31	06:00	No: data did not record	2023061806		
18	17:30	12:00	No: data did not record	2023061812		
18	23:30	18:00	Yes	2023061818	11°53'06.0"N	066°38'56.3"E
19	05:30	00:00	Yes	2023061900	12°03'00.2"N	067°05'57.4"E
19	11:31	06:00	Yes	2023061906	12°04'11.2"N	066°42'26.4"E
19	17:30	12:00	Yes	2023061912	12°15'18.1"N	066°39'35.3"E
19	23:30	18:00	Yes	2023061918	12°15'17.8"N	067°04'24.3"E
20	05:36	00:00	Yes	2023062000	12°25'26.0"N	066°38'44.5"E
20	11:38	06:00	Yes	2023062006	11°56'40.0"N	067°13'02.1"E
20	17:30	12:00	Yes	2023062012	12°04'06.5"N	067°47'54.1"E
20	20:30	15:00	Yes (Extra)	2023062015	12°03'47.9"N	067°45'43.4"E
20	23:30	18:00	Yes	2023062018	12°03'36.9"N	067°43'36.7"E

Date 2023/06	Local Time	UTC	SUCCESS	FOLDER NAME: E	Latitude	Longitude
20 (21 local)	02:30	21:00	Yes (Extra)	2023062021	12°04'14.3"N	067°47'47.2"E
21	05:32	00:00	Yes	2023062100	12°04'01.5"N	067°45'40.9"E
21	11:30	06:00	Yes	2023062106	12°04'00.4"N	067°46'59.1"E
21	17:30	12:00	Yes	2023062112	12°03'57.4"N	067°43'17.1"E
21	20:30	15:00	Yes (Extra)	2023062115	12°04'06.0"N	067°41'51.1"E
21	23:30	18:00	Yes	2023062118	12°03'56.1"N	067°47'18.5"E
21 (22 local)	02:30	21:00	Yes(Extra)	2023062121	12°03'42.8"N	067°44'59.2"E
22	05:31	00:00	Yes	2023062200	12°04'02.1"N	067°42'58.8"E
22	11:30	06:00	Yes	2023062206	12°02'05.7"N	067°45'16.5"E
22	17:30	12:00	Yes	2023062212	12°02'23.9"N	067°44'52.9"E
22	20:30	15:00	Yes (Extra)	2023062215	12°03'29.2"N	067°45'10.3"E
22	23:30	18:00	Yes	2023062218	12°04'13.2"N	067°48'16.5"E
22 (local 23)	02:30	21:00	Yes (Extra)	2023062221	12°04'32.3"N	067°44'05.8"E
23	05:35	00:00	Yes	2023062300	12°04'13.5"N	067°45'43.5"E
23	11:31	06:00	Yes	2023062306	12°02'15.2"N	067°46'28.1"E
23	17:30	12:00	Yes	2023062312	12°03'55.7"N	067°46'16.4"E
23	20:30	15:00	Yes (Extra)	2023062315	12°03'35.3"N	067°42'58.7"E
23	23:30	18:00	Yes	2023062318	12°03'22.0"N	067°45'56.5"E
23 (local 24)	02:30	21:00	Yes	2023062321	12°04'11.8"N	067°48'27.9"E
24	05:35	00:00	Yes	2023062400	12°03'48.6"N	067°44'22.2"E
24	11:30	06:00	Yes	2023062406	12°02'40.0"N	067°46'48.2"E
24	17:30	12:00	Yes	2023062412	12°04'04.4"N	067°46'59.4"E

Table 12. *Telemetry data of the radiosondes (iMetOS-II Manual)*

– Time (from launch) – Pressure – Temperature – Humidity – Longitude – Latitude – Geometric altitude above ground level – Geometric altitude above mean sea level – Geopotential above ground level – Geopotential above mean seal level – North offset from launch site – East offset from launch site – Wind speed – Wind direction – Wind north component – Wind east component – Virtual temperature – Dew point – Air density – Vapour pressure – Ascent rate – Mid-Level geopotential – Height:Layer thickness ratio – Standard Atmosphere temperature – Standard Atmosphere pressure – Standard Atmosphere density	– Mid-Level temperature – Mid-Level pressure – Mid-Level density – Mid-Level Standard Atmosphere temperature – Mid-Level Standard Atmosphere pressure – Mid-Level Standard Atmosphere density – Delta Standard Atmosphere temperature – Delta Standard Atmosphere pressure – Delta Standard Atmosphere density – Layered Delta Standard Atmosphere temperature – Layered Delta Standard Atmosphere pressure – Layered Delta Standard Atmosphere density – Ground range – Slant range – Azimuth angle between antenna and radiosonde – Elevation angle between antenna and radiosonde – Mixing ratio – Saturation vapour pressure – Solar angle – Solar temperature corrections – UTC date of data sample – UTC time of data sample – Ozone pressure

Table 13. *Deployment and recovery times of the Sea Snake*

Deployment		**Recovery**	
Date/Time [Local time]	Date/Time [UTC]	Date/Time [Local time]	Date/ Time [UTC]
2023/06/14 18:50	2023/06/14 13:20	2023/06/20 06:00	2023/06/20 00:30
2023/06/20 16:39	2023/06/20 11:09	2023/06/24 19:50	2023/06/24 14:20

Table 14. *Licor and radiometer clean schedule*

Licor Clean [Local time]	**Radiometer Clean [Local time]**
15^{th} of June 12:00	16^{th} of June 12:26
16^{th} of June 12:22	17^{th} of June 12:45
17^{th} of June 12:41	18^{th} of June 12:56
18^{th} of June 12:50	19^{th} of June 12:24
19^{th} of June 12:20	20^{th} of June 12:33
20^{th} of June 12:20	21^{st} of June 12:30
21^{st} of June 12:33	22^{nd} of June 12:31
22^{nd} of June 12:26	23^{rd} of June 12:13
23^{rd} of June 12:10	24^{th} of June 12:51
24^{th} of June 12:49	

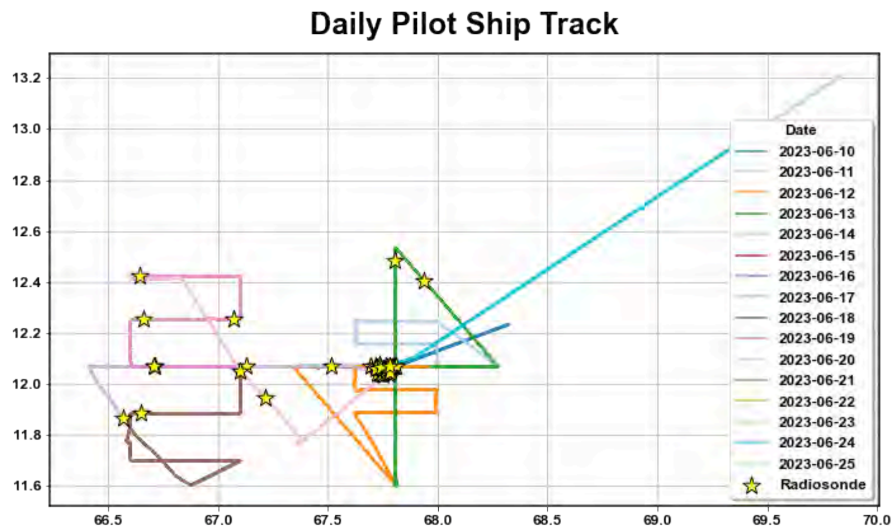

Figure 24. *Ship track. Stars mark radiosonde launches and line color indicates date.*

Figure 25. *A successful radiosonde release.*

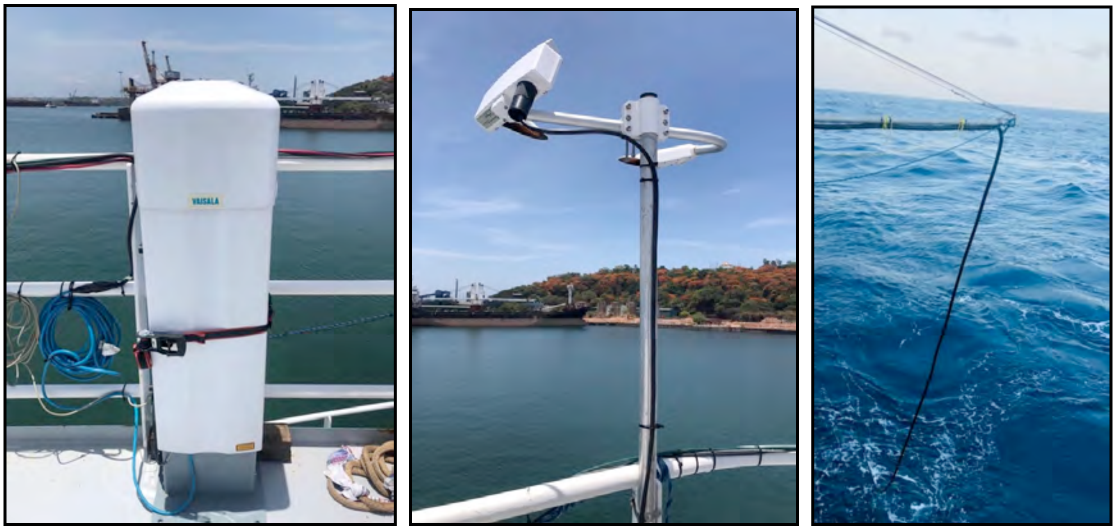

Figure 26. *(left) Vaisala CL-31 Ceilometer, (center) PWD 22, and (right) Sea Snake, as deployed for the EKAMSAT/ASTraL 2023 pilot cruise.*

3. RESULTS AND DISCUSSION

June Climatology in the Arabian Sea

The southwestern monsoon in India sets over the state of Kerala, typically around 1 June of each year. The lower tropospheric southwesterly Somali jet transports moisture as it crosses the Arabian Sea and helps this onset. The low-pressure system forms at around 10°N and moves northward (*Vinayachandran et al*., 2007). According to the IMD, the monsoon onset for 2023 was on 8 June, which is seven days later than usual. In fact, monsoon onset is this late only ten percent of the time (Fig. 27). The development of Cyclone Biparjoy in the southeast Arabian Sea pulled moisture out of the Kerala coast, causing this delay.

Atmospheric Profile Measurements from the Radiosondes

Presence of a Mid-Tropospheric Dry Layer

Figure 28 (a–c) shows the vertical distribution of atmospheric temperature during the EKAMSAT pilot cruise on June 14, 17, and 21, derived from rawinsonde sounding data. These figures provide a snapshot of the general atmospheric conditions present throughout the entire cruise. The atmospheric profile reveals several distinct layers that remain consistent during the cruise.

Below the ~950 hPa level, the temperature lapse rate is approximately dry adiabatic, indicating a well-defined atmospheric mixed layer. Above this mixed surface layer, a sharp inversion is observed around ~800–850 hPa (~1.4–1.9 km), characterized by a rapid drop in dew point temperature (Fig. 28). Relative humidity (RH) is predominantly above 80% near the base of this inversion but falls sharply to less than 20–40% at the top (Fig. 29).

At approximately 600 hPa (~4.2 km), a second inversion layer is noted, marked by a steep decline in dew point temperature and very low RH levels (Fig. 28). Specifically, RH drops sharply from 50–60% to ~5% within this layer (Fig. 29). These decreases in humidity resemble the warm, dry layers observed in the TOGA COARE (1992) soundings in the western Pacific warm pool region (*Mapes and Zuidema*, 1996; *Parsons et al*., 2000), and findings from the ARMEX 2002 experiment in the Arabian Sea (*Bhat*, 2005).

The EKAMSAT Rawinsonde data highlight several distinct RH levels (Fig. 29).

- Below the ~800 hPa level (1.9 km), RH values range from ~70–100%, indicating a relatively humid and moist atmospheric environment.
- Between ~800 hPa and ~600 hPa (4.2 km), a low moist–dry intermediate layer is present, with RH values of ~20–60%. This layer contains dry areas that appear as discrete pockets or patches.

- From ~600 hPa to ~300 hPa (~9 km), RH drops below 20%, which will be referred to as the mid-tropospheric dry layer (MTDL) from this point onwards.
- Above 300 hPa, RH generally ranges from ~40–80%, although some dry pockets persist in this region. The MTDL is notably warm, particularly near its base, while the layer below it shows slight moisture.

In Fig. 29, the pressure resolution is set at 5 hPa for each 6-hr interval throughout the ship's course each day.

Wind Speed Profile with Respect to the Relative Humidity Structure of the Atmosphere

The wind speed profile over the ship's track, derived from the rawinsonde data, shows wind speeds ranging from ~10 m/s to 15 m/s below ~800 hPa following the onset of the southwest monsoon (Fig. 30a).

The wind pattern indicates a prevailing southwesterly flow, as shown by the wind direction profile (Fig. 30b). These features are consistent with the characteristics of the Somali ('Findlater') jet, known for its lower tropospheric southwesterly winds. The Somali jet transports moisture across the Arabian Sea and plays a significant role in the onset of the southwestern monsoon. Its arrival typically occurs in early June, marking the beginning of the monsoon season, particularly in the southwestern region of Kerala.

- The wind speeds in the MTDL are typically very low, usually less than 5 m/s, except during the initial days of the cruise, specifically June 13–15, 2023, prior to the landfall of Cyclone Biparjoy. During this time, higher wind speeds of around 15 m/s were recorded within the MTDL, following the passage of Biparjoy. Wind direction observations indicate a weak westerly flow within the MTDL (Fig. 30b).
- Above the MTDL, the atmosphere features easterly flows with wind speeds ranging from about 15 m/s to ~25 m/s.

The presence of a dry layer in the Arabian Sea has been earlier noted by *Fletcher et al*. (2018) (see Fig. 31 for a schematic). During the final phase of the cruise, a gradual moistening of the dry layer is observed, which can be attributed to southeasterly intrusions at this level (Figs. 29 and 30).

Thermodynamic Structure of the Atmosphere (Stability)

The Brunt–Väisälä frequency is a measure of the stability of a fluid to vertical displacements. The convective or static stability of the atmosphere is characterized by the square of the buoyancy frequency N^2. The observed vertical profile of the buoyancy frequency squared (N^2) reveals significant variations in atmospheric stability across different pressure levels (Fig. 32a).

At both 800 hPa (the base of the MTDL) and 600 hPa, (the base of dry-low moist intermediate layer), N^2 values are comparatively high, approximately 2–3.5 x 10^{-4} s^{-2}, indicating strong static stability relative to other levels.

These elevated N^2 values suggest that air parcels displaced vertically within these layers experience a considerable restoring force, inhibiting vertical motion and suppressing convective activity. The presence of these stable inversions is further confirmed by the average virtual potential temperature profile (Fig. 32b). Typically, the equivalent potential temperature exhibits a minimum value at the interface between moist and dry air masses. This minimum indicates the separation level, where the presence of relatively dry layers is clearly discernible from the equivalent potential temperature profile at above mentioned levels (Fig. 33).

Between ~800 hPa and 600 hPa, there is a drastic reduction in N^2 to around 0.1 x 10^{-4} s^{-2}. This sharp decline in N^2 denotes a transition to much less stable atmospheric conditions.

This pronounced change in atmospheric stability may have important implications for the vertical mixing and overall dynamical behavior of the atmosphere in this region. Moreover, the negative gradients observed in the average equivalent potential temperature profiles within this region suggests potential instability (convective instability) with respect to saturated vertical displacements (Fig. 34).

A comparatively high vertical wind shear ($S^2=\sqrt{(\frac{du}{dz})^2 + (\frac{dv}{dz})^2}$) can be observed around 600 hPa, the bottom boundary of the MTDL (Fig. 35a) due to somewhat counterflowing winds (Fig. 30b), with lens shaped easterly intrusions.

Large vertical changes in horizontal wind combined with low static stability can lead to shear or dynamic instability. The Richardson number (Ri) is used to characterize dynamic stability and is calculated as N^2/S^2. Immediately beneath the MTDL, the presence of low Ri suggests the existence of prevailing shear instabilities (Fig. 35b). This observation indicates that the low moist-dry layer may have been formed as a result of mixing induced by these dynamic instabilities. This enhanced mixing at the edges of an intrusion has been demonstrated in the laboratory experiment of *Ching et al*. (1992), where mixing of the intrusion and outer fluid occurred across the interface by shear instabilities.

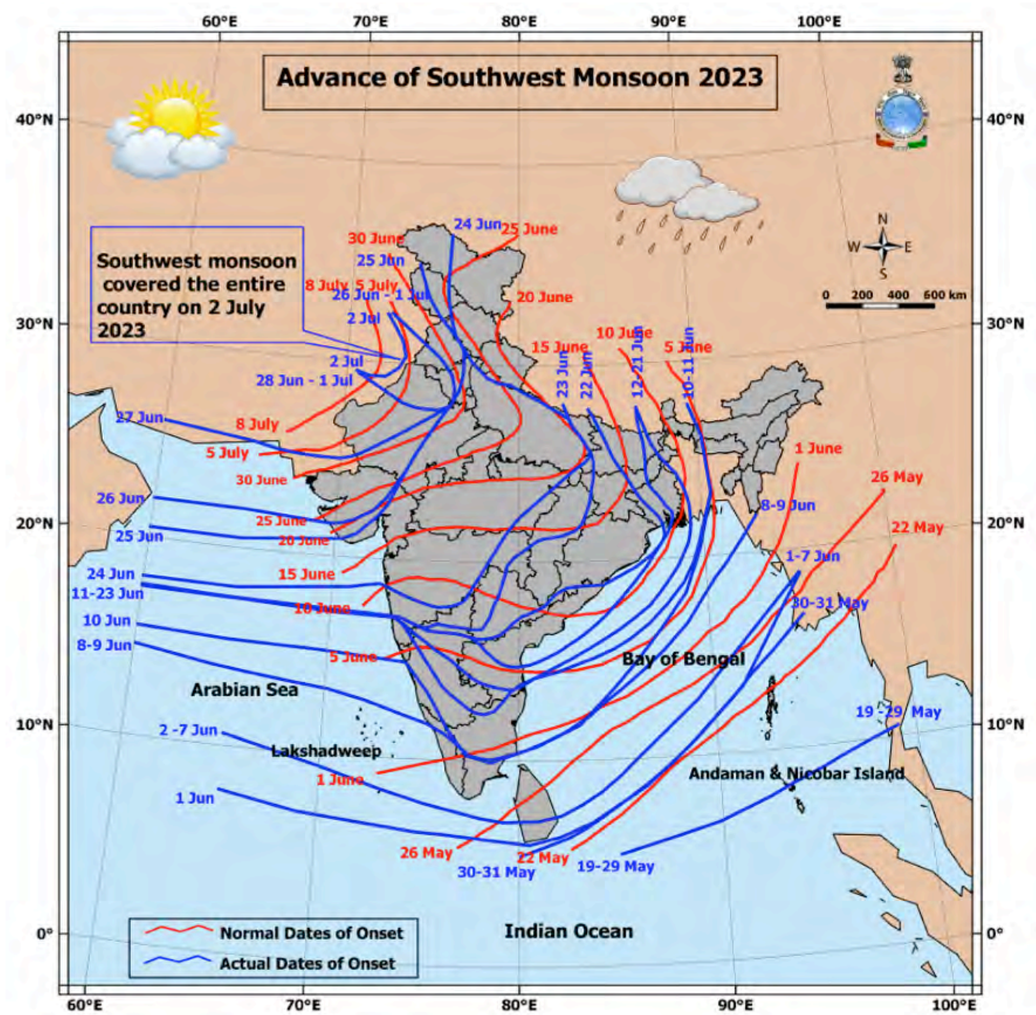

Figure 27. *Monsoon onset*

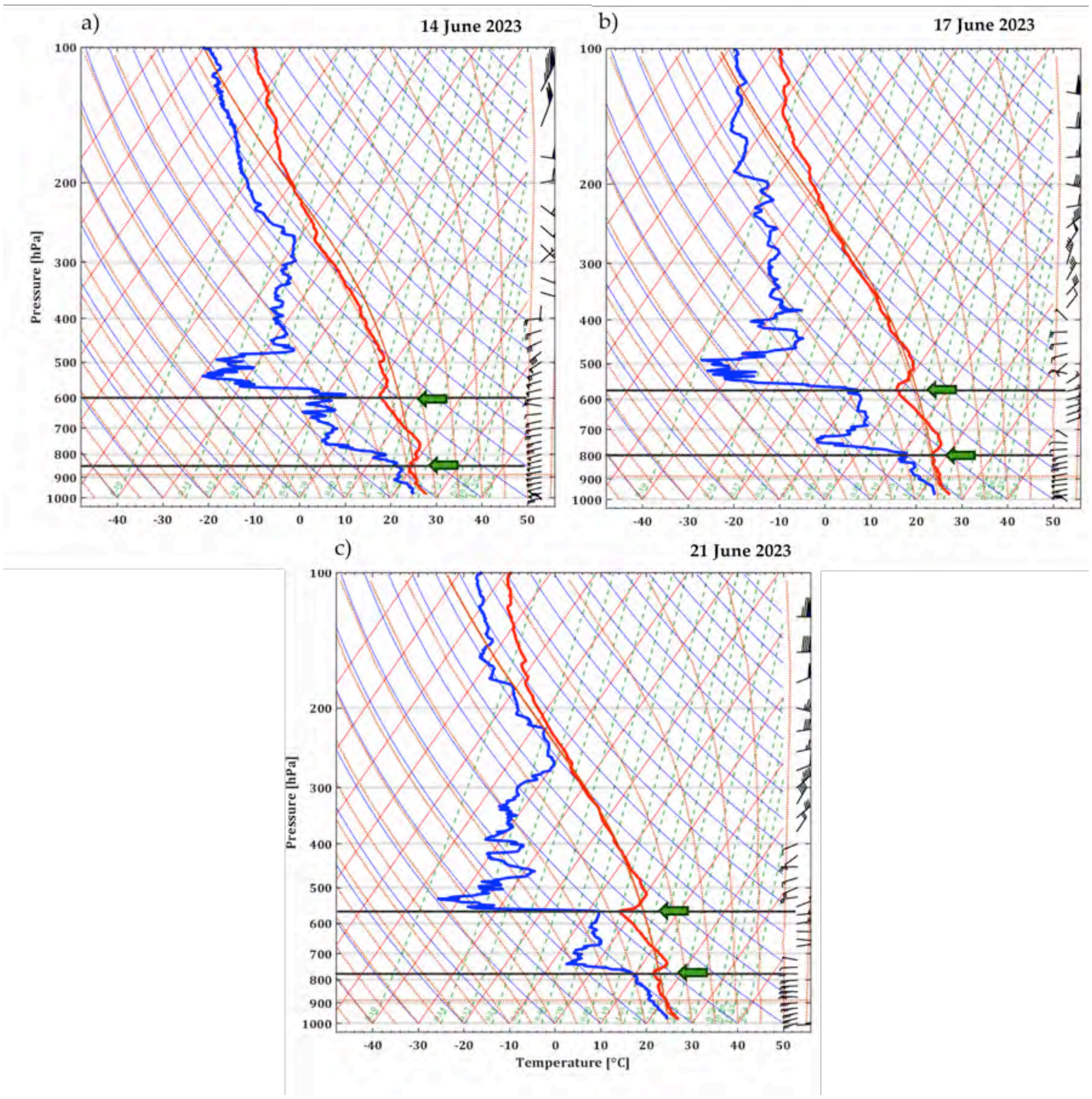

Figure 28. *Skew T-log P diagrams for EKAMSAT soundings on a) June 14, b) June 17, and c) June 21, 2023. The thick red and orange lines represent air temperature and the surface air moist adiabat, respectively. The thick blue line shows the dew point temperature. Solid dark gray lines with green arrows highlight the temperature inversion levels.*

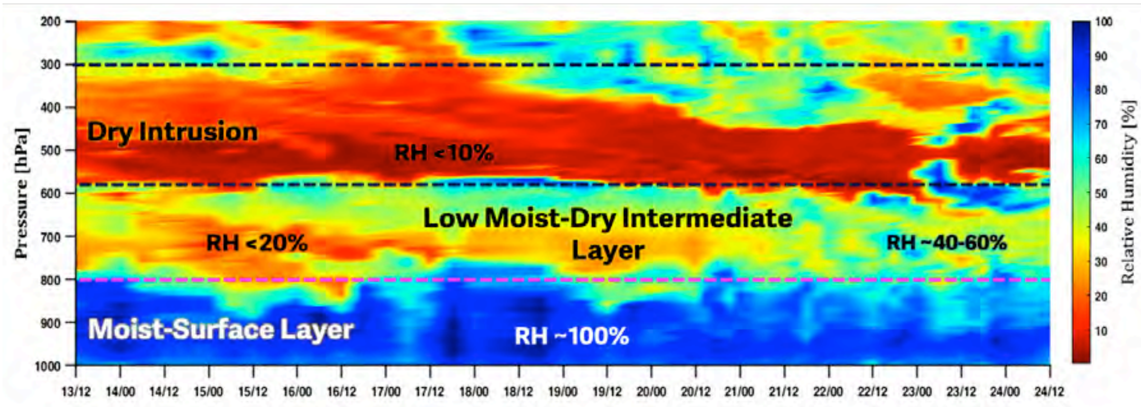

Figure 29. *The temporal evolution of relative humidity across various ship locations from rawinsonde data from the EKAMSAT pilot cruise.*

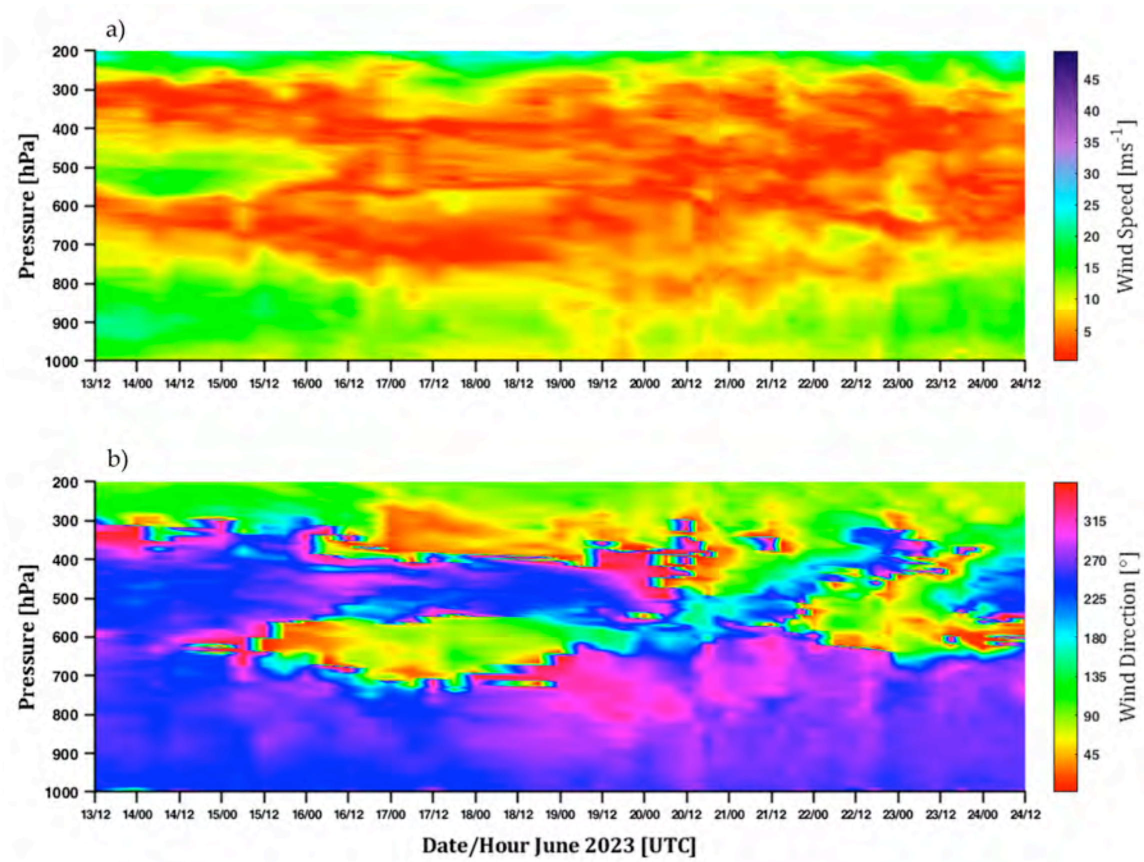

Figure 30. *The temporal evolution of a) wind speed and b) wind direction across different ship locations.*

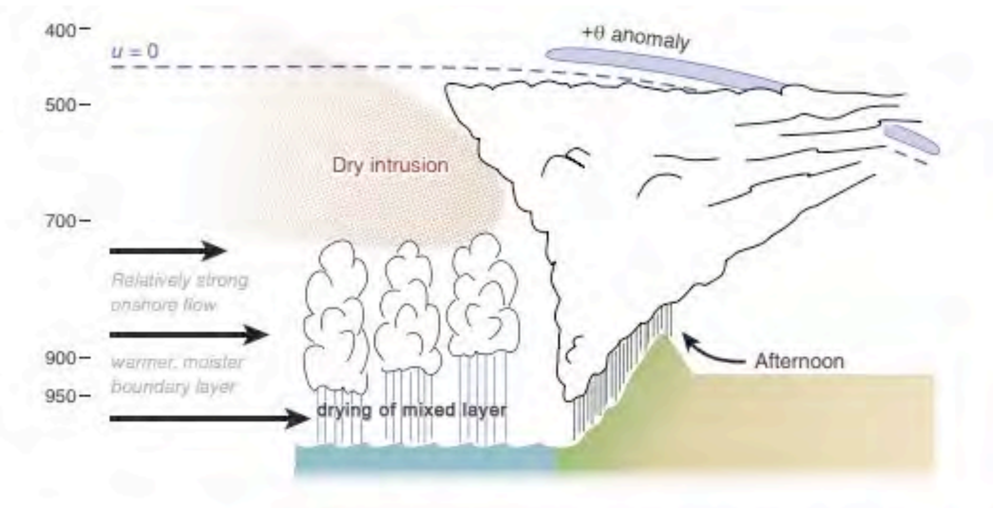

Figure 31. *Schematic of the dry layer (Fletcher et al., 2018)*

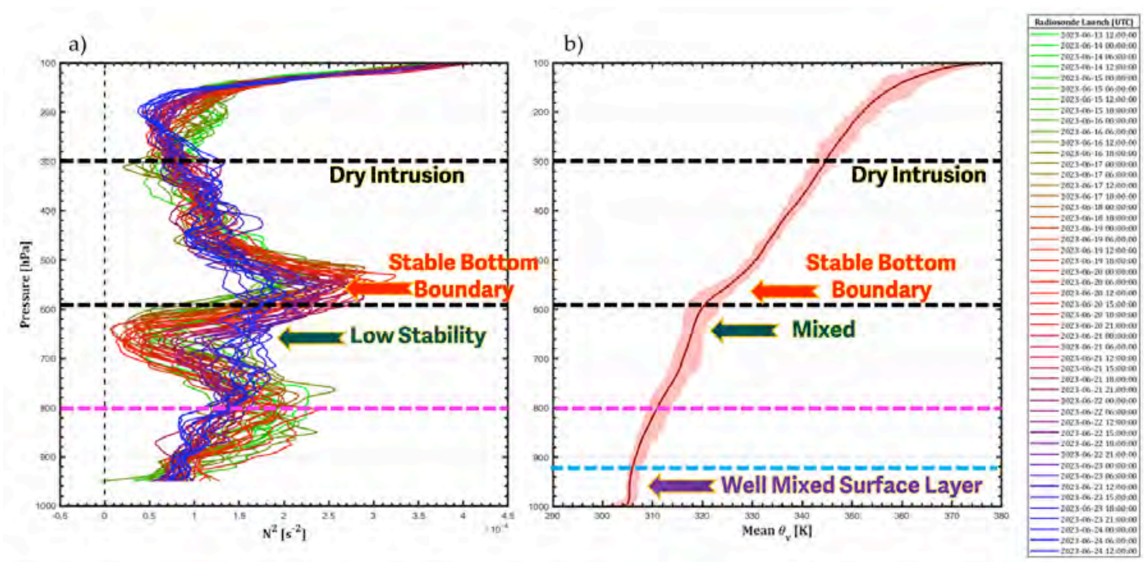

Figure 32. *The bouyancy frequency squared profile and b) the mean virtual potential temperature profile from the EKAMSAT pilot cruise soundings.*

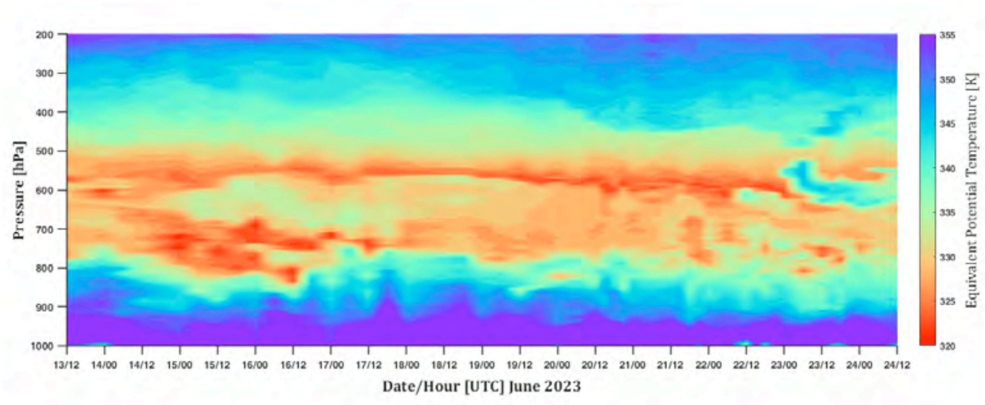

Figure 33. *Temporal variation of equivalent potential temperature across different ship locations.*

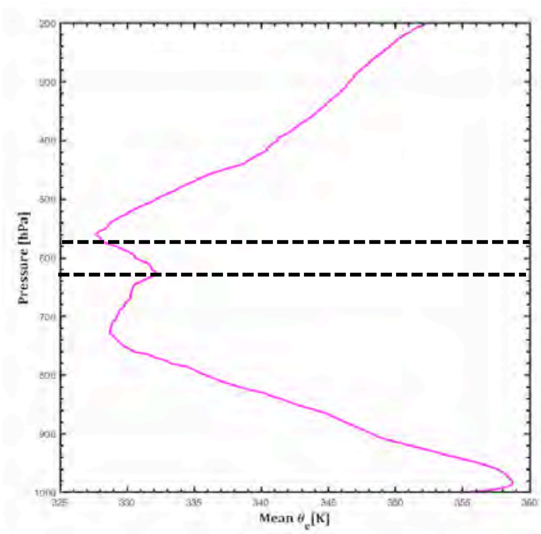

Figure 34. *Average equivalent potential temperature profile from the EKAMSAT soundings.*

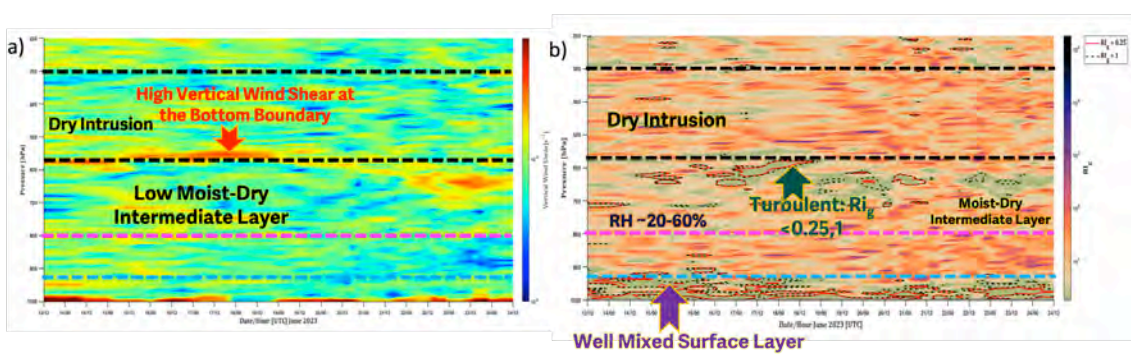

Figure 35. *a) Vertical wind shear profile and b) gradient Richardson number profile from the EKAMSAT radiosondes.*

Cloud Base Heights Measurement Using Ceilometer Data

Figure 36a represents an attenuated backscatter profile obtained from the CL-31 Ceilometer. From June 11 to 13, 2023, the ship was located near the outer bands of Cyclone Biparjoy (Fig. 36c). During this period, sea surface temperatures (SSTs) recorded were the highest of the entire cruise period, exceeding 29.5°C (Fig. 36b, d). Additionally, the attenuated backscatter profiles revealed significant diurnal variations in the boundary layer structure, with heights ranging from approximately 600 m and reaching over 1.5 km at around 12:00 UTC (17:30 Local Time).

On June 16, 2023, Cyclone Biparjoy made landfall, later inducing oceanic upwelling that resulted in the formation of a cold filament along its track (Fig. 37d). R/V Roger *Revelle* entered this cold filament on June 17. From June 17 to 19, observed SSTs were the lowest values recorded during the cruise. During this time, the atmospheric boundary layer remained at approximately 600 m, with minimal convective growth (Fig. 37a), as observed in high SST conditions (Fig. 36a). Hence it is evident that local SST variations might have played a role in modulating the boundary layer heights. Following June 19, 2023, the SSTs began to recover as the cold filament dissipated (Fig. 37b). However, SSTs did not reach the ~30°C levels observed during the initial phase of the cruise, as the Arabian Sea mini warm pool had already started to dissipate with the onset of the southwest monsoon. During the cruise, SSTs exceeded 28°C, a threshold for potential deep convective systems, but the CL-31 attenuated backscatter data did not reveal any such systems apart from the diurnal variation of the convective boundary layer, which reached up to ~1.5 km. This lack of deep convection may be due to the high stability conditions observed at the base of the low moisture to dry layer (Figs. 32 and 35), which acted as a barrier to convective development.

From 19 June onwards, another moist system started approaching the ship location from the east (Figs. 29 and 30). This is clear from the integrated water vapor transport (IVT) calculations, which were made using the radiosonde data (Fig. 38).

$$IVT = \sqrt{\left(\frac{1}{g}\int_{P_{surface}}^{P} q.u.dp\right)^2 + \left(\frac{1}{g}\int_{P_{surface}}^{P} q.v.dp\right)^2},$$

where g is the gravitational acceleration, $P_{surface}$ the surface pressure, q the specific humidity and u and v are the zonal and the meridional components of the wind, respectively. On 13 June a peak in IVT is evident, which gradually diminishes by 17 June (Fig. 38a). The decrease in IVT can be attributed to both the reduction in wind speeds (Fig. 38b) and the lower evaporation rates (Fig. 41b) and atmospheric moisture content associated with comparatively lower sea surface temperatures (SSTs).

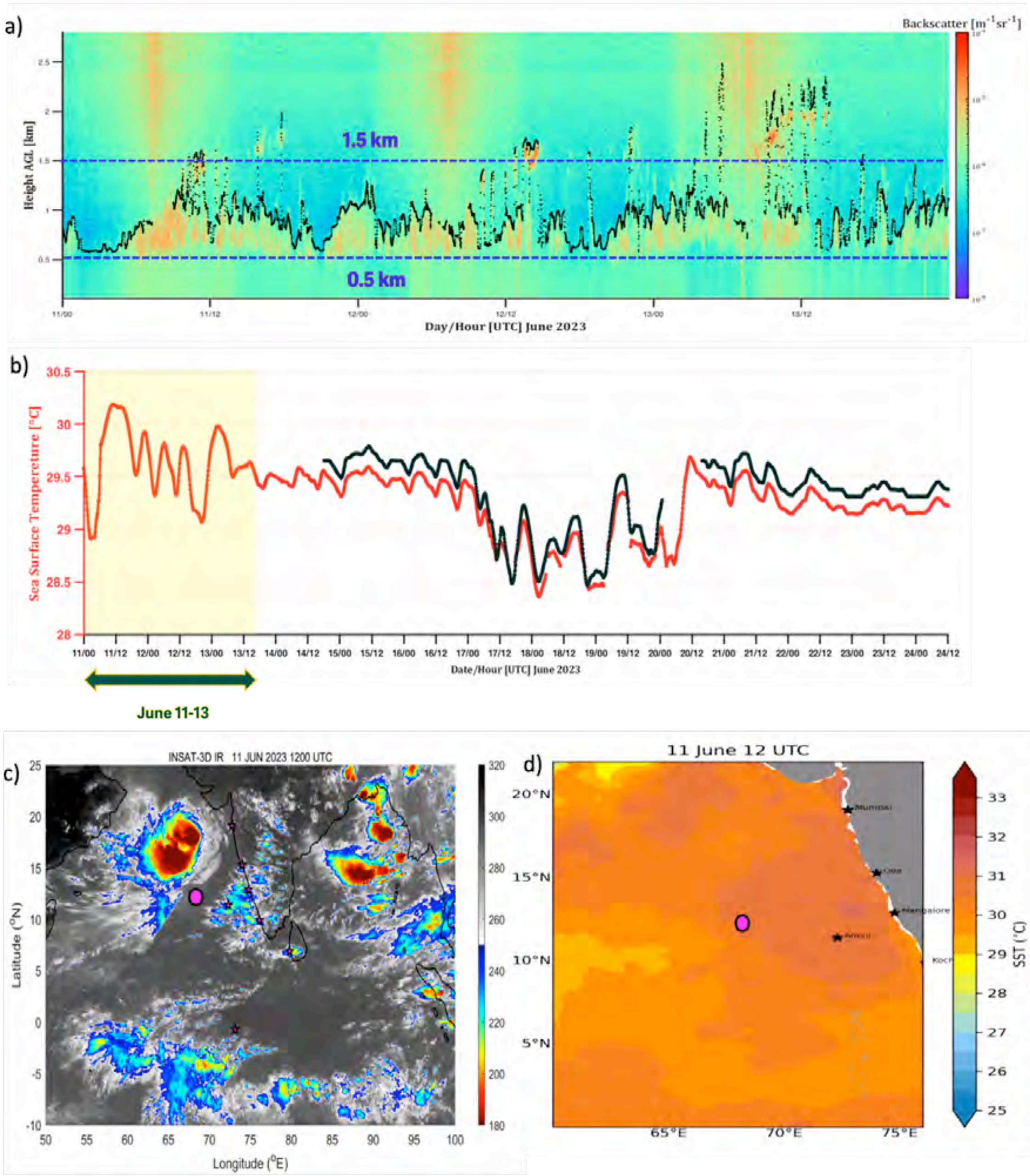

Figure 36. *a) Attenuated backscatter profiles with boundary layer heights from CL-31 11–13 June 2023. b) Temporal variation of skin SST (Red) and Sea Snake SST (Black). c) INSAT IR: 11 June 2023 and d) OISST: 11 June 2023 with respect to R/V* Roger Revelle *represented by pink marker.*

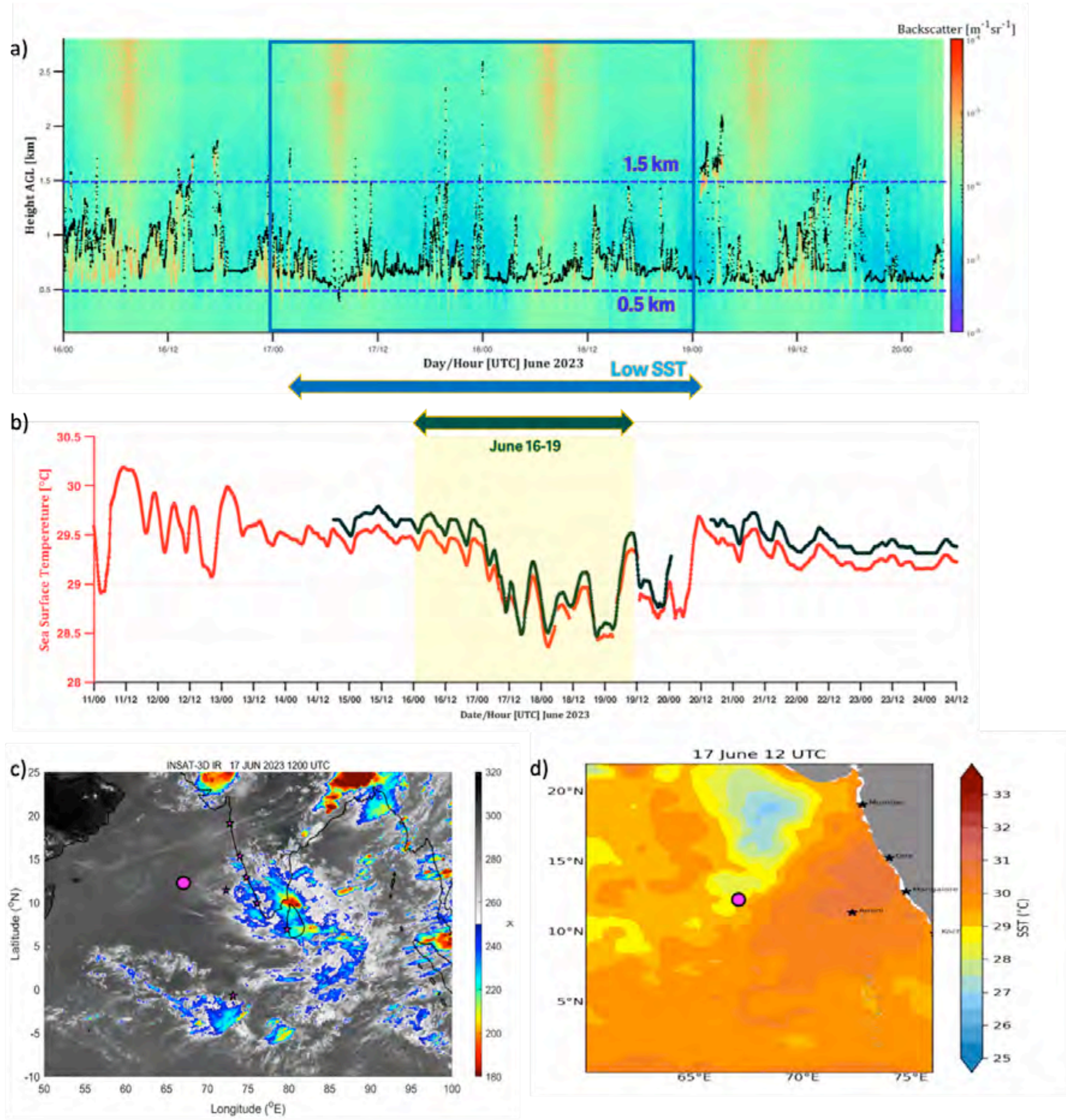

Figure. 37. *a) Attenuated backscatter profiles with boundary layer heights from CL-31 16–20 June 2023. b) Temporal variation of skin SST (Red) and SST Sea Snake (Black). c) INSAT IR: 17 June 2023 and d) OISST: 17 June 2023 with respect to R/V* Revelle *represented by the pink marker.*

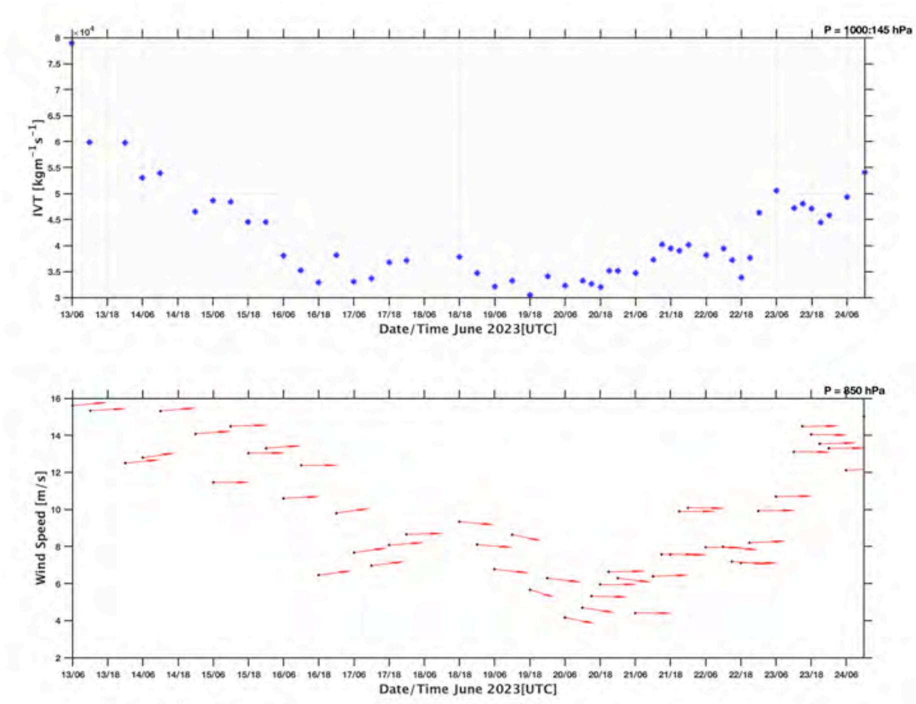

Figure 38. *a) IVT and b) wind speed and direction at 850 hPa from EKAMSAT radiosondes.*

Bow Mast Measurements

Figure 39a shows the 10-m adjusted air temperature measurements from the Visalia HMT337 temperature–humidity sensor, while Fig. 39b displays the T_{skin}–T_{air} (2-m adjusted) difference. It is evident that from 17 to 19 June, the air temperature was higher than the sea surface temperature, which can be attributed to the previously mentioned ocean upwelling.

Comparatively high net heat flux into the ocean in this cold filament from 17 to 19 June, where the air temperature is higher than the SST, implies a significant transfer of heat from the warm air to the colder ocean surface (Fig. 40). During the day, the combination of sensible heat flux and solar radiation might have contributed to the warming of the cold filament. At night, the net heat flux out of the ocean is comparatively low during this period. This reduced nighttime cooling might have allowed the cold filament to retain more heat, contributing to the SST recovery. As a result, the cold filament might have gradually warmed up, eventually leading to its dissipation. This is further supported by the outgoing longwave radiation and evaporation plots Fig. 41.

Future studies will involve a more detailed analysis including these flux measurements.

Meteorological Analysis from PWD 22

A dry phase lasted throughout the EKAMSAT 2023 pilot cruise period. The weather code based on 15-min averages for the entire period of the cruise is shown in Fig. 42. A fog condition was recorded by PWD on 15 June around 3:00 UTC (08:30 IST), which was not recorded in the weather briefings, and hence can be considered as an anomaly. According to the PWD22, rain conditions were encountered very few times, on 13 and 14 June. These were light rains that did not last for a long time. Rains were observed visually on 13 July at ~ 11:45 am (Local time) (06:15 UTC) and 18 June 1:05 am (Local time) (17 June 19:30 UTC).

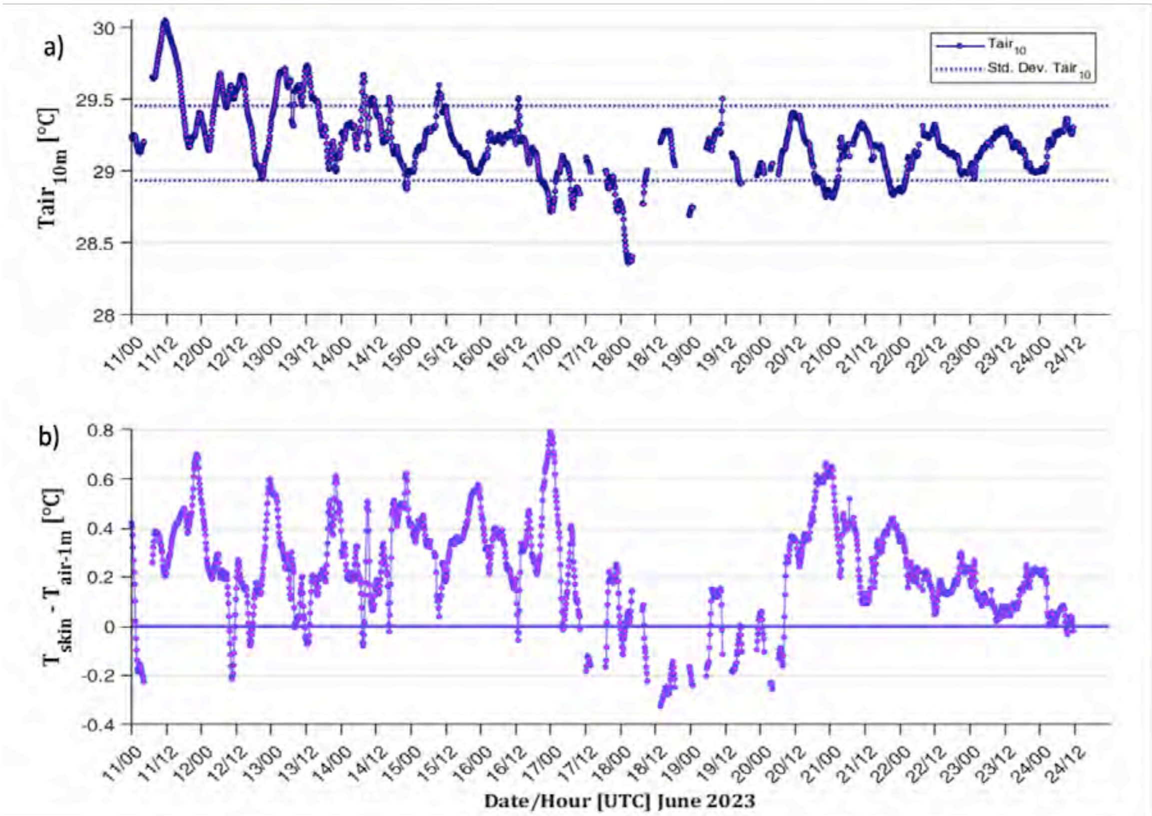

Figure 39. *a) Air temperature (10-m adjusted) b) T_{skin}–T_{air} (2-m adjusted)*

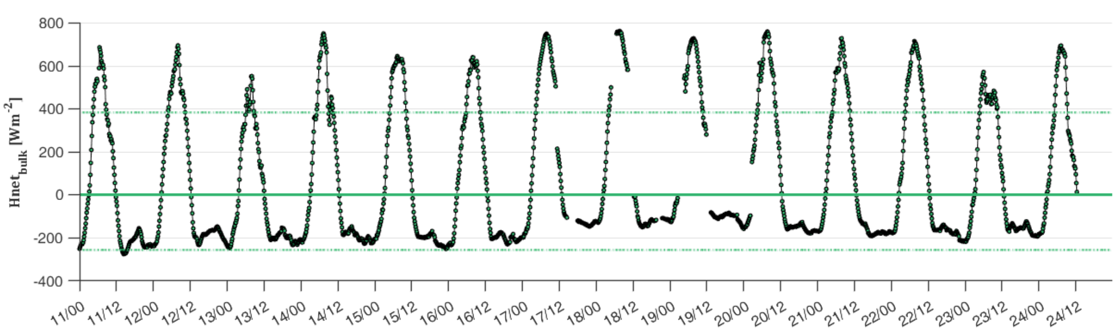

Figure 40. *Bulk downward net heat flux (H_{net} > 0 heating the ocean)*

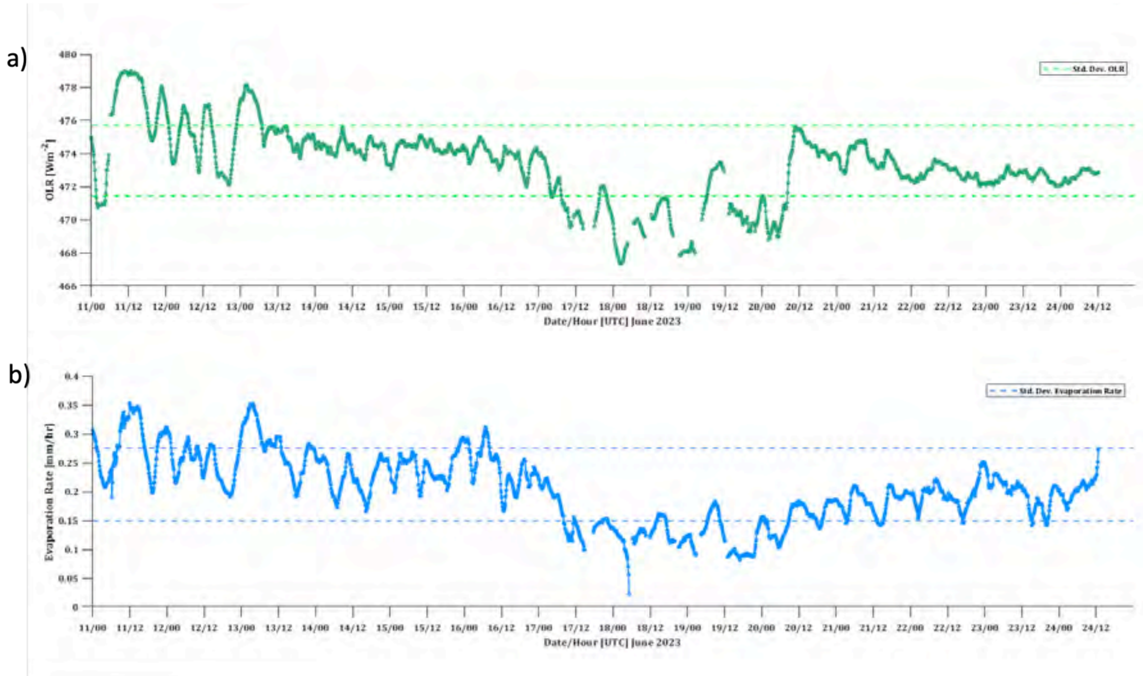

Figure 41. *Upwelling longwave radiation (positive out from the ocean) and b) evaporation rate*

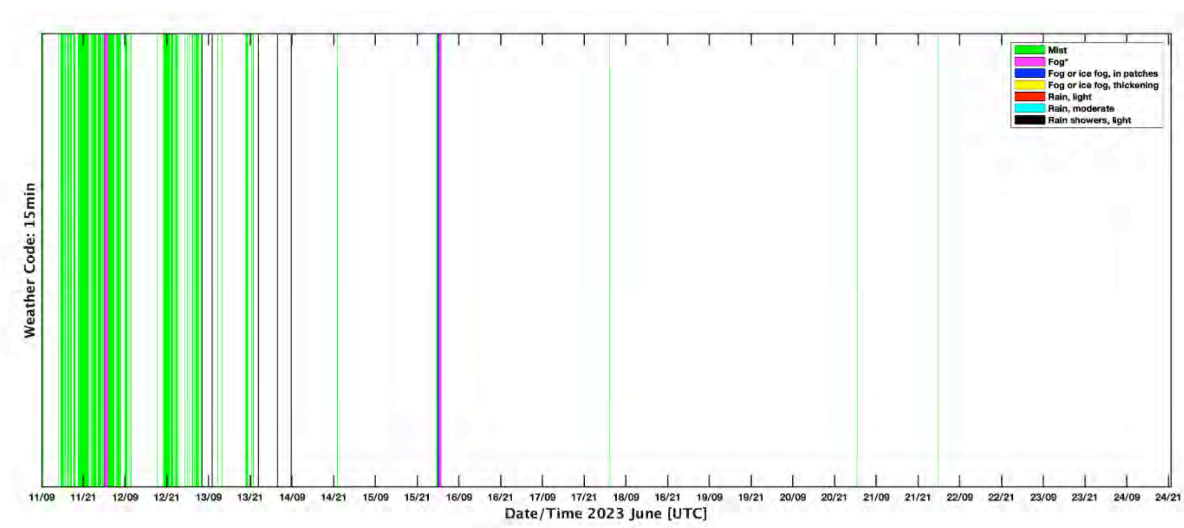

Figure 42. *15-minute averaged PWD weather code*

4. CONCLUSIONS

Atmospheric observations indicated:

- Two temperature inversions existed within the atmospheric profile. The first was observed at ~800 hPa and the second inversion was encountered at ~600 hPa. The bottom boundary of these inversions was highly stable, which was evident from the buoyancy frequency profiles.
- The presence of a dry layer in the atmosphere around ~500 – 600 hPa that might have formed due to intrusion of northwesterly winds to a dense layer and then spreading horizontally and slowly as a gravity current.
- Atmospheric profiles indicated several thermodynamic regions.
    - Below ~900 hPa: Well mixed surface layer
    - Below ~800 hPa: Moist layer
    - ~800 hPa – 600 hPA: Low moist-dry intermediate layer
    - ~600 hPa~300 hPa: Mid-tropospheric dry layer

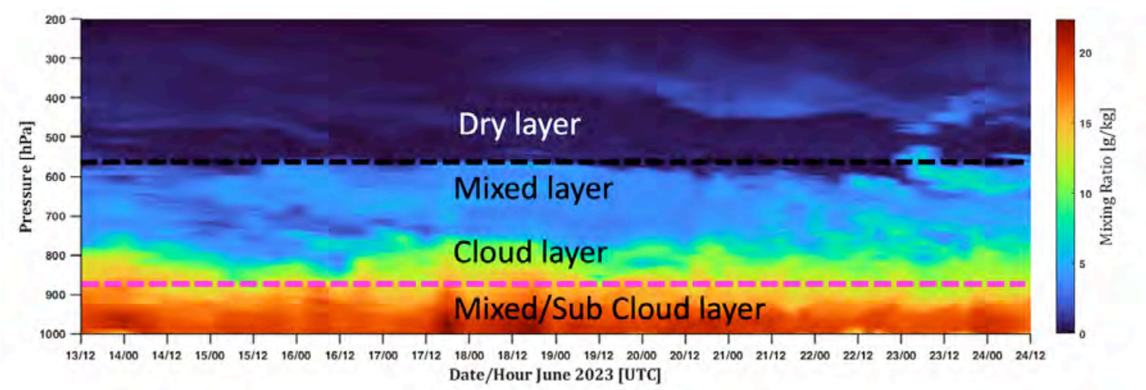

Figure 43. *Thermodynamic regions observed in the atmosphere 13–24 June 2023.*

- High shear and low Ri below this MTDL imply shear induced mixing of moisture from the bottom layer towards the dry layer resulting in the varied RH in the low-moist to dry layer. Moist easterlies penetrate the upper most dry layer from 18 June onwards.
- Ceilometer data indicate varying cloud heights (600 m – 1.5 km) that could be correlated with the local SST. In addition to this direct atmospheric effect, the SST within the warm pool was affected by the cyclone wherein colder water is pumped upward and produced islands of low SST in the wake of Biparjoy. The minimum temperature in the campaign area (~11.6°N – 12.5°N and ~66.5°E -67.2°E) was recorded

around 17 June and the cold pool disappeared around 20 June, indicating a decaying period of cold islands as ~3 days.

- SSTs exceeded 28°C throughout the entire cruise, which is considered as a necessary but not the only condition for the development of deep convective systems. Convection never penetrated the low-moist to dry intermediate layer.
- The (weak) stability at the low moist-dry intermediate layer might have prevented the development of deep convection.
- The bow mast data support the interpretations of atmospheric and oceanic conditions during the period of cold filament development. A more detailed study of these measurements will be carried out in the future.

Biogeochemical Sampling, Clouds and Aerosols

Overview

The Indian participants were active in data collection and got acquainted with state-of-the-art equipment such as the UCTD, radiosonde, VMP, drifters, sun photometer, CTD etc. The INCOIS team collected water samples at selected locations along the track and at the area of an observed chlorophyll bloom after the passage of Cyclone Biparjoy. The measurement of atmospheric black carbon was carried out with the real time seven wavelength Aethalometer AE-33 from IITM Pune. IITM Pune also collected atmospheric aerosol samples on filter paper for further electron microscopic and chemical analysis of atmospheric particles. The visual observations of cloud characteristics were carried out by the NIOT participant. The meteorological measurements, specifically the vertical structure of the atmosphere, is proposed to be utilized for calibrating and validating the NCMRWF weather prediction models.

Radiation and Clouds (NIOT)

One of the objectives under the EKAMSAT collaboration is to estimate the basin specific coefficients of radiation parameters in the Arabian Sea. At present the coefficients that are utilized in radiation parameters are either developed for other basins or developed using limited and/or remote measurements. Errors in these coefficients significantly affect the accuracy of the numerical models and hence necessitates basin specific coefficients for the Arabian Sea, which can reduce the systematic errors in numerical models.

The cruise aboard R/V *Roger Revelle* was focused to collect meteorological parameters, particularly radiation and cloud measurements. The aerosol optical depth measurements for fine tuning the estimation of shortwave radiation and the derived values of integrated water vapor measurement for estimating the effective emissivity will also be utilized.

Regular visual measurements of appearance of sky and cloud characteristics at an interval of one hour during 06:30 – 18:30 IST (1:00 – 13:00 UTC) was carried out during the cruise period 10–25 June 2023. A few snap shots of the cloud images along with the remarks indicating the general appearance (clear sky, cloudy, etc.), cloud amount in octas, the type of cloud, distribution of cloud, etc. were recorded (Fig. 44). It is proposed to utilize these measurements along with the measurements of meteorological parameters carried out onboard the ship to develop an equation for estimating emissivity under clear sky conditions (Fig. 45). The air temperature, relative humidity, air pressure, latitude, and downwelling longwave radiation will be utilized for this study.

The preliminary analysis of the measured data indicates predominantly clear sky conditions during 17 and 18 June and intermittent clear skies during 19 and 20 June (Fig. 45). The number of data points under clear sky conditions are limited (14 values; Fig. 46) and requires more observations to carry out a statistically significant line fitting and thereby to estimate the effective emissivity coefficients. The present observations will be utilized along with moored buoy measurements and other ships of opportunity for the proposed work.

Atmospheric Aerosols

The carbonaceous aerosols are the significant constituents of atmospheric aerosols and carry substantial uncertainties in climate models, mainly due to poorly constrained emissions, optical properties, atmospheric transformation, and aerosol-cloud interactions. Black carbon (BC) is the dominant light-absorbing constituent of carbonaceous aerosols. Fresh BC is hydrophobic; it ages and mixes with other hydrophilic components within the atmosphere. The aged BC can act as a cloud condensation nuclei (CCN), which has significant implications in cloud albedo, lifetime, and precipitation.

South Asia is home to one-fourth of the world's population, and a large share of the economy depends on the summer monsoon (June to September). As winter ends, warm and moist air from the southwest Indian Ocean blows toward South Asia and carries significant rain. The Arabian Sea, the northern part of the Indian Ocean, is significantly influenced by the particulate pollutions from the neighboring hot-spot regions (Fig. 47). During the summer monsoon months, African savanna burning can contribute up to 50% of total BC over the Arabian Sea. A previous study also showed that the increase in BC fate can lead to a gradient in the sea surface temperature, which further helps in intensifying Arabian Sea tropical cyclones. Hence, a study on BC and other aerosol constituents during the summer monsoon period over the Arabian Sea is of prime importance for better understanding and reducing uncertainties over South Asia.

Figure 44. *Sun behind the thick cumulus cloud on 15 June and clear sky observed on 19 June.*

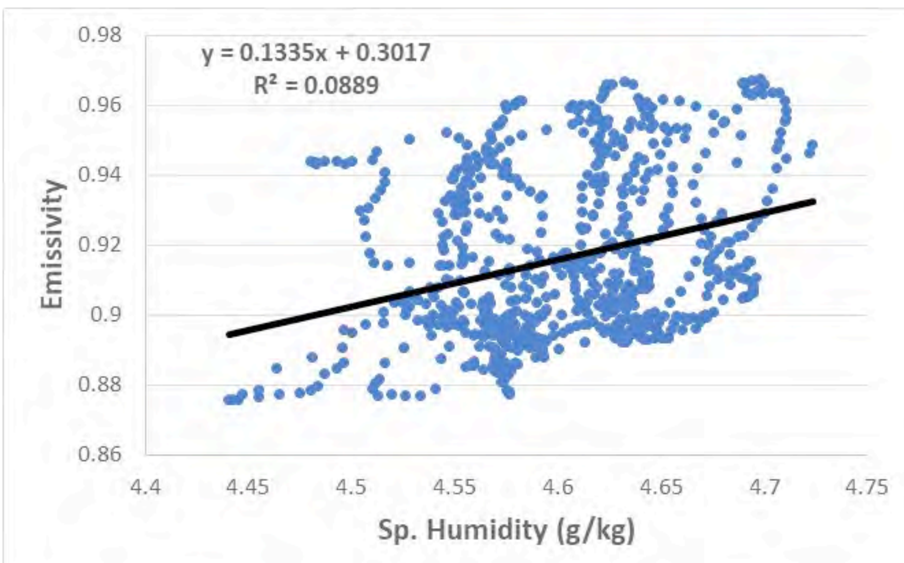

Figure 45. *Scatter plot of specific humidity vs. emissivity during 15–22 June.*

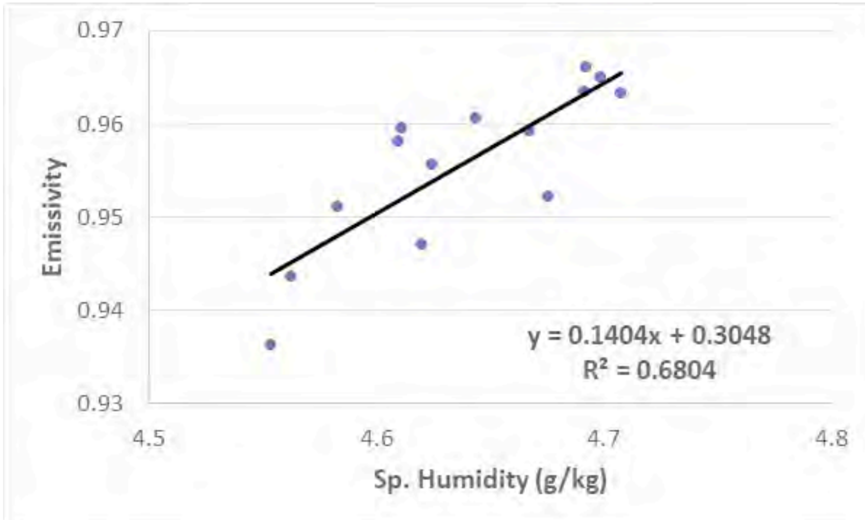

Figure 46. *Scatter plot of specific humidity vs. emissivity during clear sky conditions observed during 15–22 June.*

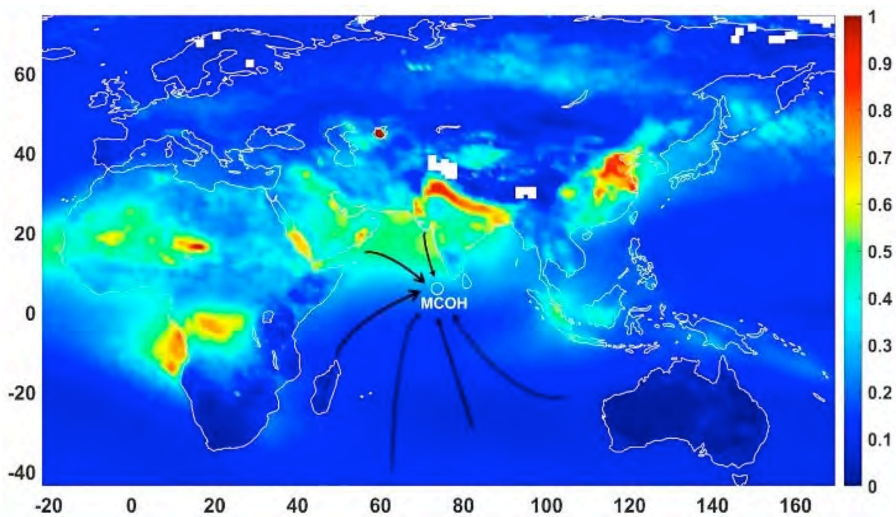

Figure 47. *Aerosol optical depth May to October 2013 to 2017 (graphic from Budhavant et al., 2023)*

The key deliverables include: (1) generating datasets of key pollutant-BC aerosol over the strategic location of the Arabian Sea; (2) studying the microphysical and chemical properties of atmospheric aerosols; and (3) radiative forcing of atmospheric aerosols and their role in sea surface temperature.

To fill the knowledge gap, IITM Pune measured atmospheric BC aerosols over the Arabian Sea during the EKAMSAT pilot cruise (8–26 June 2023). These are the first of their kind measurements during the summer monsoon period over the important geographical region. For the generation of quality data, several precautionary measures were implied. For instance, the setup of inlets was far from the local emission sources, a nafion dryer was used to limit the relative humidity in the air stream, the length of inlet tubing was minimized to avoid loss of particles in the wall of the inlet tube, etc. The atmospheric aerosol samples were also collected on filter paper to study particle shape and size using the electron microscope and chemical compositions to understand its microphysical and chemical properties better. At the same time, particles deposited on the sea surface water were also collected through filtration to study wet scavenging of atmospheric BC and its role in warming sea surface temperatures.

Phytoplankton and Pigments

The LDEO group funded by NASA undertook high-resolution measurements of chlorophyll *a* (Chl *a*), phytoplankton functional types, phytoplankton size classes, and phytoplankton photosynthetic quantum efficiencies in near surface (~5 m) seawater samples pumped continuously through R/V *Roger Revelle's* uncontaminated seawater flow-through system. These measurements compliment continuous flow-through measurements of seawater temperature, salinity, conductivity, and pCO_2 conducted routinely onboard R/V *Roger Revelle*. Along with the above, samples were also collected from three to four discrete depths in the water column using a CTD rosette wherein the above measurements, together with filtration and non-filtration based collections for ocean biological and biogeochemical constituents, were performed (see details below). All filtered samples will be analyzed upon return to LDEO. Additionally, at select stations, deck-based 24-hr incubations were undertaken to estimate rates of net primary productivity.

Station – Discrete Samples

Water samples were collected from a total of 25 stations (Fig. 48), mostly around the highly oligotrophic waters of the warm pool with a few in the path of Cyclone Biparjoy, whose passage coincided with the EKAMSAT pilot cruise. At each station seawater samples were collected at three or four depths in the water column for the following biological and bio-optical constituents:

1. Counting, imaging, and size estimations of phytoplankton and other detrital particles using a Fluid Imaging Technologies, Inc., FlowCAM
2. Microscopic counts of phytoplankton functional types, fluorometric estimations of Chl *a* and cyanobacterial phycobilipigments, HPLC

determinations of phytoplankton pigments, spectrophotometric and spectrofluorometric measurements of colored dissolved organic matter (CDOM), flow-cytometric determinations of cyanobacteria, and spectrophotometric determinations of phytoplankton spectral absorption coefficients

3. Fluorescence based estimates of Chl-*a*, CDOM, phycobilipigments and variable fluorescence (F_v/F_m), a measure of phytoplankton photosynthetic efficiency, using a WET Labs advanced laser fluorometer (ALF)
4. Measurements of F_v/F_m and the functional absorption cross-section of photosystem II (σ_{PSII}) and electron transport rates (*ETR*) in a fluorescence induction and relaxation (FIRe) fast repetition rate fluorometer (FRRF)

Details of the measurements made at the CTD stations are shown in Table 15.

Underway Flow-Through Measurements

Between stations, the ALF, the FlowCAM, and a FIRe were connected in parallel to the ship's seawater flow-through system, allowing for continuous in-water measurements of phytoplankton community composition, phytoplankton size, phycobilipigment types, and photosynthetic efficiency. With the exception of a few breaks during stations and for reconditioning, all four instruments were operated over the entire cruise track, providing several thousand fluorescence-based measurements of Chl-*a*, CDOM, cyanobacteria and cryptophytes, F_v/F_m and σ_{PSII}, p (a measure of electron transport between the PSII and PSI). Continuous flow-through measurements of phytoplankton species distribution and cell size distribution along the cruise track will provide useful information for interpreting the optical measurements for phytoplankton functional types (PFTs) over the study area.

Data obtained with the flow-through instrumentation will provide us with a synoptic picture of biological oceanographic conditions during the cruise. Preliminary plots using partial, non-quality controlled data of some variables measured along the cruise track are shown in Fig. 49. These datasets reveal that the warm pool, where the core physical oceanographic and atmospheric measurements were made, were extremely oligotrophic waters in which Chl *a* concentration seldom rose above 0.1 mg m^{-3}. Here small, round (< 6 µm diameter) cyanobacteria were the dominant phytoplankton functional types. A few diatoms with epiphytic cyanobacterial populations were observed at depth in the western side of the warm pool. Surprisingly, values of variable fluorescence (F_v/F_m) and other photosynthetic rate parameters in the warm pool were indicative of a population that was by and large photosynthetically active and not stressed.

West of our core study area, ship transects across the region impacted by Cyclone Biparjoy revealed substantial (~2^{o} C) cooling of the surface waters, and elevated phytoplankton biomass (Fig. 49a, c, d) and an actively photosynthesizing phytoplankton population (Fig. 2b) consistent with the notion that the passage of the cyclone helped entrain and recharge the warmer, highly stratified, nutrient poor, oligotrophic waters that typify the pre-monsoonal upper Arabian Sea euphotic column, with deeper, colder nutrient rich waters. The impact of this entrainment was also visible in the form of a dramatic shift in phytoplankton functional types from small round cyanobacteria to chlorophyll rich diatoms (Fig. 50).

The passage of Cyclone Biparjoy was unanticipated, but it served as an excellent analog for monsoonal wind driven impacts on biological processes and how ocean biological community productivity and biogeochemistry are strongly interconnected with and linked to coupled atmospheric–oceanic processes. The increase in Chl *a* in the wake of the cyclone and the contrast in biological and bio-optical properties between the region in the warm pool and to the west of it were clearly visible in ocean color images obtained roughly 6 days after the passage through this region (Fig. 51).

Time series ocean color derived maps of Chl *a* revealed a gradual northward progression of the region of elevated Chl *a* as the cyclone progressed northeastwards off the coast of India. Eight-day composite images for periods before and after the passage of Cyclone Biparjoy resulted in elevated Chl *a* over an area covering ~5000 km^2 in the eastern Arabian Sea (Fig. 52).

Radiometric measurements made at several stations (Table 15) within the warm pool and to the west of it within the elevated plume of Chl *a* provided immediate indication of the contrasting optical properties of these waters. Representative remote sensing reflectance (R_{rs}) spectra obtained from within these two locations (Station 2 – Warm Pool, Station 16 – elevated Chl *a* plume) using a Spectra Vision Corporation (SVC) radiometer are shown in Figs. 53a and b.

In addition to the radiometric measurements, we also made measurements of aerosol optical depth, aerosol optical thickness, aerosol optical properties, water vapor, etc. using a Microtops sunphotometer. The list of locations and times at which sunphotometer measurements were made are shown in Table 16.

Our goal is to use our above water radiometric (see Tables 11 and 12) and in-situ measurements to: 1) calibrate and validate satellite ocean color data products, 2) develop Arabian Sea specific algorithms for phytoplankton functional types for net primary productivity, and 3) study coupled atmospheric–oceanographic processes and mechanisms associated with the formation of the band of elevated Chl *a*.

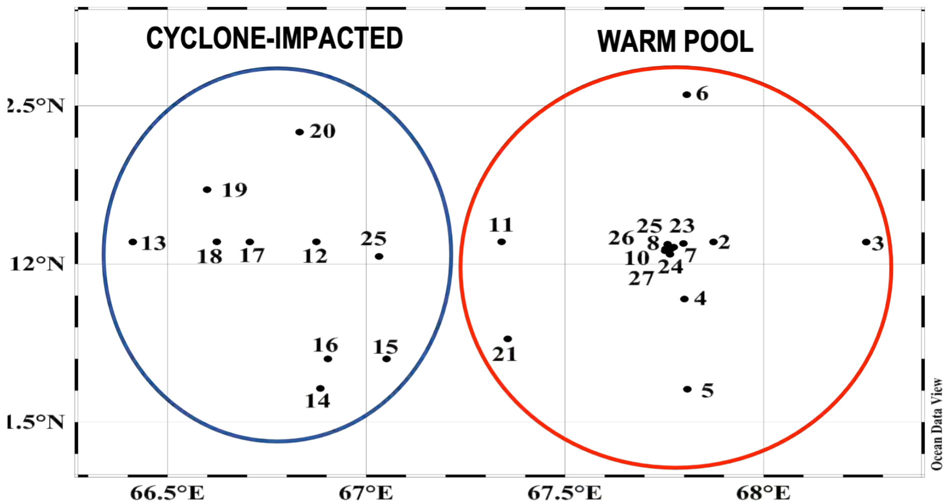

Figure 48. *Distribution of CTD stations and collection of discrete depth water samples in the warm pool and in the path of the cyclone to the west.*

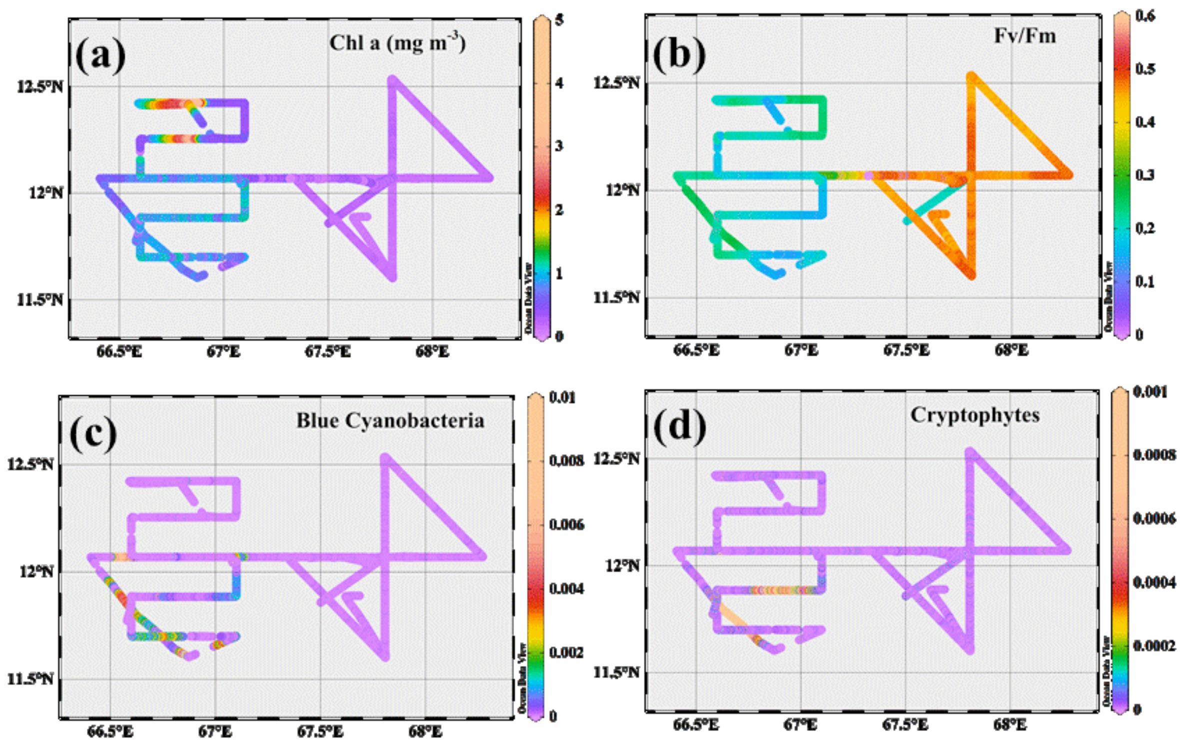

Figure 49. *Partial, non-QC'd seawater flow-through datasets showing the distribution of a) Chl a, b) F_v/F_m, c) blue water cyanobacteria, and d) cryptophytes.*

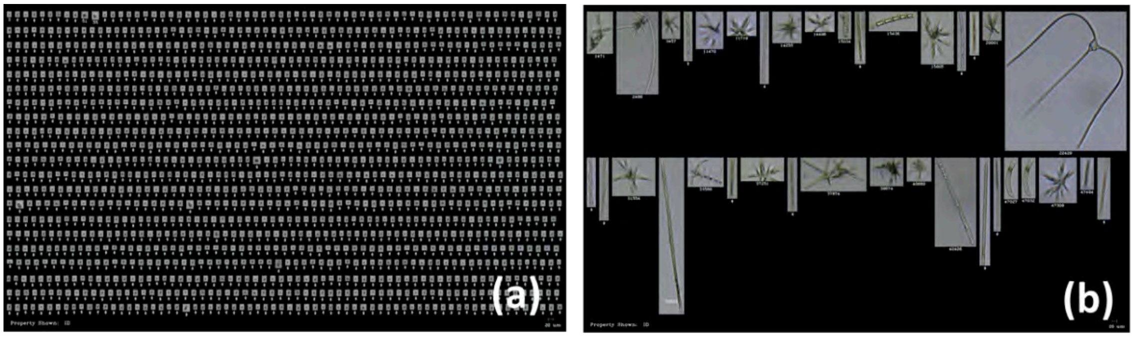

Figure 50. *FlowCAM-derived phytoplankton functional types showing dominance of a)* Synechococcus *sp. in the warm pool and b) diatoms in region of elevated Chl* a *to the west.*

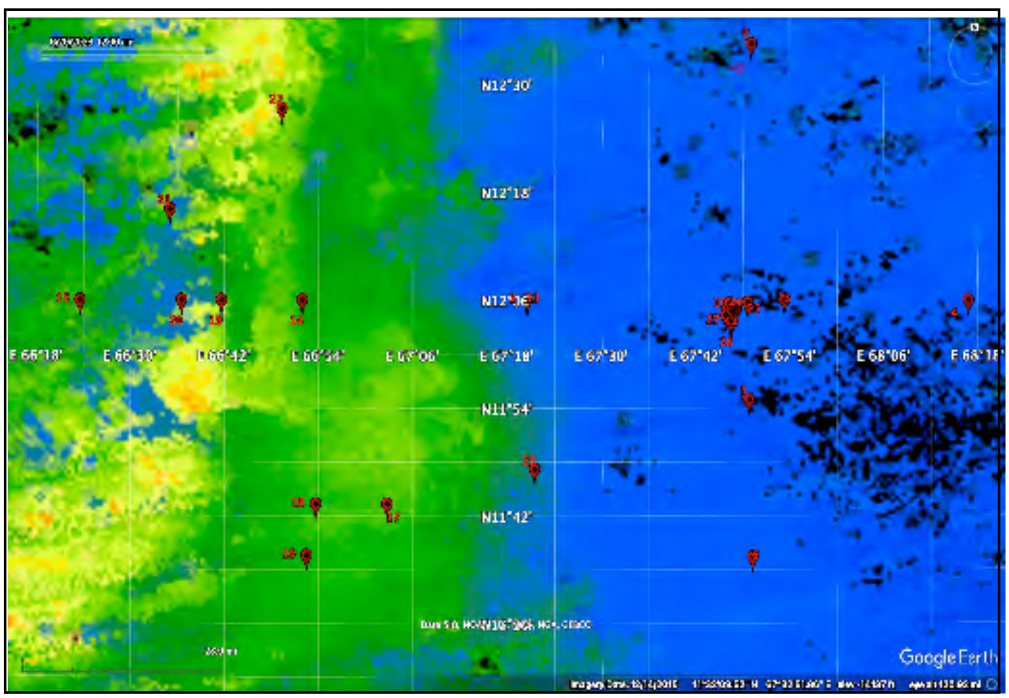

Figure 51. *NOAA-20 ocean color satellite map showing elevated Chl* a *concentration to the west of the warm pool.*

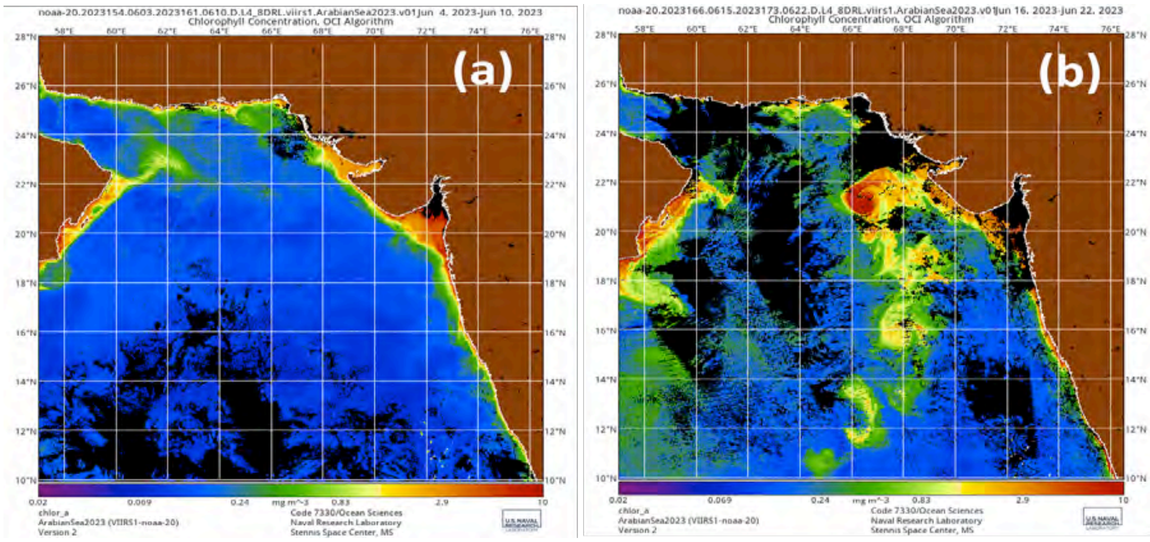

Figure 52. *NOAA-20 ocean color satellite derived 8-day composite images of the Arabian Sea before and after the passage of Cyclone Biparjoy.*

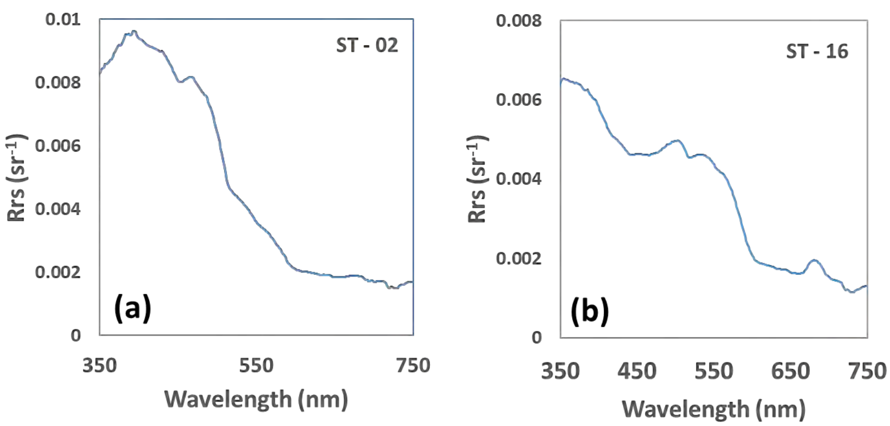

Figure 53. *Representative remote sensing reflectance spectra from the a) warm pool and b) elevated Chl a plume.*

Table 15. *Stations occupied for CTD profile and biological and radiometric measurements*

Date	Station ID	Latitude N	Longitude E	Depths (m) Sampled	Measurements	SVC	Microtops
6/11/2023	**2**	12.0703	67.3407	0,20,50,75	Chl a, HPLC, Phyco, Aph, CDOM, Cyanos	✓	✓
6/11/2023	**3**	12.0695	67.8738	0,50,75	Chl a, HPLC, Phyco, Aph, CDOM, Cyanos	✓	
6/11/2023	**4**	12.0692	68.2583	0,50,75	Chl a, HPLC, Phyco, Aph, CDOM, Cyanos		
6/12/2023	**5**	11.8892	67.8007	0,50,80,100	Chl a, HPLC, Phyco, Aph, CDOM, Cyanos	✓	✓
6/12/2023	**6**	11.6041	67.8079	0,50,75,100	Chl a, HPLC, Phyco, Aph, CDOM, Cyanos		
6/13/2023	**7**	12.5353	67.8067	0,40,65,80	Chl a, HPLC, Phyco, Aph, CDOM, Cyanos, NPP	✓	
6/14/2023	**9**	12.0477	67.7670	0,50,75,100	Chl a, HPLC, Phyco, Aph, CDOM, Cyanos,	✓	✓
6/15/2023	**10**	12.0475	67.7530	0,50,85,100	Chl a, HPLC, Phyco, Aph, CDOM, Cyanos, NPP	✓	✓
6/16/2023	**11**	12.0530	67.7738	0,50,75,100	Chl a, HPLC, Phyco, Aph, CDOM, Cyanos, NPP	✓	✓
6/16/2023	**12**	12.0420	67.7518	0,50,75,100	Chl a, HPLC, Phyco, Aph, CDOM, Cyanos	✓	✓
6/17/2023	**13**	12.0702	67.3403	0,50,75,100	Chl a, HPLC, Phyco, Aph, CDOM, Cyanos	✓	✓
6/17/2023	**14**	12.0701	66.8746	0,38,50,75	Chl a, HPLC, Phyco, Aph, CDOM, Cyanos, NPP		
6/18/2023	**15**	12.0699	66.4123	0,42,60,80	Chl a, HPLC, Phyco, Aph, CDOM, Cyanos		
6/18/2023	**16**	11.6068	66.8843	0,12,50,75	Chl a, HPLC, Phyco, Aph, CDOM, Cyanos	✓	✓
6/18/2023	**17**	11.7000	67.0510	0,30,75,100	Chl a, HPLC, Phyco, Aph, CDOM, Cyanos	✓	✓
6/18/2023	**18**	11.6998	66.9032	10,20,50,75	Chl a, HPLC, Phyco, Aph, CDOM, Cyanos	✓	✓
6/19/2023	**19**	12.0698	66.7070	0,38,50,75	Chl a, HPLC, Phyco, Aph, CDOM, Cyanos	✓	✓
6/19/2023	**20**	12.0700	66.6240	0,40,60,80	Chl a, HPLC, Phyco, Aph, CDOM, Cyanos	✓	✓
6/19/2023	**21**	12.2353	66.5992	0,36,50,75	Chl a, HPLC, Phyco, Aph, CDOM, Cyanos, NPP	✓	✓
6/20/2023	**22**	12.4168	66.8321	0.10,40,75	Chl a, HPLC, Phyco, Aph, CDOM, Cyanos,NPP		
6/20/2023	**23**	11.7633	67.3558	0,30,48,75	Chl a, HPLC, Phyco, Aph, CDOM, Cyanos, NPP	✓	✓
6/21/2023	**24**	12.0625	67.7585	0,50,75,100	Chl a, HPLC, Phyco, Aph, CDOM, Cyanos, NPP	✓	✓
6/22/2023	**25**	12.0650	67.7981	0,60,75,100	Chl a, HPLC, Phyco, Aph, CDOM, Cyanos		
6/23/2023	**26**	12.0310	67.7645	0,68,78	Chl a, HPLC, Phyco, Aph, CDOM, Cyanos	✓	✓
6/12/2023	**27**	12.1657	67.4491	0,60,75,100	Chl a, HPLC	✓	

Table 16. *Times and positions for sunphotometer measurements*

DATE	TIME	LATITUDE	LONGITUDE
6/11/23	4:00	12.07	67.34
6/11/23	11:32	12.07	68.28
6/12/23	7:52	11.89	66.84
6/12/23	11:23	11.78	67.70
6/14/23	7:05	12.05	67.76
6/15/23	5:43	12.06	67.77
6/15/23	11:57	12.06	67.79
6/16/23	4:39	12.06	67.79
6/16/23	7:05	12.05	67.77
6/16/23	10:43	12.04	67.75
6/16/23	13:32	12.07	67.81
6/17/23	2:06	12.04	67.76
5/11/21	5:06	12.07	67.59
6/17/23	7:25	12.07	67.34
6/17/23	8:56	12.07	67.31
6/18/23	7:16	11.70	67.07
6/18/23	10:48	11.70	66.90
6/18/23	11:57	11.70	66.79
6/19/23	5:48	12.07	66.71
6/19/23	6:59	12.07	66.63
6/19/23	8:21	12.14	66.60
6/19/23	9:30	12.20	66.60
6/19/23	11:29	12.26	66.66
6/20/23	5:09	12.03	67.12
6/20/23	6:06	11.91	67.26
6/20/23	6:54	11.80	67.36
6/20/23	7:03	11.78	67.37
6/20/23	8:31	11.81	67.43
6/21/23	5:55	12.07	67.78
6/21/23	6:08	12.07	67.78
6/21/23	8:16	12.06	67.78
6/21/23	13:11	12.07	67.71

Meandering Dense Filament

A quick shipboard synthesis of the throughflow, UCTD, and ADCP velocity structure suggests the presence of a density filament that weakened over the sampling period. The first pass of the filament SC2E-SC2W (Fig. 13) shows an intense positive buoyancy gradient close to (12.2°N, 67°E) and a weaker negative buoyancy gradient at (12.2°N, 66.5°E). These gradients encompass colder and saline, and hence denser, cyclone wake water. The ADCP section shows near surface northward flow in the eastern buoyancy gradient region, with convergence implied by the reversing near-surface zonal flow component, with relatively deeper mixed layers, and shallower southward flow with shallower mixed layers below the weaker buoyancy gradients to the west (Figs. 54 and 55). The southwest monsoon winds have a northward component, which acts on the eastern gradients in the downfront sense, possibly promoting vertical mixing, while the western flank of the dense filament is undergoing upfront Ekman forcing, and hence undergoing a rapid re-stratification by the upfront Ekman flow, resulting in shallower mixed layers, and weaker buoyancy gradients.

Another dynamical impact is that on the barrier layer thickness. On the eastern region of the filament, the mixing appears to progressively erode the salinity "nose" at the base of the deep mixed layers. On the western side of the filament, because mixing is inhibited by the shallow stratification created by the upfront winds, the relaxation of the horizontal salinity gradients below the 60-m layer is evident.

The meandering filament shows processes involved in the re-stratification of the eastern edge of the wake of Cyclone Biparjoy during southwest monsoon conditions. In the presence of southwest winds, the baroclinic instability of the gradients to the east develop into strongly non-linear meanders, which, due to the orientation of the southwest winds with respect to the cyclone wake meandering and folding over, forms dense filaments that have both upfront and downfront sides. The upfront regions stratify rapidly, leading to shallow mixed layers and downfront regions that are frontogenetic with deeper mixed layers (Fig. 56). The vertical circulation at these filaments promotes blooms (Fig. 52).

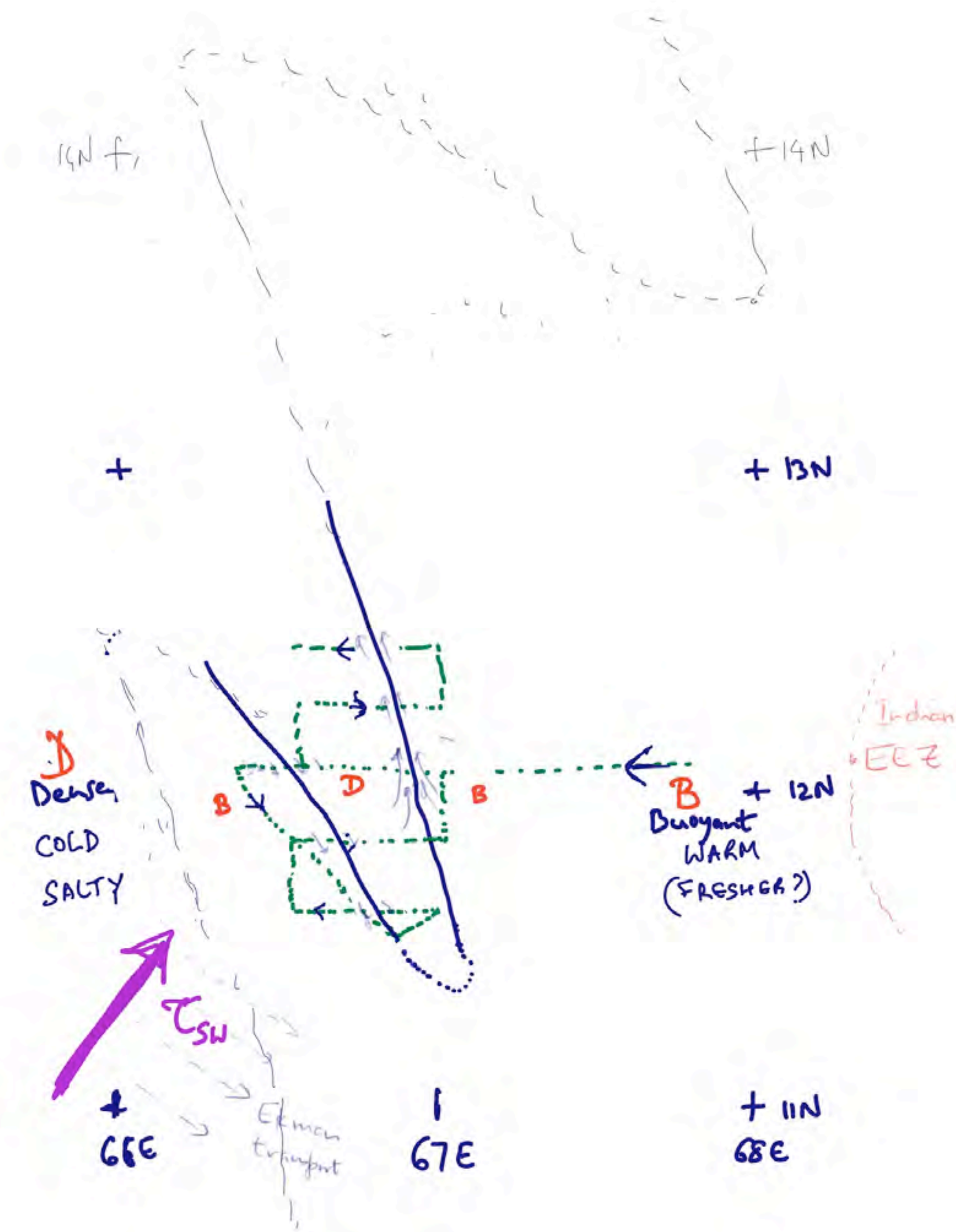

Figure 54. *A schematic of the meandering dense filament sampled by the Zonal-2 and Filament Survey sections. The buoyant and dense waters are marked B and D. The green broken lines mark Zonal-2 and Filament Survey sections. The southwest monsoon is shown as the purple arrow, with Ekman transport in dashed arrows. The flow along the filament is implied by the near surface flow shown in the ADCP.*

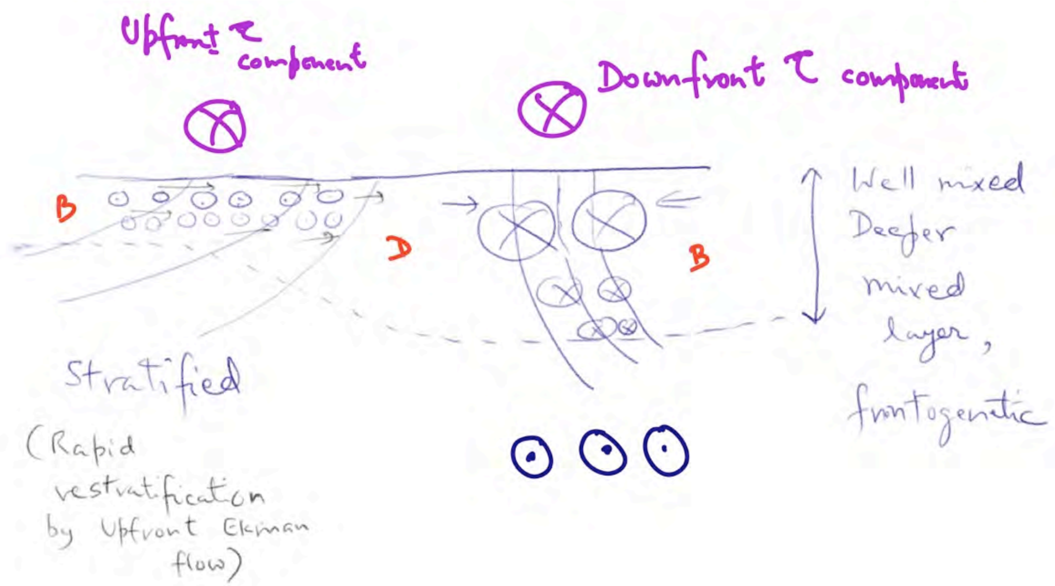

Figure 55. *A schematic of the side view of the dense filament sampled in the Zonal-2 and Filament Survey sections. Note the deeper mixed layers to the east and the shallower mixed layers at the western edge, possibly due to the southwest monsoon winds inducing a downfront component and the upfront component of Ekman buoyancy flux.*

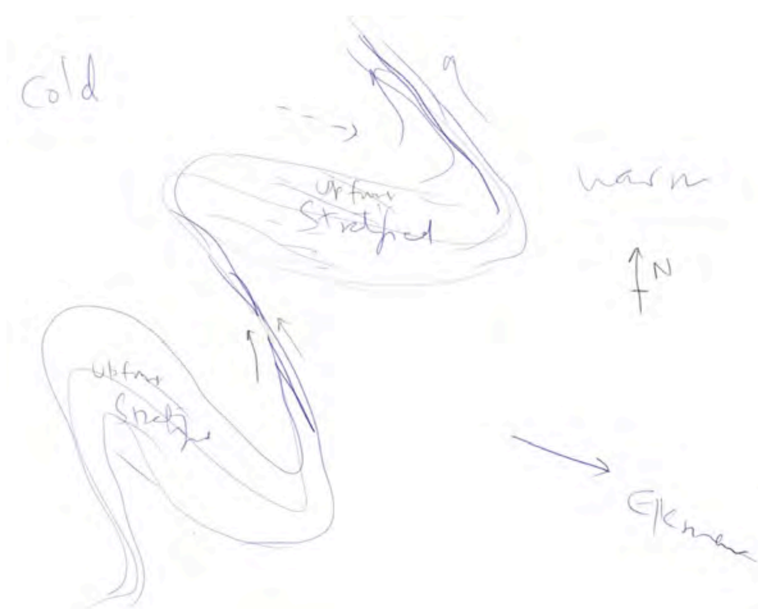

Figure 56. *A schematic for re-stratification in the Arabian Sea on the eastern flank of a wake following a cyclone, during the southwest monsoon: The eastern edge of the wake goes unstable to large-scale meanders due to baroclinic instability. As the meander grows and gets nonlinear, both upfront stratified and downfront frontogenetic regions develop as shown. An improved schema would need to consider the impact of pre-existing mesoscale eddies in the Arabian Sea.*

5. REFERENCES

Bhat, G.S., 2005. Convection inhibition energy of the inversion and the suppressed rainfall over the Arabian Sea during July 2002. *Mausam*, 56, 89-96.

Budhavant, K., Andersson, A., Holmstrand, A., and Gustafsson, Ö., Black carbon aerosols over Indian Ocean have unique source fingerprint and optical characteristics during monsoon season, *Proc. Natl. Acad. Sci*., 120, doi: 10.1073/pnas.2210005120, 2023.

Ching, C.Y., Fernando, H.J.S., and Noh, Y., 1993. Interaction of a negatively buoyant line plume with a density interface. *Dyn. Atmos. Ocean.*, 19, 367–388.

Fletcher, J.K., Parker, D.J., Turner, A.G., Menon, A., Martin, G.M., Birch, C.E., Mitra, A.K., Mrudula, G., Hunt, K.M.R., Taylor, C.M., Houze, R.A., Brodzik, S.R., and Bhat, G.S., 2020. The dynamic and thermodynamic structure of the monsoon over southern India: New observations from the INCOMPASS IOP. *Quart. J. Royal Meteor. Soc.*, 146, 2867–2890.

Mapes, B.E., and Zuidema, P., 1996. Radiative-dynamical consequences of dry tongues in the tropical troposphere. *J. Atmos. Sci*., 53, 620-638.

Parsons, D.B., Redelsperger, J.L., and Yoneyama, K., 2000. The evolution of the tropical western Pacific atmosphere–ocean system following the arrival of a dry intrusion. *Quart. J. Royal Meteor. Soc*., 126, 517-548.

Vinayachandran, P.N., Shankar, D., Kurian, J., Durand, F., and Shenoi, S.S.C., 2007. Arabian Sea mini warm pool and the monsoon onset vortex. *Current Sci*., 93.

6. APPENDIX A: CRUISE PARTICIPANTS

Name	Institution	Role
Craig Lee	Applied Physics Lab, Univ. of Washington	Chief Scientist
Amit Tandon	Univ. of Massachusetts, Dartmouth	Scientist
Siddhant Kerhalkar	Univ. of Massachusetts, Dartmouth	Scientist
Janet Sprintall	Scripps Institution of Oceanography	Scientist
Justine Damaris Parks	Scripps Institution of Oceanography	Technician
Ankitha Kannad	Scripps Institution of Oceanography	Scientist
Griffin Michael Modjeski	Univ. of Notre Dame	Scientist
Devmi Gamage	Univ. of Notre Dame	Scientist
Selina Bolella	Univ. of Notre Dame	Scientist
Maria Laura Zoffoli	Consiglio Nazionale delle Ricerche	Scientist
Joaquim Ignacio Goes	Lamont Doherty Earth Observatory at Columbia Univ.	Scientist
Rohan Armando Jordan Carneiro Menezes	Dartmouth College	Scientist
Charles William Kovach	NOAA Center for Weather and Climate Prediction	Scientist
Emma Renee Robertson	Pennsylvania State Univ.	Scientist
Melanie Faire McCoy	Whatcom Community College	Scientist
Alexander Brown Kinsella	Woods Hole Oceanographic Inst.	Scientist
Mr. R Chandra Sekhar Naik	INCOIS	Project Scientist-I
Mr. Harsa Bardhan Dalabehera	INCOIS	Project Scientist-II
Ms. Anupama Sahoo	INCOIS	Junior Research Fellow
Dr. Jossia Joseph	NIOT	Scientist-E
Dr. Asish Soni	IITM Pune	Postdoc Project Scientist-I
Mr. Pawan Soyam	IITM Pune	Research Scholar (grad student)
Dr. K.B.R.R. Hari Prasad	NCMRWF	Scientist-C
Debarshi Sarkar	Univ. of Massachusetts, Dartmouth	Beginning Grad Student (BSME)

7. APPENDIX B: CRUISE NARRATIVE

5 June

Arrive in Goa. Early arrivals clear port pass process.

Cyclone Biparjoy forecast to develop south of the work area, propagating northward to either be over the site or between Goa and the worksite on 9–10 June. Significant wave heights of 6+ m forecast.

IITM group requests permission to install two aerosol sampling instruments, one of which uses a radioactive component. Due to insufficient time to complete safety analysis, our request to include this instrument is denied.

6 June

Remainder of the team arrives in Goa.

Visit R/V *Revelle* after the ship arrives to discuss loadout plan and weather, and to coordinate activity for 6 June.

7 June

Loadout begins. All gear except the surface drifters delivered to the ship. The port pass process and port security make for a late morning start. INCOIS team assembles Lagrangian float and filtering station.

We encounter some difficulty finding a location that meets the requirements for aerosol sampling (forward of stacks, high, within a 5-m tubing run of an interior lab). Site the instrument in the analytical lab, but the team is concerned about the tubing being bent to exit out the gooseneck on the 01. Further searching fails to reveal a better solution, so they proceed with installation in the analytical lab.

8 June

Science team signs onto *Revelle* in the morning. The team works aboard the ship through the morning, walking out to process through immigration and customs in two waves. This avoids the entire team spending the morning in the immigration office waiting until everyone completes the process.

Loadout continues. Lagrangian float and SG530 self-tested. UCTD assembled and tested. VMP assembly begins.

MicroSVP drifters delivered early evening after being expedited through customs.

The forecast shows a tropical storm propagating northward over the AD07 site around our 10 June arrival date, with significant wave heights of 5–7 m. Seas are not forecast to drop to 3–4 m until Thursday/Friday (15–-16 June). We thus switch to target mooring AD08, which has peak significant wave heights of 5 m, dropping to 3 m Tuesday/Wednesday.

Swell at the pier severe enough that *Revelle* is parting mooring lines. After being unable to secure an alternate berth and being denied permission to anchor off in the harbor, *Revelle* decides to depart Mormugao, leaving the dock at roughly 20:00 local time and steaming to a position 12 nm offshore. The ship then holds station to allow us to finish set-up and securing of gear.

9 June

Science team finishes securing the labs shortly after breakfast. Depart for AD08 at 09:00 local time. Sea state is modest offshore of Goa, with roughly 3 m significant wave height, but worsens as we move offshore.

Plotting survey waypoints reveals that AD08 sits well inside the Indian EEZ, far enough that the entire original UCTD survey would have been inside the EEZ boundary. We shift 50 nm west to avoid the EEZ.

Internet connection fails late in the night.

10 June

Internet connection down the entire day.

Exit Indian EEZ around 20:00 and begin science sampling with underway systems.

Radiosonde team's field laptop fails, and we are unable to configure a spare because it requires drivers that must be downloaded from the Internet. Radiosonde launches on hold until new laptop can be configured.

Hyperspectral profiler also non-functional, so no optics casts until the issue can be identified and addressed.

11 June

Internet connection down the entire day.

Arrive at S1-W, 2000-m CTD cast. INCOIS decides that they no longer want the MLF deployed at the westernmost station, but would instead like to use the easternmost point.

Transit to S1-C and conduct 2000-m CTD cast.

Transit to S1-E, arriving late afternoon. Deploy MLF, followed by 2000-m CTD cast

Transit to start of SVP grid. Begin deployment of SVP array, and begin experimenting to see if UCTD is operable in current wave state.

12 June

Continue deploying SVP array, sampling with UCTD throughout.

Conduct 200-m CTD cast timed for optics. Finish deploying SVP array around 16:00 local time.

Transit to S1-S for 2000-m CTD cast, then begin the 'butterfly' UCTD survey. Routing chosen to place a 2000-m CTD cast later in the evolution, to allow Restech Mason to get some rest. We conduct the survey as S1-S – S1-W – S1-E – S1-N – S1-S.

13 June

UCTD 'butterfly' survey.

Deploy BGC float.

14 June

Drop into flux sampling at S1-C. Point ship into the wind and move forward at a rate just fast enough to ensure that the UCTD line does not pass under the ship.

Dual noon CTD cast (200 m followed by 2000 m) due to water budget issues.

Deploy SG530 following CTD cast.

15 June

UCTD at S1-C while pointed into the wind and making minimal way. It requires roughly 1 kt to stream the line, so we gradually move away from the site. Once we reach 5 nm separation, we reposition back to the center. Sample with UCTD while repositioning unless the ship needs to pump sewage, in which case we simply transit back to center.

CTD cast (200 m) at 13:00 local time, coincident with satellite overpasses.

After CTD cast, perform trials with the VMP system. Start with winch tests, deploying and recovering the UCTD dummy probe. After testing winch functionality, we do four casts with the VMP (fitted with dummy probes) to figure out overboarding and profiling procedures.

16 June

Still sunny with few clouds and no precipitation. Continue UCTD time series at S1-C. CTD casts at 12:00 and 15:00 local time, both 200 m. VMP profiling between the CTD casts, collecting 12 profiles while moving 1 kt through the water.

17 June

Forecast shows possible rain in the 4–5 days out, though perhaps not the start of an active period. The next few days will bring more of what we've seen during the time series sampling thus far. We thus decide to end the first time series and shift west to sample the bloom signature seen in ocean color images. The high chlorophyll region sits roughly under the path of the cyclone, and appears to be in the north-going branch of a meander or eddy. We anticipate seeing a northward jet with maximum velocity near the center of our survey pattern. Plan a 100-km butterfly survey (identical to the initial survey, just shifted to the west to capture the high chlorophyll region), with CTD sampling along the zonal leg. We'll deploy the second SVP array along the survey track, and launch the optical drifter at the southern apex.

The second CTD cast (at S2-C, in the feature) shows elevated chlorophyll and a weak salinity stratified layer at roughly 10 m, sitting atop a mostly mixed layer that extends to roughly 40 m. Below that is a region of interleaving, but the prominent salinity maximum that was present to the east is absent.

The LDEO team reports smaller cells indicative of early stages of a bloom.

Evening (just past dusk) VMP sampling reveals ML base at ~20 m, with regions of active mixing at 35–45 m, just below the ML base, and 95–105 m, where the ADCP shows elevated shear.

18 June

Morning finds us at the southern segment of the survey. MLD is less than 20 m, with salinity increasing slightly below and a muted salinity maximum at 85 m. LDEO team reports a mix of small and large cells, with a bloom well in progress.

Rather than occupy the meridional section of the butterfly, we switch to a radiator survey designed to span the high-chlorophyll/strong gradient region, with six 54-km zonal sections separated at 20-km spacing.

Deploy the optical drifter slightly NE of the southernmost waypoint (S2-S) during the transit to S3-E1. Begin UCTD survey S3-E1 to S3-W1, then continue on the pattern. Deploy the last of the SVP microdrifters on the first segment of this pattern.

Three CTD casts — morning, noon, and afternoon — to sample variability across the bloom region.

VMP at 20:00 local time.

19 June

VMP at 05:00 local time.

Continue UCTD survey.

Three CTD casts arrayed around noon. These show weakening bloom signatures. Speculation is that the large region of elevated chlorophyll has been advected northward.

VMP at 20:00 local time.

20 June

Bio team elects to skip the scheduled 02:00 local CTD cast, as it falls outside the high-chlorophyll region. After completing the meander section, we recover Sea Snake and UCTD and head toward optical drifter recovery at full speed. Drifter is reporting GPS positions at 15-min intervals. Follow a dog-leg transit to allow for one final CTD cast in the high-chlorophyll region, and then head directly for the drifter.

Calm seas make the optical drifter easy to spot. Grapple the recovery float and bring it aboard by manually hauling drifter and drogue over starboard rail. Conduct a calibration cast at the drifter recovery site and then begin transit back to time series site S1-C.

Resume time series sampling at S1-C. Shift VMP ensemble to 18:00 local time to coincide with the Q_{net} transition from warming to cooling.

21 June

VMP sampling at 05:00 local, near the end of the nighttime cooling period.

Continue S1-C time series.

Finalize VMP sampling to 04:00–07:00 and 17:00–20:00 local.

22 June

Continue time series sampling at S1-C, UCTD, VMP, CTD, and radiosondes.

Bow thruster fails mid-morning. Continue operations using only the Z-drives, but minimum speed jumps from 0.5 kt to > 1 kt. Profiles take longer to reach the same depth and time between resets decreases.

Brief moment of early evening rain during the 17:00–20:00 local VMP period.

23 June

Time series sampling at S1-C.

Convective clouds and rain to the north of us, but nothing near S1-C. We consider breaking off early to run north before turning back inside the Indian EEZ to make for Goa, but the high-chlorophyll signals are too far north to reach in the remaining time.

24 June

Finish time series at S1-C. Conclude science operations and begin transit to Goa.

25 June

Transit to Goa.

26 June

Arrive Goa 08:00 local time. Immigration and customs are time-consuming, but science team is off the ship by late afternoon.

8. APPENDIX C: DAILY WEATHER BRIEFINGS

Analysis by Selina Bolella

10 June 2023

Captured: 13:39 IST

Briefing: Partly cloudy skies with sun throughout the day. Winds maxed at about 20 knots. Possible chance of spotted showers as ship was located east to intensifying tropical Cyclone Biparjoy.

11 June 2023

Captured: 11:05 IST

Captured: 14:16 IST

Briefing: Mainly cloudy skies, cloud coverage increased throughout the day and overnight. Winds maxed around 20 knots. Scattered showers throughout the day.

12 June 2023

Captured: 13:30 IST

Captured: 13:52 IST

Briefing: Mainly clear skies with scattered clouds throughout the day into the night. Winds maxed around 26 knots from the southwest. Temperatures reached high 80s (87).

13 June 2023

Captured: 14:55 IST

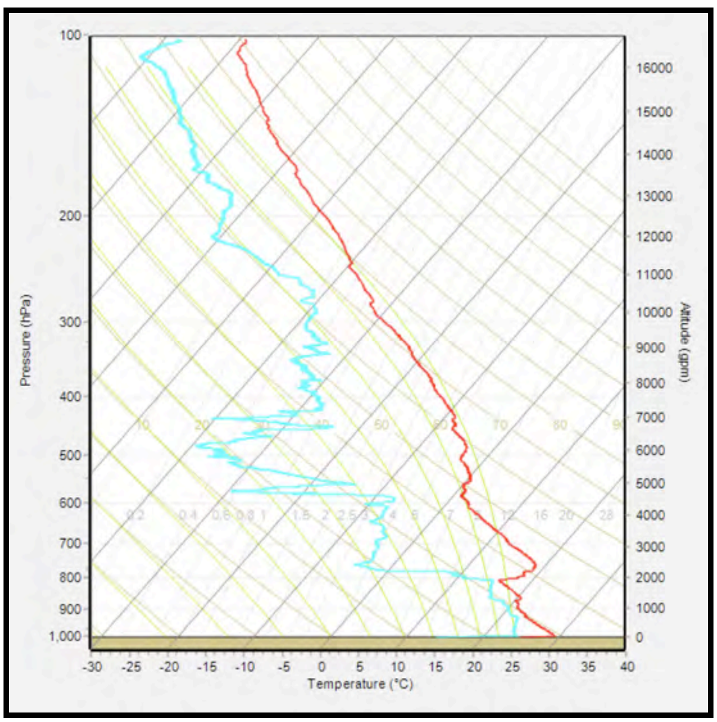

Ship Radiosonde: 12 UTC (15:30 IST)

Briefing: Cloudy sky coverage from the day into the night. Light drizzle of rain throughout the day with maximum winds of 26 knots from the southwest. Temperatures remained in mid-80s.

14 June 2023

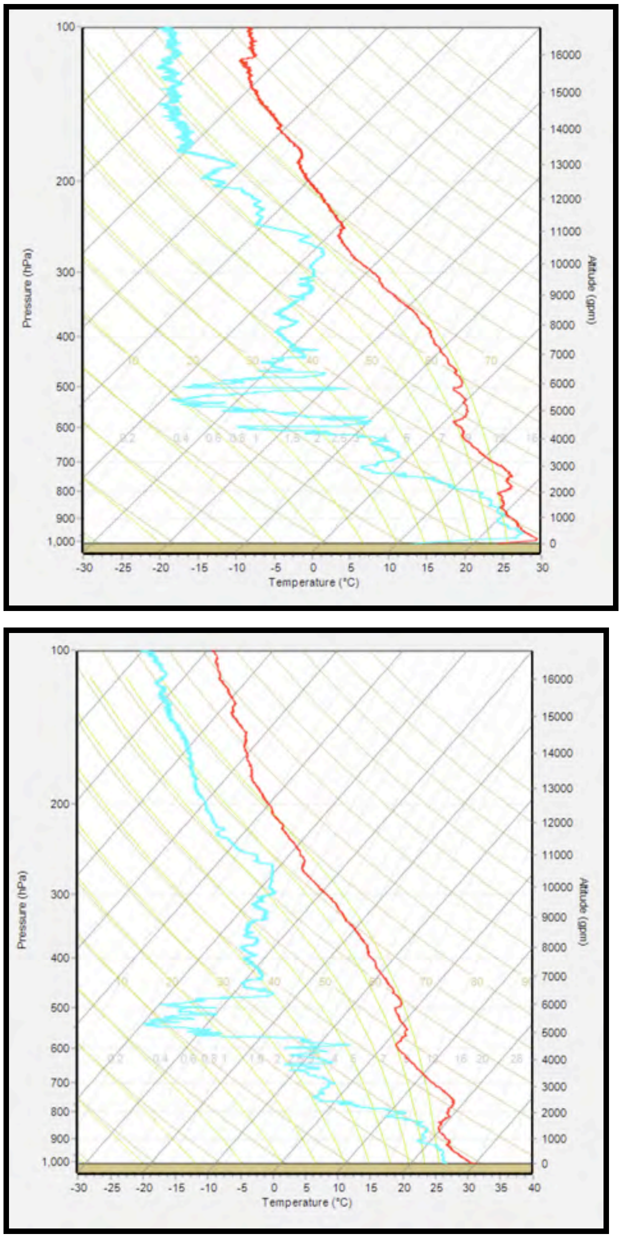

Ship Radiosonde: 0 UTC (05:30 IST) and 06 UTC (11:30 IST)

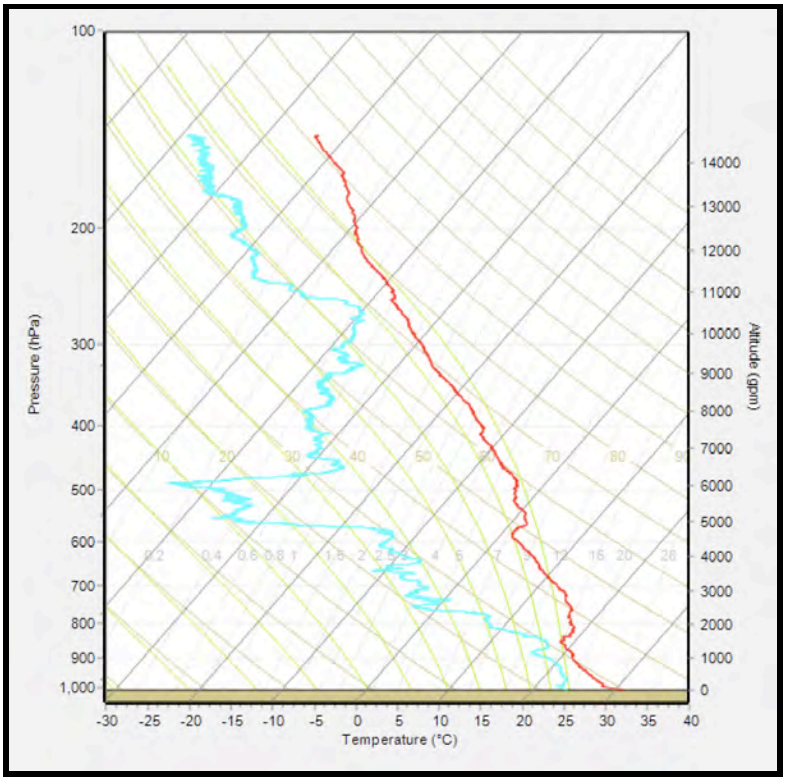

Ship Radiosonde: 12 UTC (15:30 IST)

Captured: 14:32 IST

Captured: 15:54 IST

Briefing: Passing rain drizzle in the early morning hours. Skies cleared and remained mainly sunny for the remainder of the day. Temperature remained in the mid-80s throughout the day. Max wind was about 26 knots and on average 24 knots.

15 June 2023

Captured: 13:39 IST

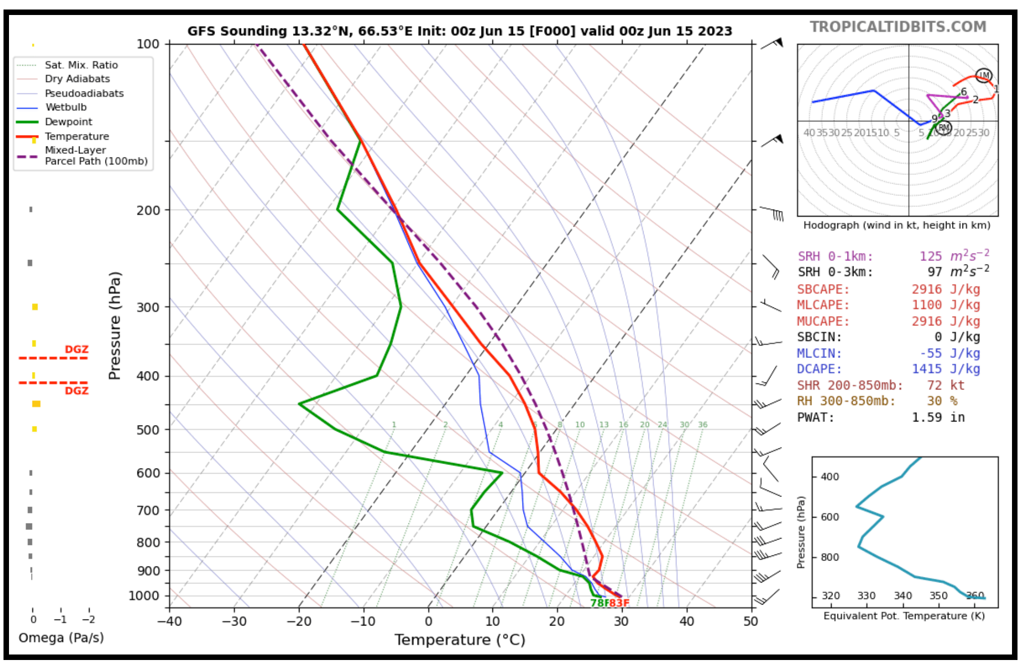

GFS Model Skew-T: 0 UTC

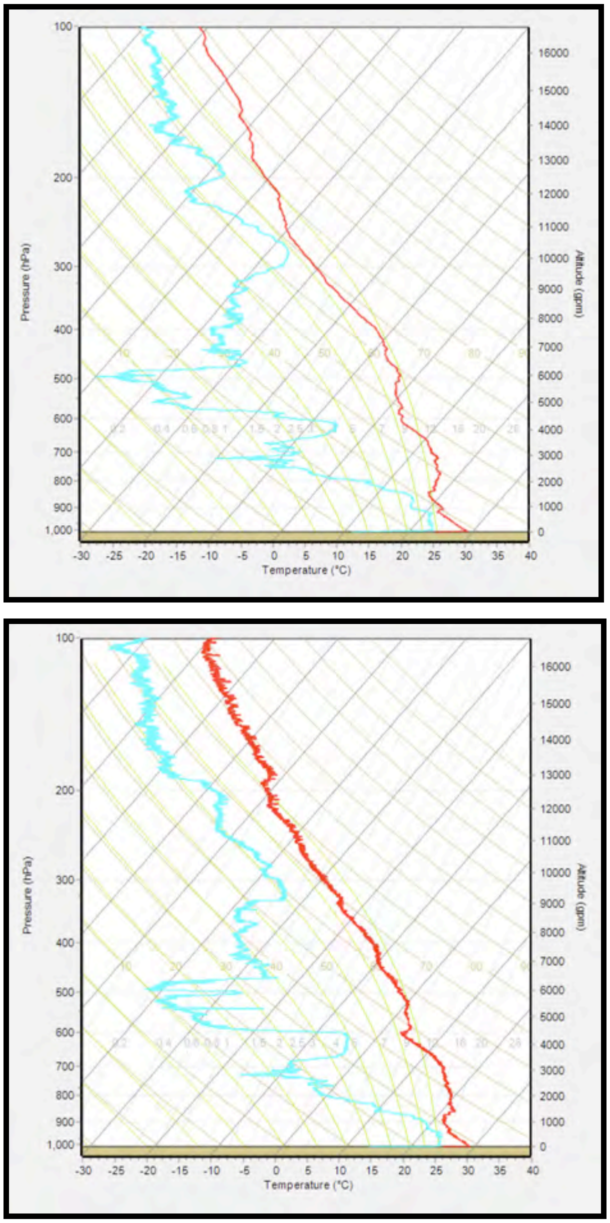

Ship Radiosonde: 0 UTC (05:30 IST) and 06 UTC (11:30 IST)

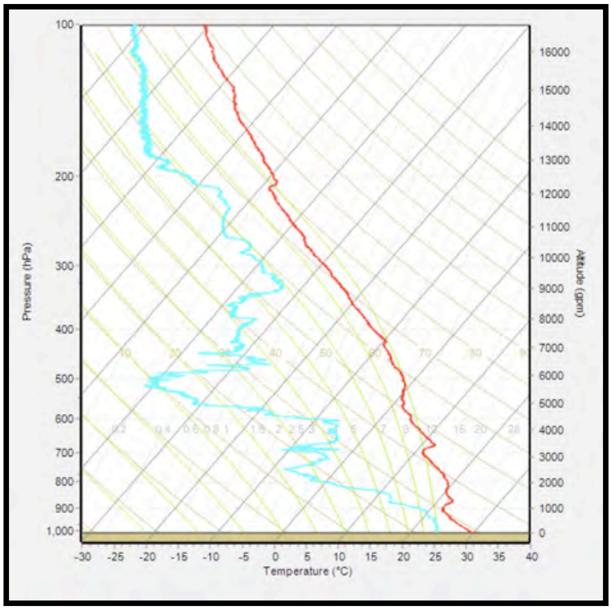

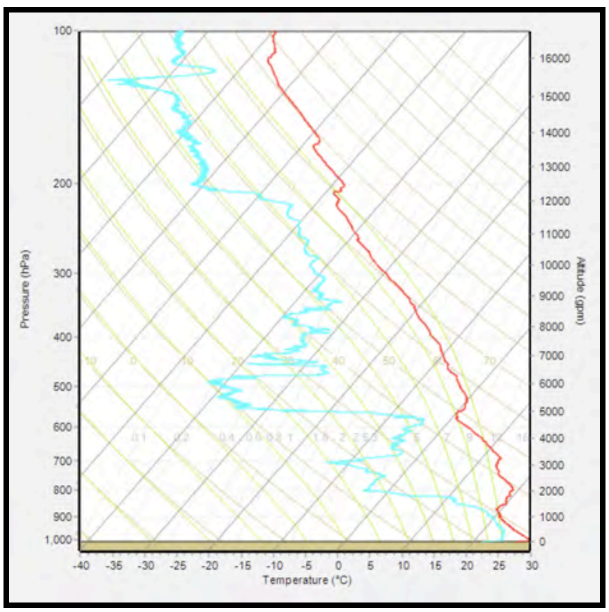

Ship Radiosonde: 12 UTC (15:30 IST) and 18 UTC (23:30 IST)

Briefing: Temperatures remain in mid-80s. Wind averaged 24 knots in the early daylight and 21 knots for the remainder of the day. Wind gusts up to 32 knots. Dry layer located at 600–400 mb.

16 June 2023

Captured: 13:06 IST

Captured: 11:24 IST

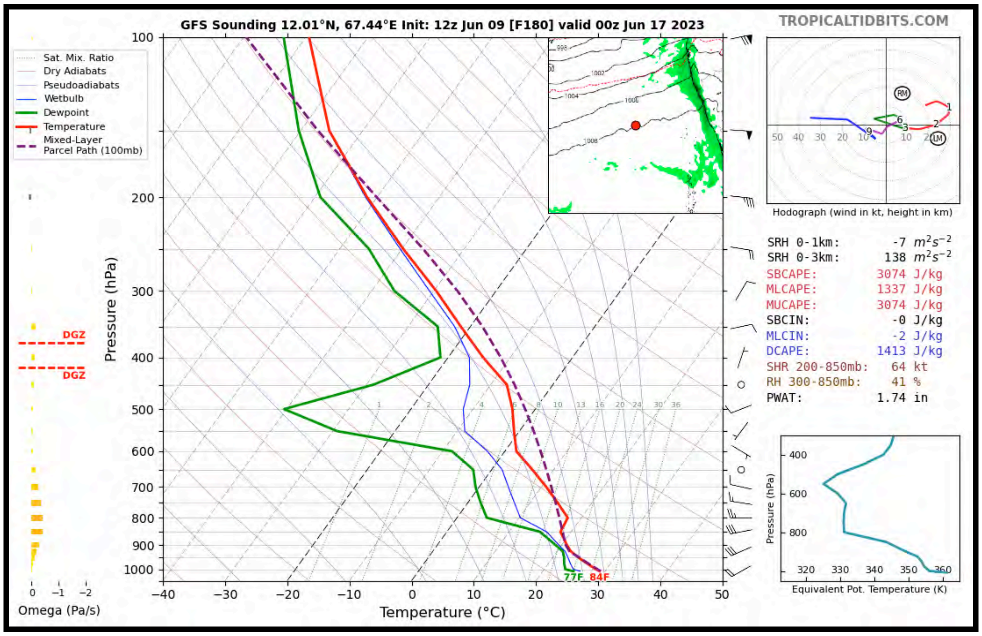

GFS Model Skew-T: 0 UTC (05:30 IST)

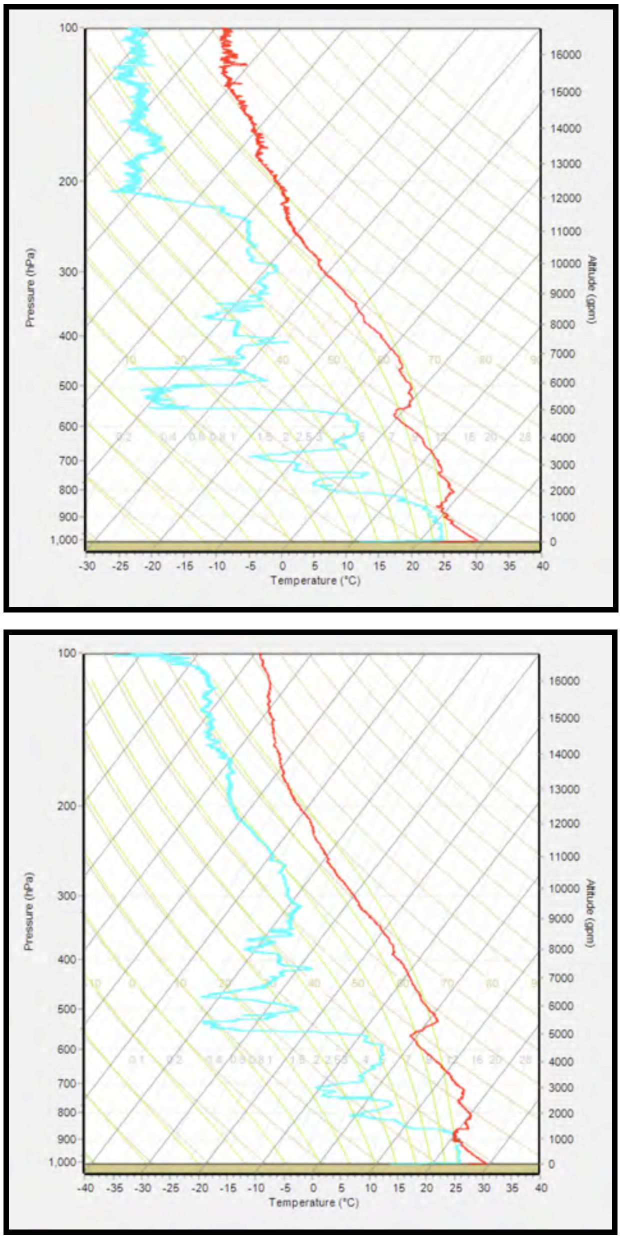

Ship Radiosonde: 0 UTC (05:30 IST) and 06 UTC (11:30 IST)

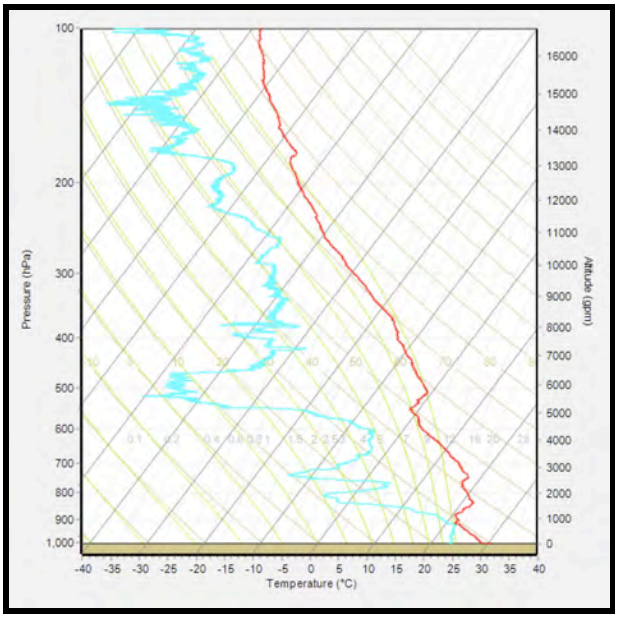

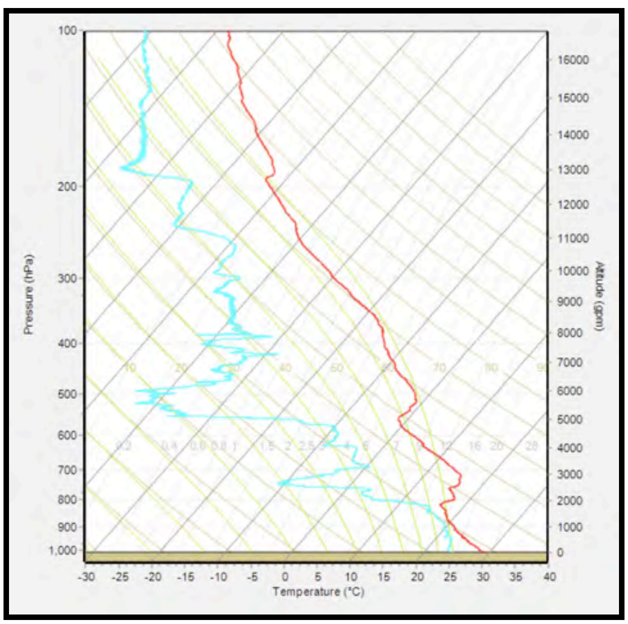

Ship Radiosonde: 12 UTC (15:30 IST) and 18 UTC (23:30 IST)

Briefing: Winds reach 22 knots throughout the day. Temperature remains consistent over sea in the mid-80s. Partly cloudy skies during the day into the night. Cloud coverage is scattered. Cloud coverage increased overnight. Dry layers in the mid-atmosphere continue.

17 June 2023

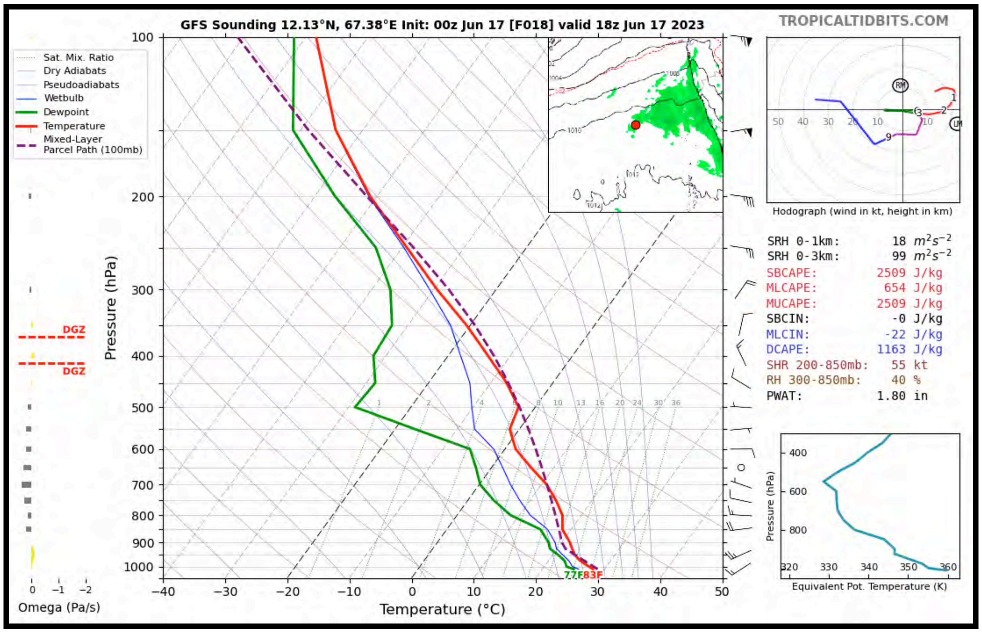

GFS Model Skew-T: 0 UTC (05:30 IST)

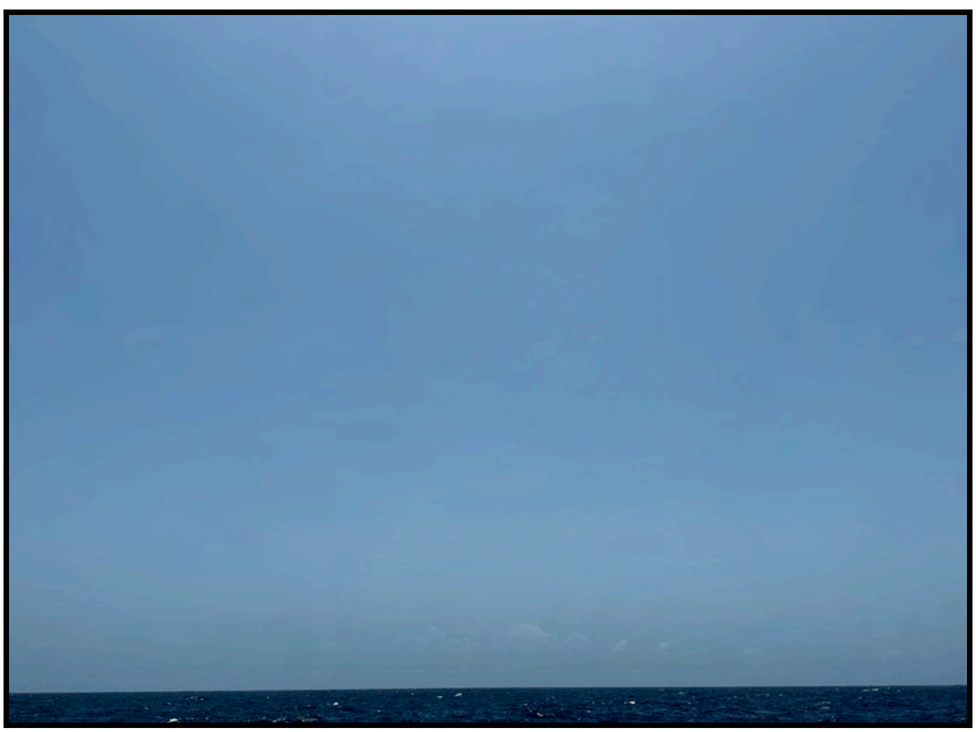

Captured: 13:27 IST

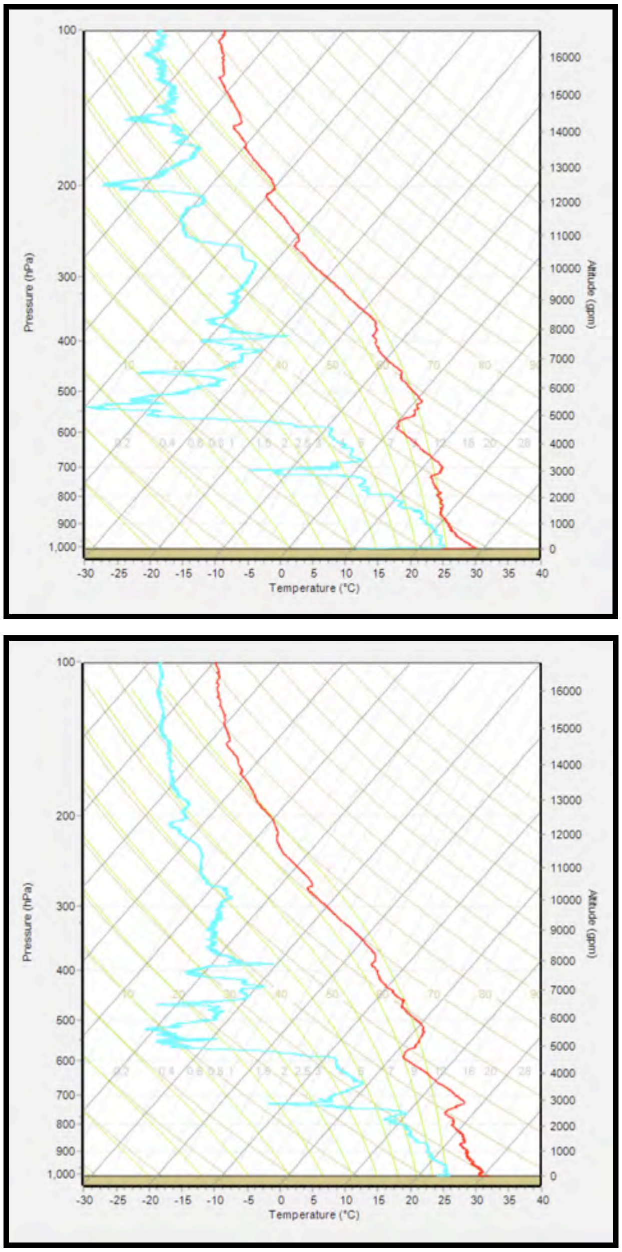

Ship Radiosonde: 0 UTC (05:30 IST) and 06 UTC (11:30 IST)

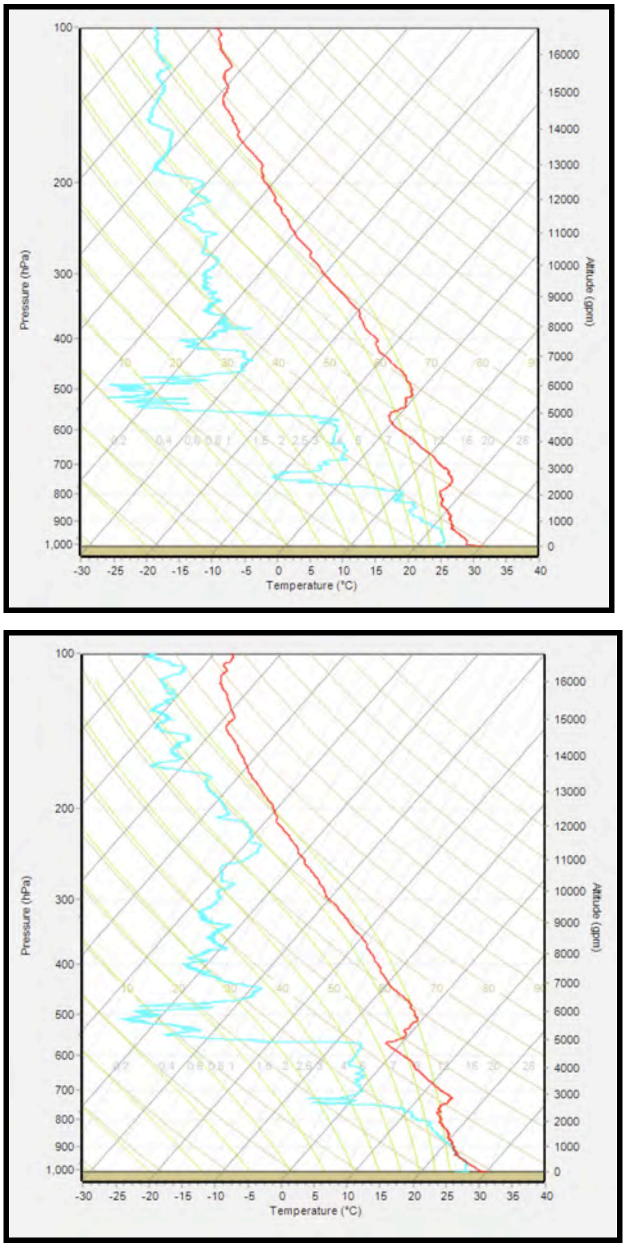

Ship Radiosonde: 12 UTC (15:30 IST)& 18 UTC (23:30 IST)

Briefing: Little cloud coverage, predominantly sunny skies. Temperature consistently in the low-80s (84) throughout the day. Winds maxed around 19 knots. Overall winds are calmer in comparison to the past few days.

Dry layer located at 500 mb: Due to proximity of Cyclone Biparjoy, cyclonic circulation is advecting dry air down from Saudi Arabia region down into Arabian Sea region.

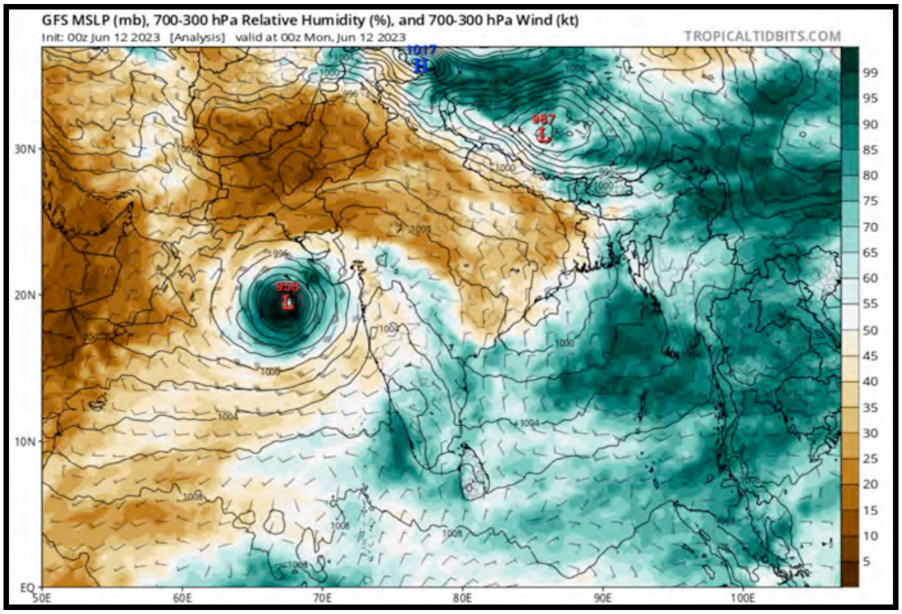

GFS: June 12th @ 0 UTC (05:30 IST)

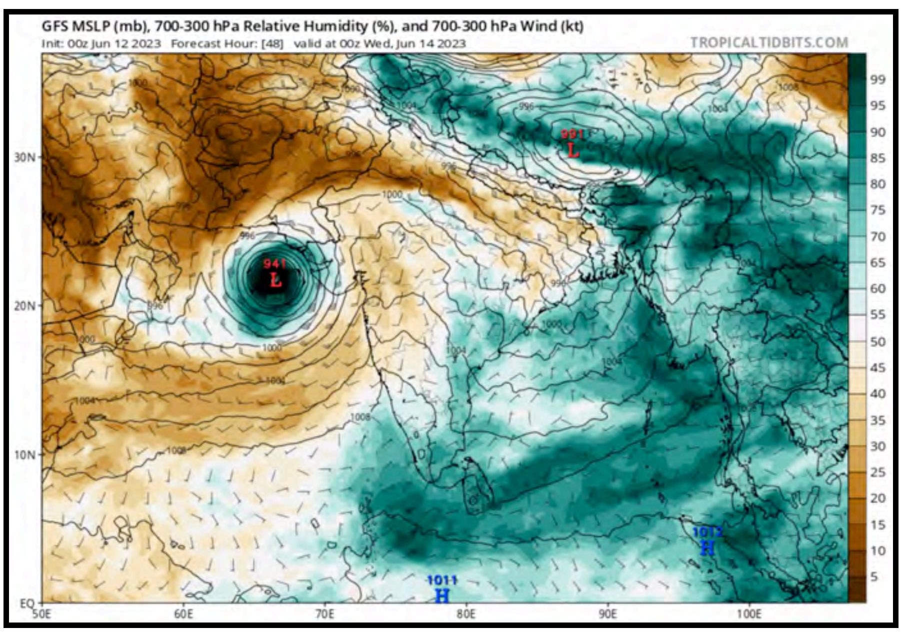

GFS: June 14th @ 0 UTC (05:30 IST)

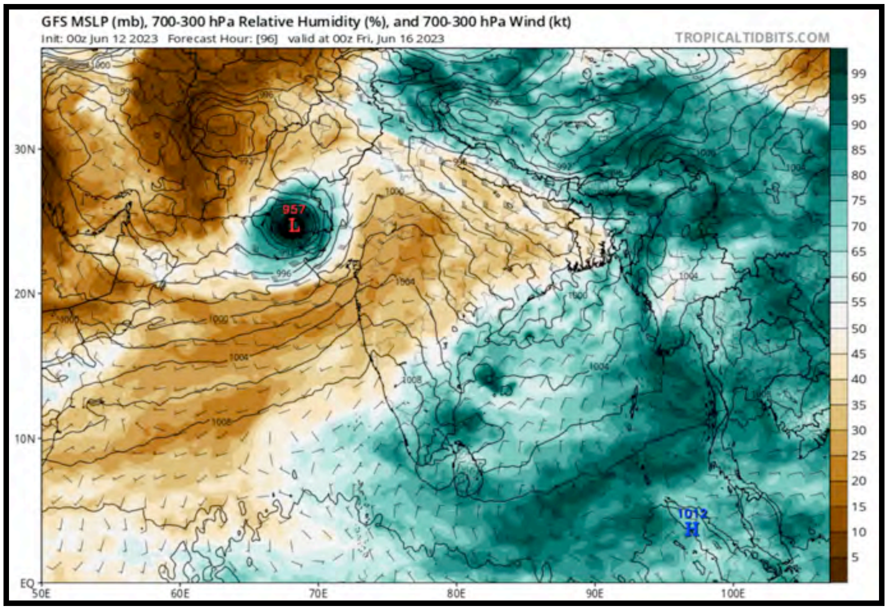

GFS: June 16th @ 0 UTC (05:30 IST)

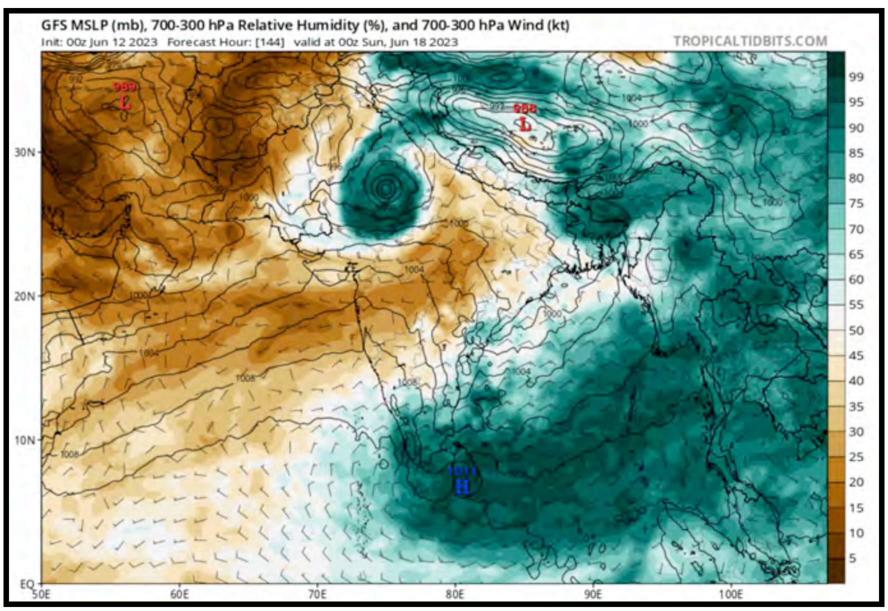

GFS: June 18th @ 0 UTC (05:30 IST)

Investigation: Relative humidity from 700–300 mb (used to distinguish 500 mb layer). Warm/dry air is advected from the northwest due to cyclonic circulation of Cyclone Biparjoy. Hence moisture being blocked off from the Arabian Sea region, creating drier conditions.

18 June 2023

Captured: 12:43 IST

Captured: 14:53 IST

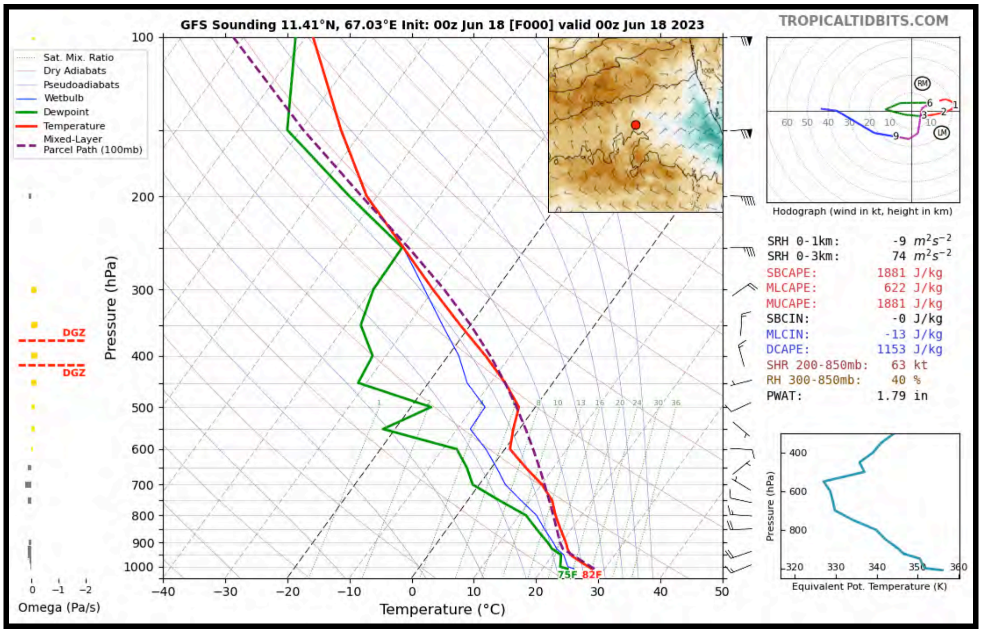

GFS Model Skew-T: 0 UTC (05:30 IST)

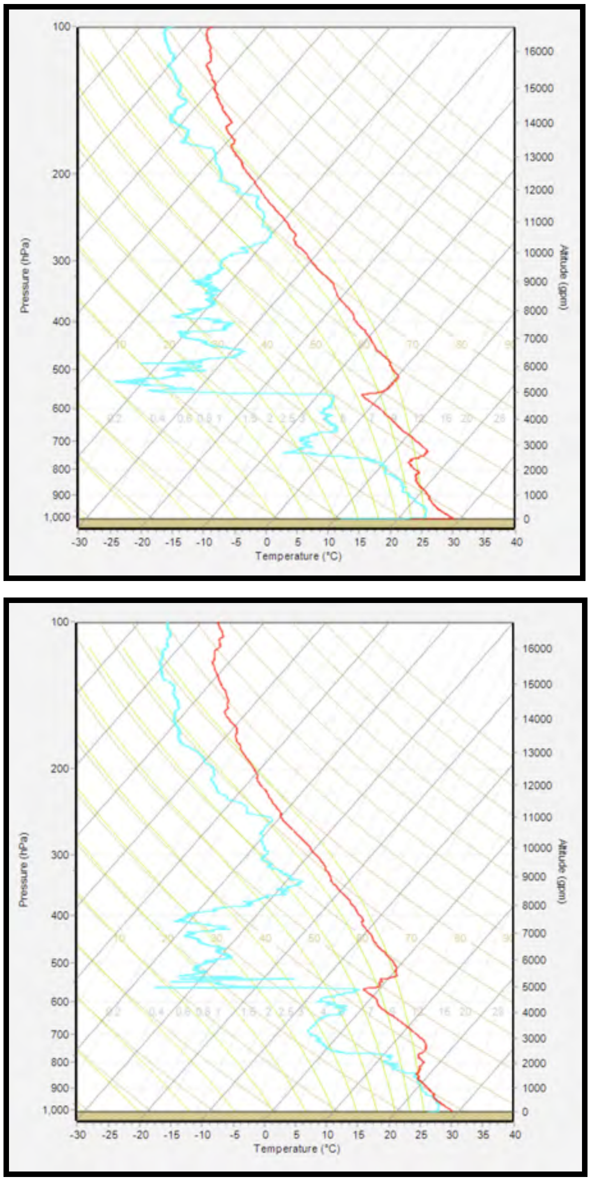

Ship Radiosonde: 0 UTC (05:30 IST) and 18 UTC (23:30 IST)

Briefing: Scattered clouds with sun. However, hazy skies are present where the appearance of the typical blue skies look to be slightly gray. Due to increased moisture and humidity in the air, particulate matter aloft for several days at a given time can cause a hazy-like appearance within the sky. Winds averaging around 18 knots throughout the day. Scattered drizzle throughout the day. Dry layer remains present. Temperature remains in lower-80s throughout the day.

19 June 2023

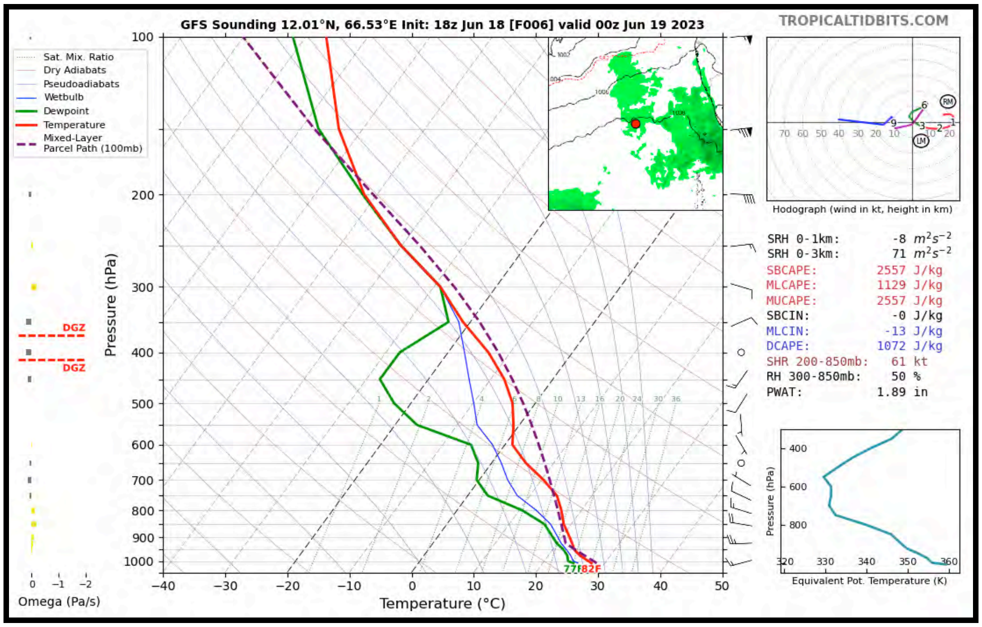

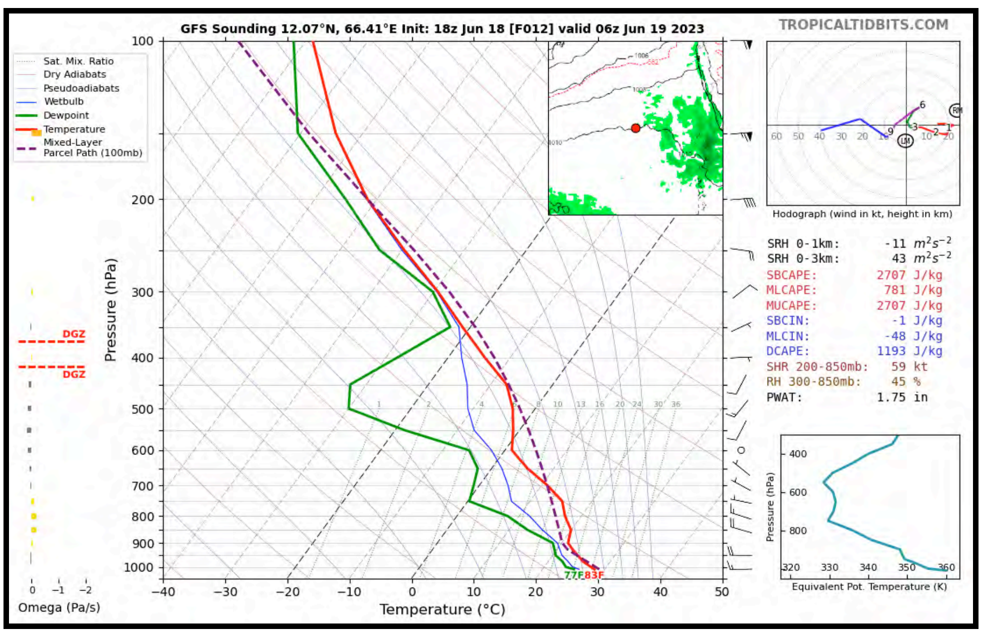

GFS Model Skew-T: 0 UTC (05:30 IST) and 06 UTC (11:30 IST)

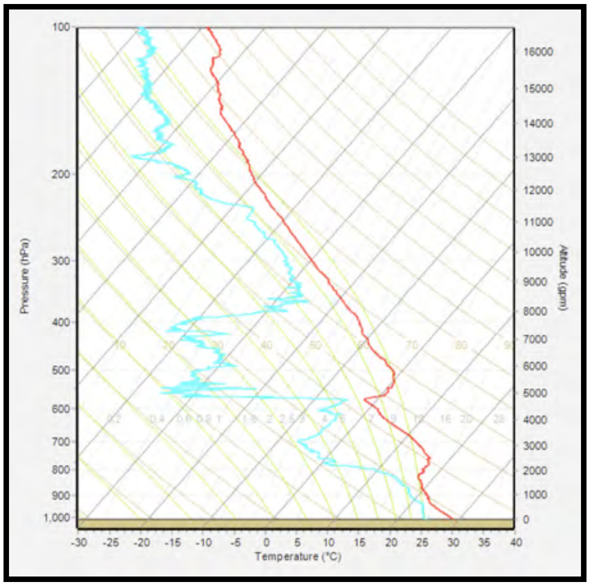

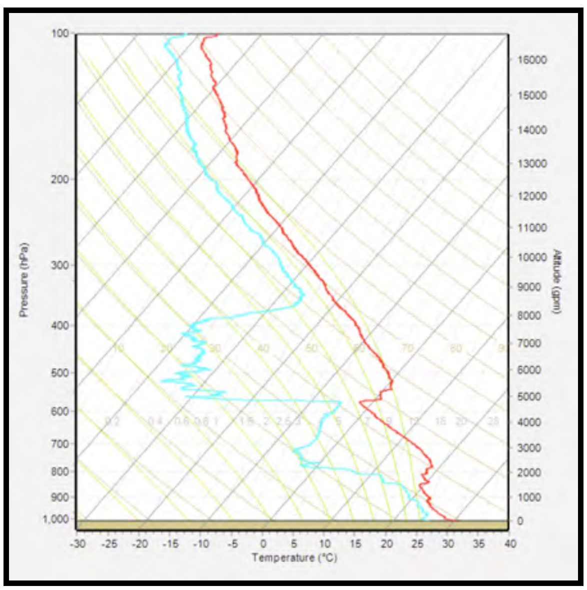

Ship Radiosonde: 0 UTC (05:30 IST) and 06 UTC (11:30 IST)

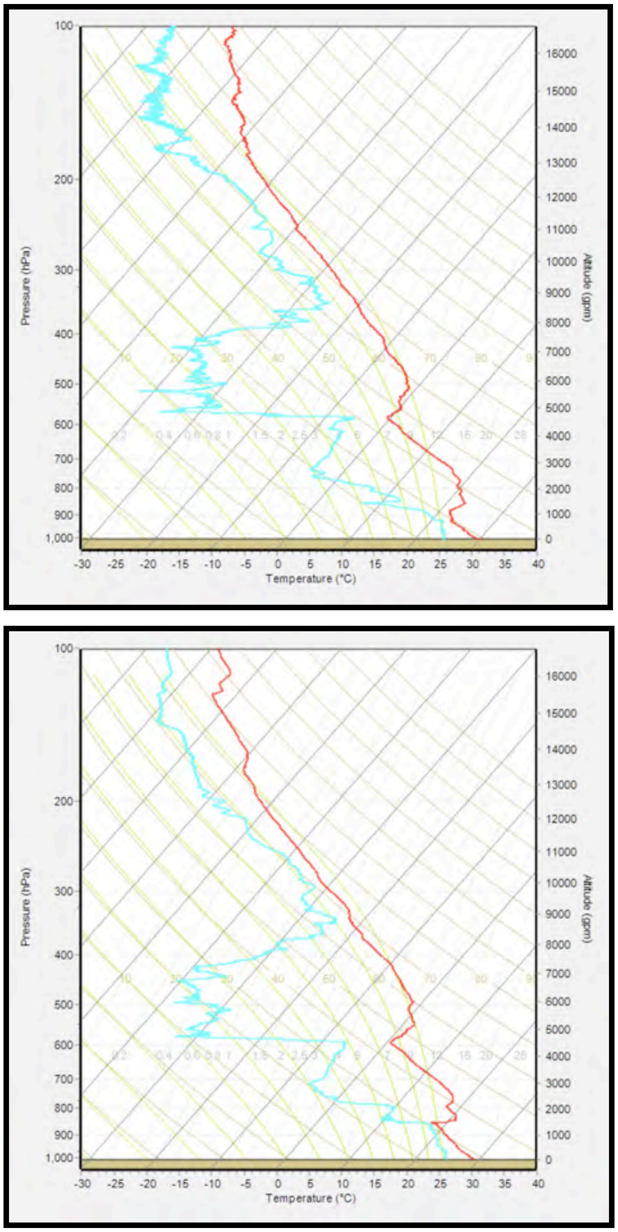

Ship Radiosonde: 12 UTC (15:30 IST) and 18 UTC (23:30 IST)

Captured: 13:45 IST (top and bottom)

Captured: 18:45 IST

Briefing: Light scattered showers in the early hours (0500) and calm conditions for the remainder of the day. Temperature remained in lower-80s (84). Wind averaged around 17 knots throughout the day. Sunny skies with sparse cloud coverage. Cirrus and cumulus clouds present.

Captured: 07:23 IST via Griffin Modjeski

20 June 2023

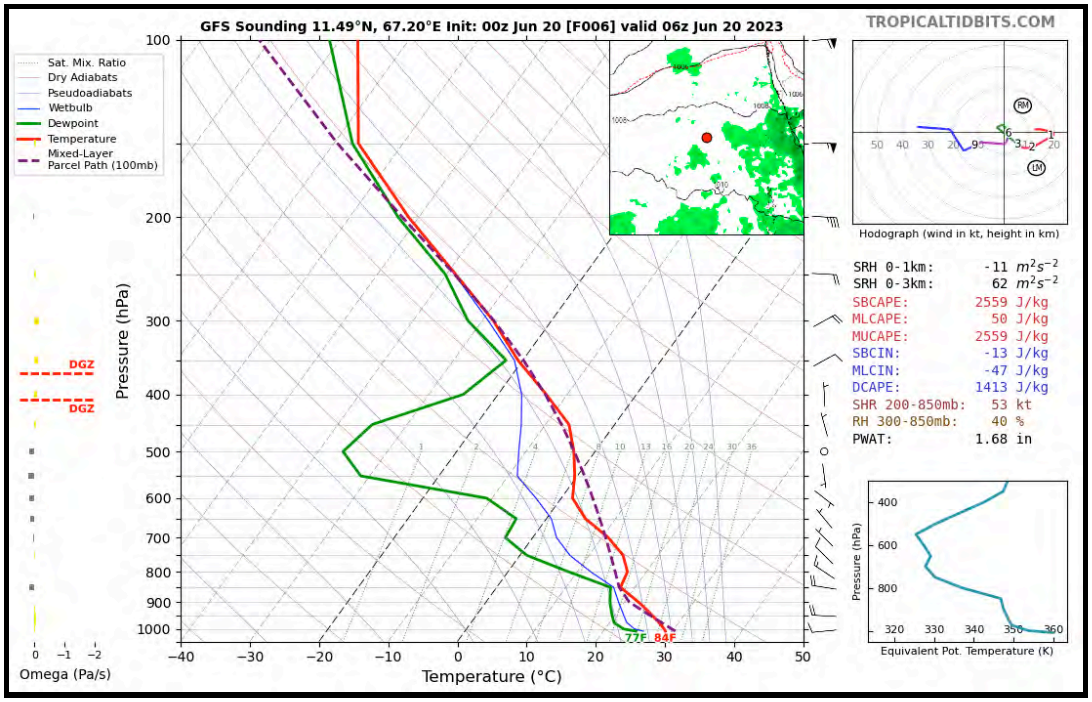

GFS Model Skew-T: 0 UTC (05:30 IST)

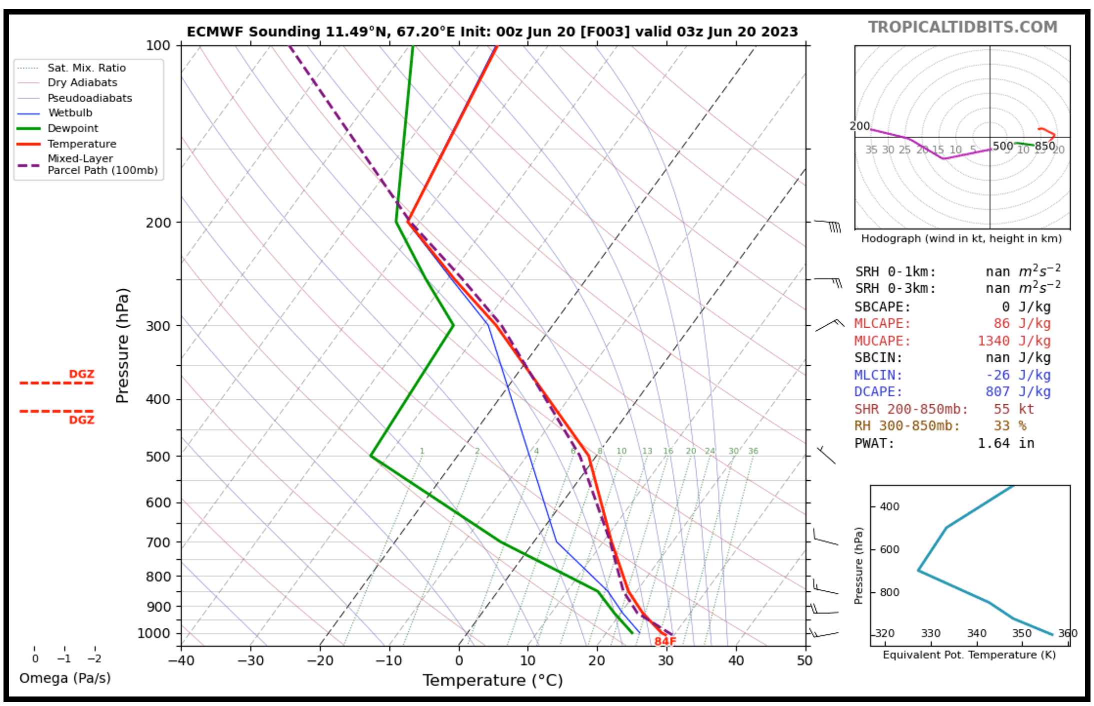

ECMWF Model Skew-T: 0 UTC (05:30 IST)

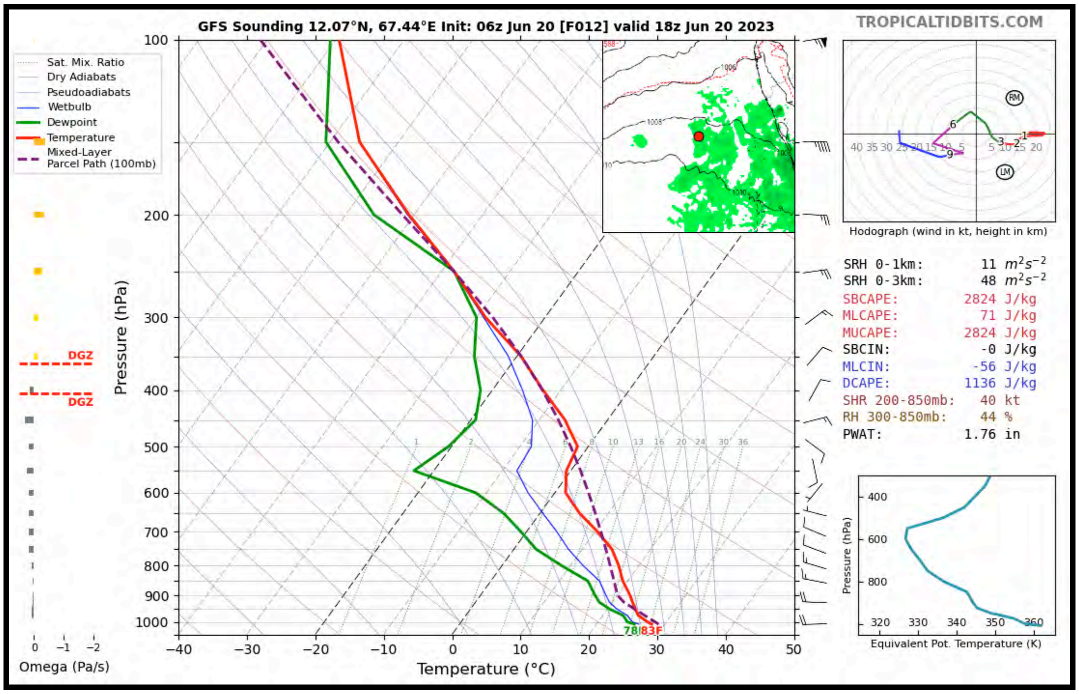

GFS Model Skew-T: 18 UTC (23:30 IST)

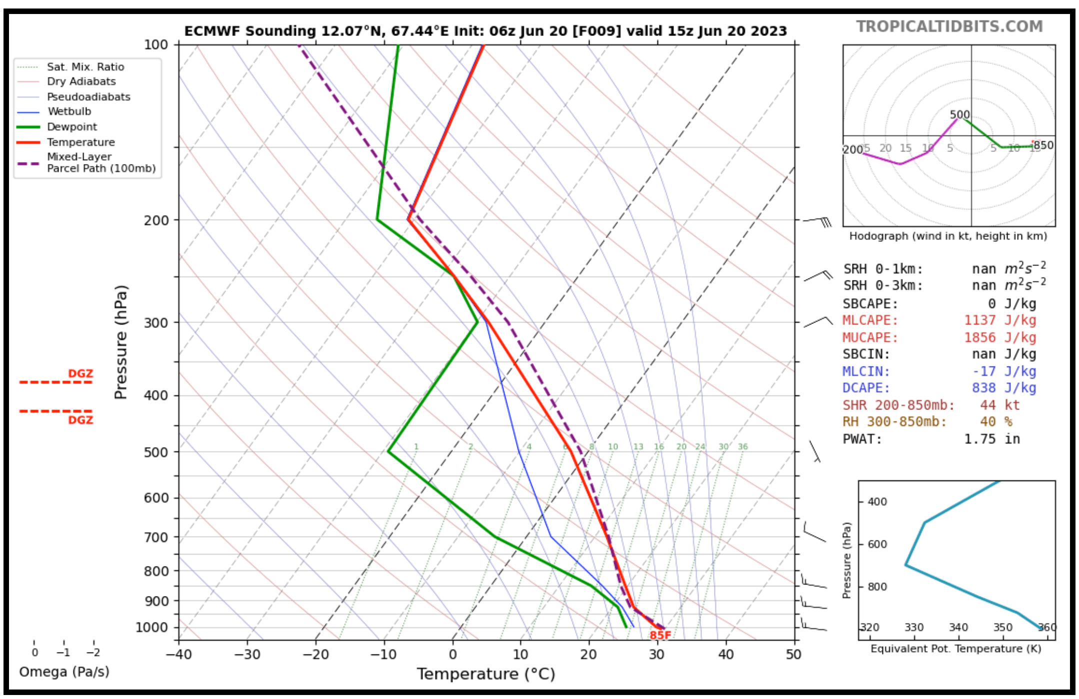

ECMWF Model Skew-T: 18 UTC (23:30 IST)

Captured: 13:00 IST (top) and 13:56 IST (bottom)

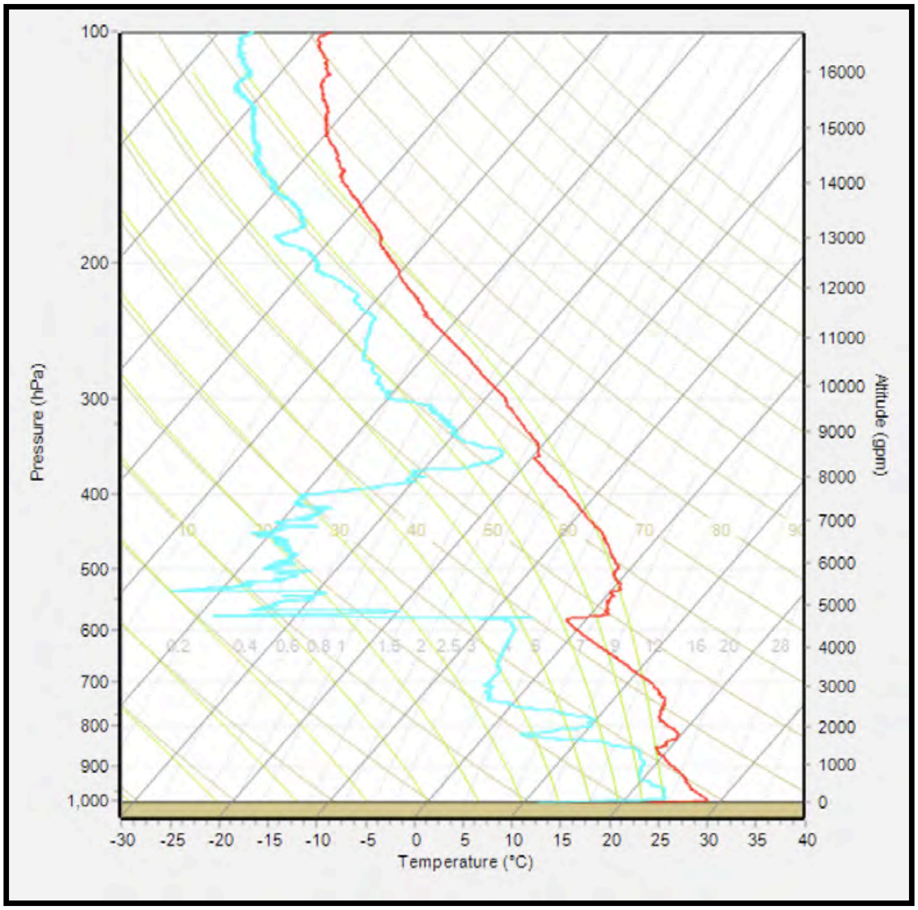

Ship Radiosonde: 0 UTC (05:30 IST)

Briefing: Seasonal temperatures in low-80s (84). Winds max about 16 knots and average around 15 knots throughout the day. Possible chance of scattered showers in the evening. Models, GFS & ECMWF, show a chance of precipitation around 18 UTC. Possible for rain to evaporate before meeting the surface due to the remaining/present dry layer at about 500 mb. Hazy skies throughout the day with partly cloudy conditions.

Captured: 18:21 & 18:26 IST

Captured: 18:21 IST

Special note: Extra ship radiosondes will be launched at 20:30 and 02:30 IST, in addition to the set launch schedule of 05:30, 11:30, 15:30, and 23:30 IST. GFS and ECMWF show potential for precipitation due to increased moisture observed in environmental soundings. Coordinates: 12.03°N 67.46°E.

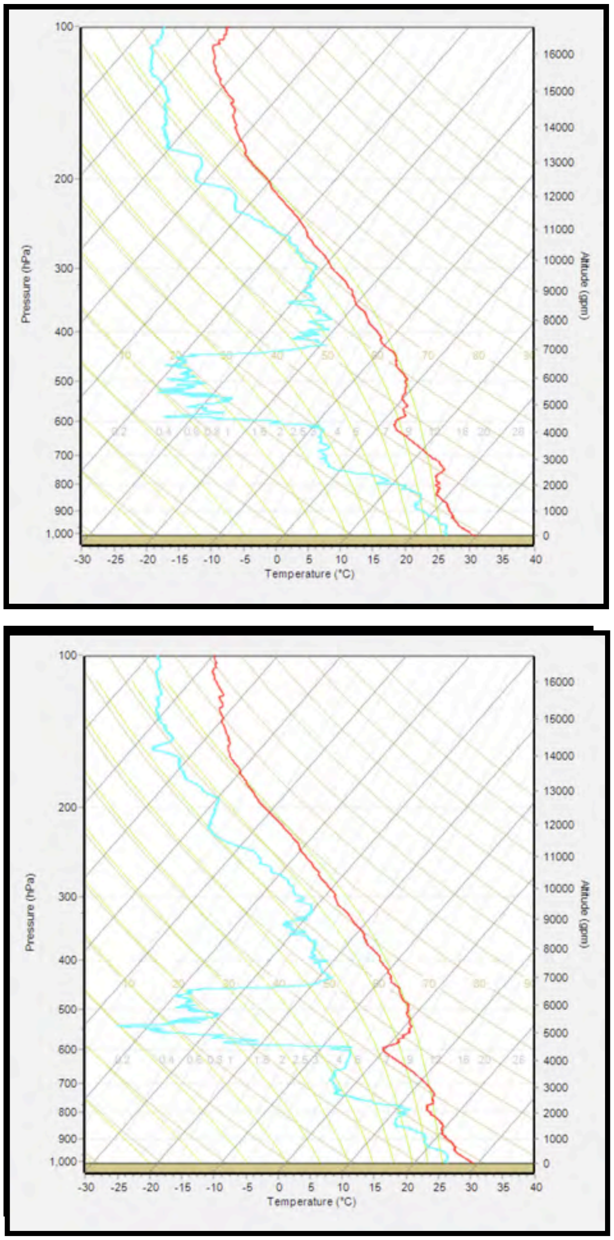

Ship Radiosonde: 15 UTC (20:30 IST) and 18 UTC (23:30 IST)

Ship Radiosonde: 21 UTC (02:30 IST)

Radiosondes have shown dry soundings, indicating no precipitation. Conclude that the environment is still too dry for development of precipitation.

21 June 2023

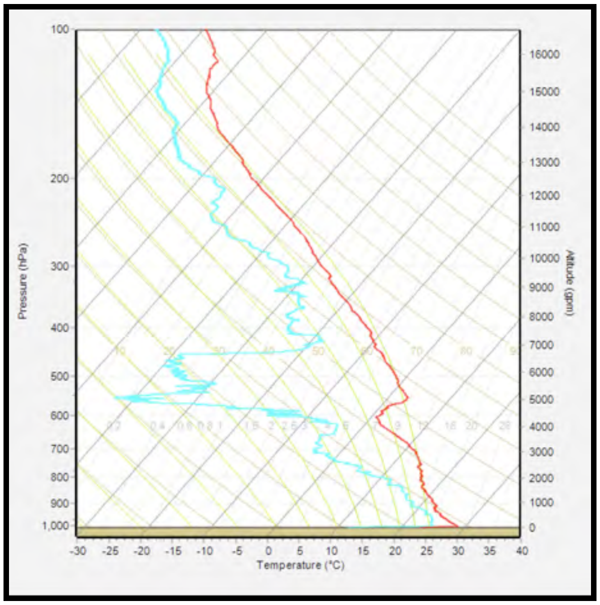

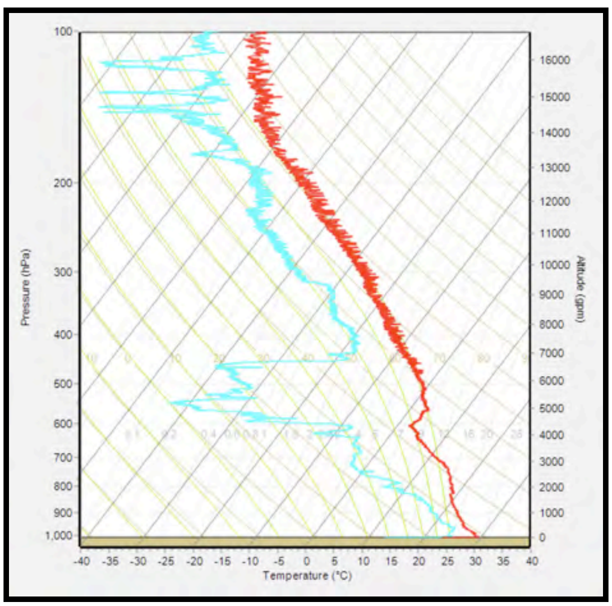

Ship Radiosonde: 0 UTC (05:30 IST) and 6 UTC (11:30 IST)

Captured: 13:40 IST

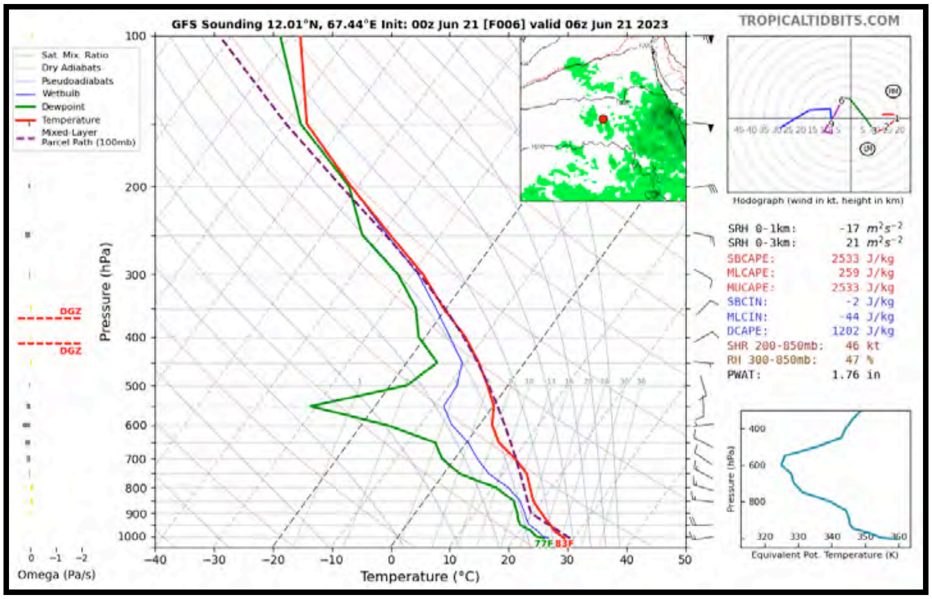

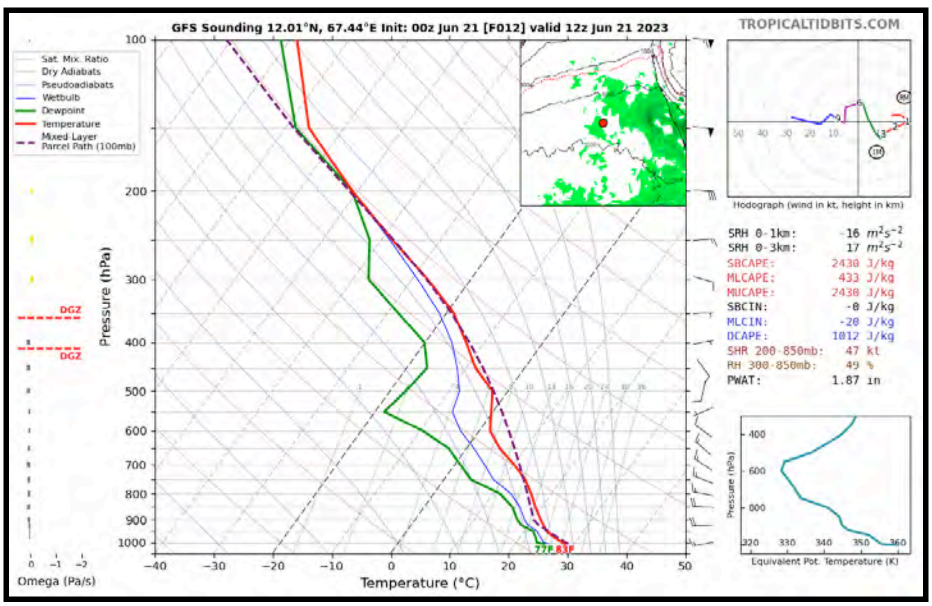

GFS Model Skew-T: 06 and 12 UTC (11:30 and 15:30 IST)

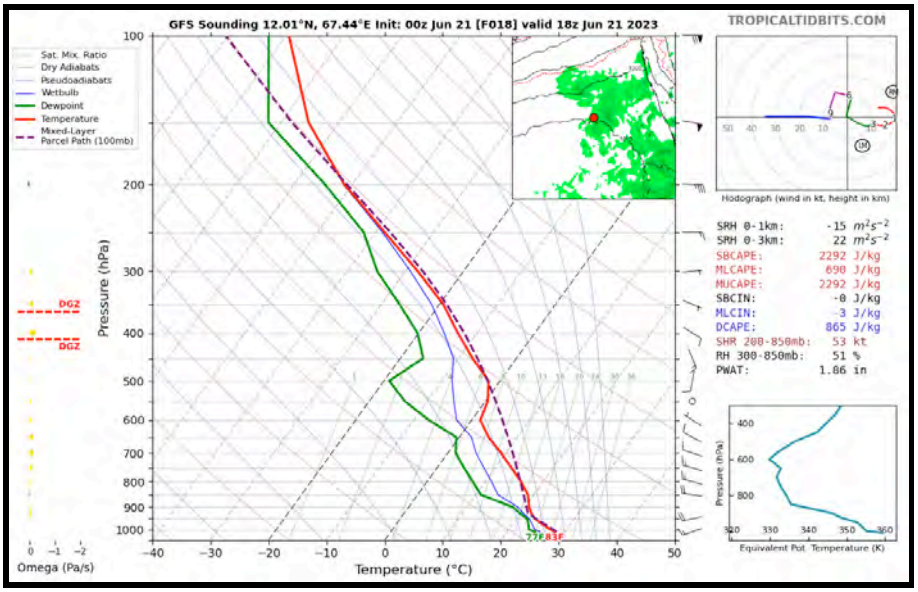

GFS Model Skew-T: 18 UTC (23:30 IST)

Captured: 18:34 IST

Briefing: Partly cloudy skies with haze. Temperatures remain consistent in the low-80s (84). Winds 16–18 knots throughout the day. Dry layer remains, but more moisture may accumulate as the day progresses.

22 June 2023

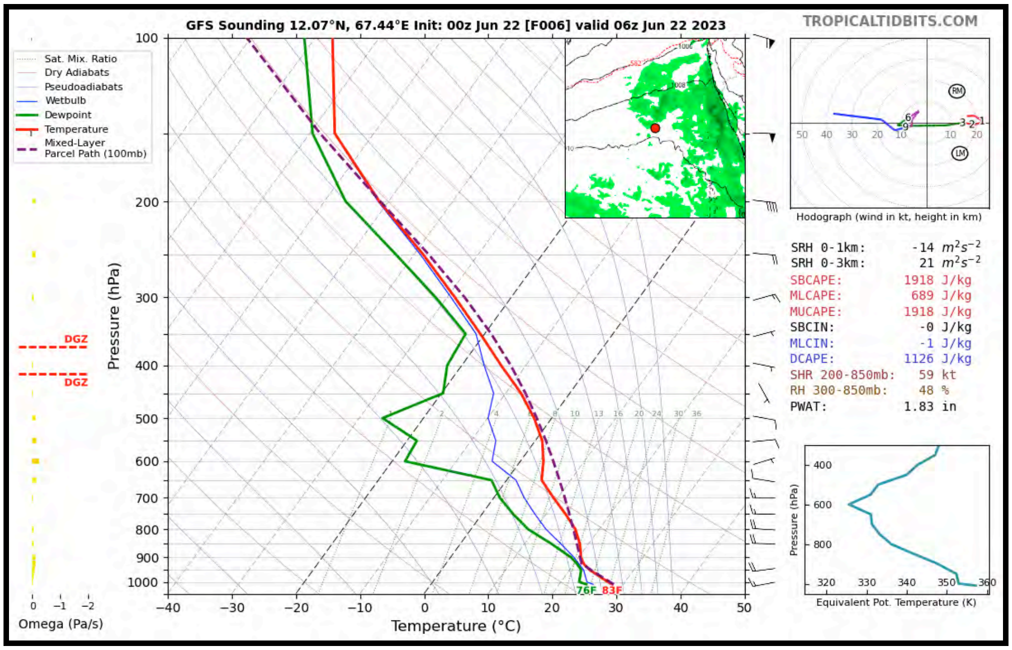

GFS Model Skew-T: Valid for 06 UTC (11:30 IST)

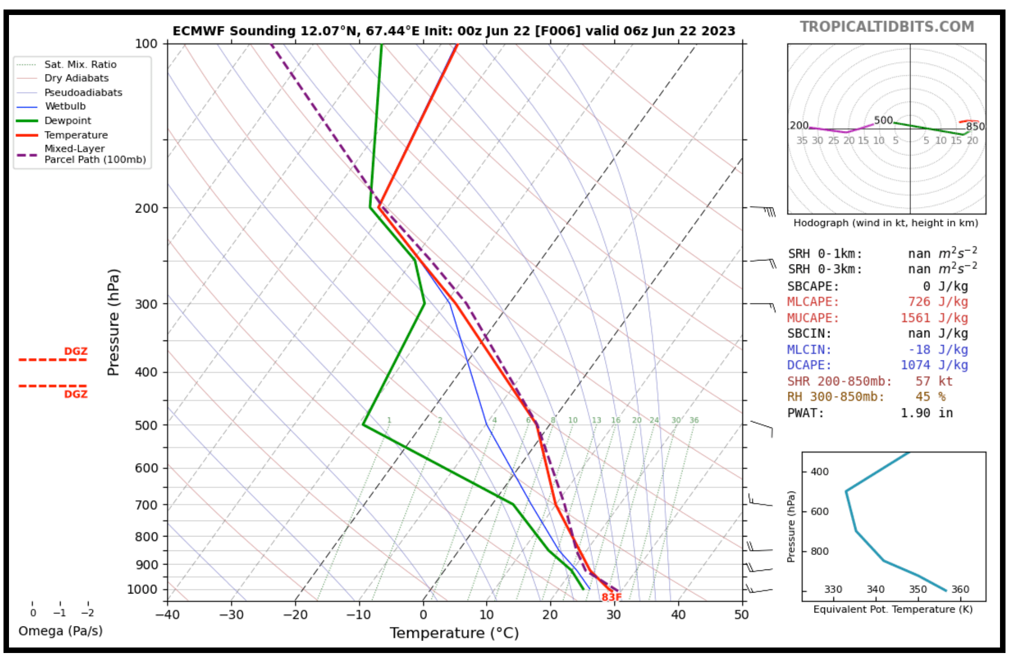

ECMWF Model Skew-T: 06 UTC (11:30 IST)

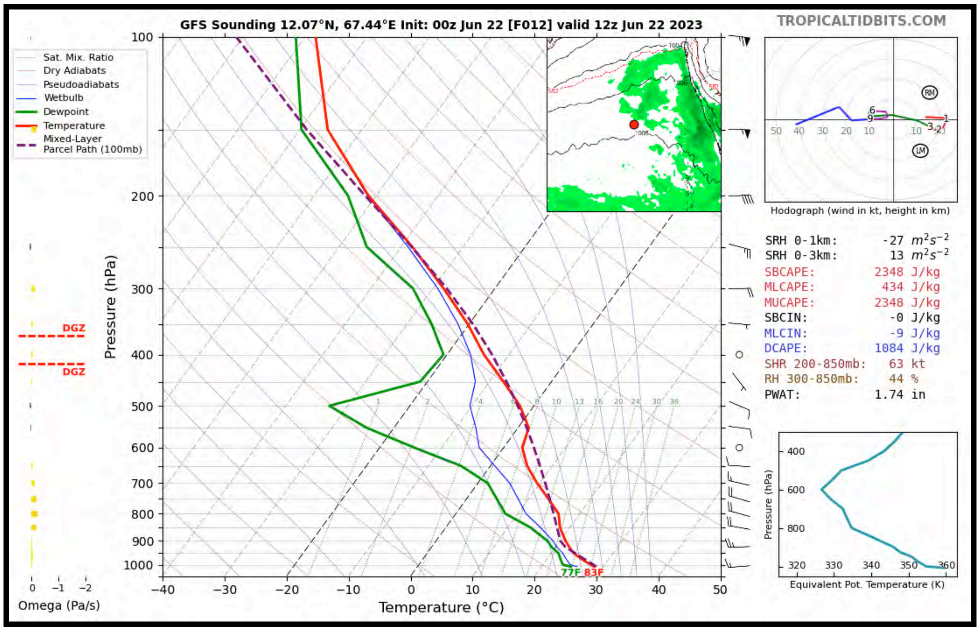

GFS Sounding: 12 UTC (15:30 IST)

Captured: 13:13 IST

Captured: 14:29 IST

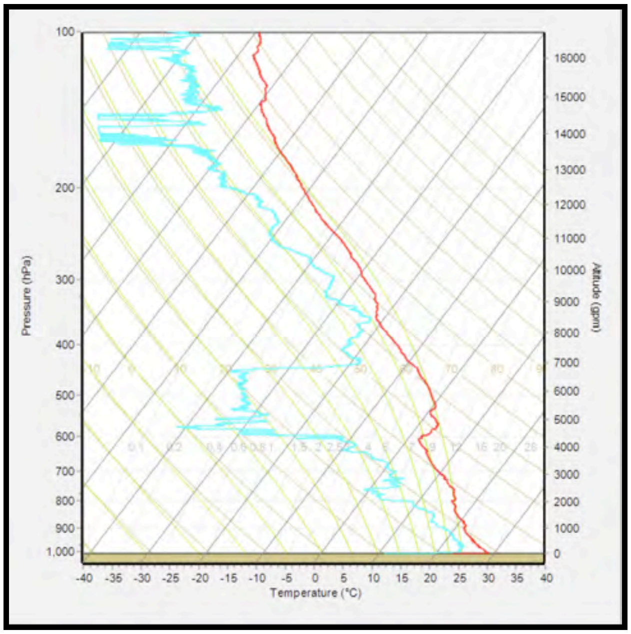

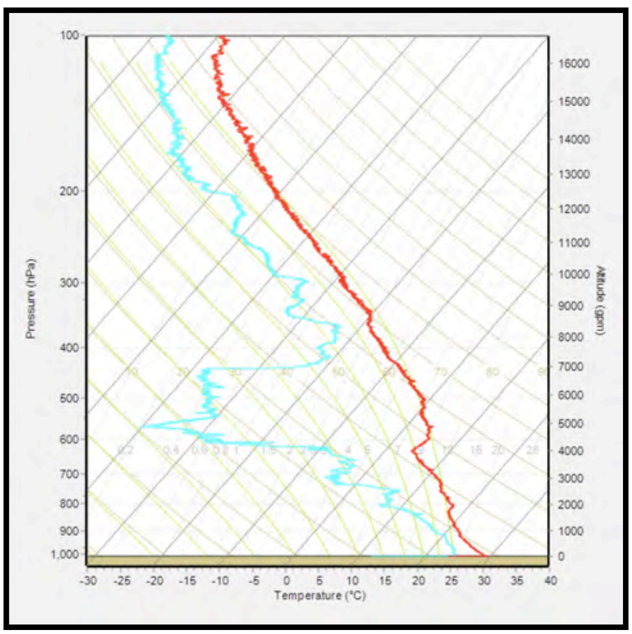

Ship Radiosonde: 0 and 06 UTC (05:30 and 11:30 IST)

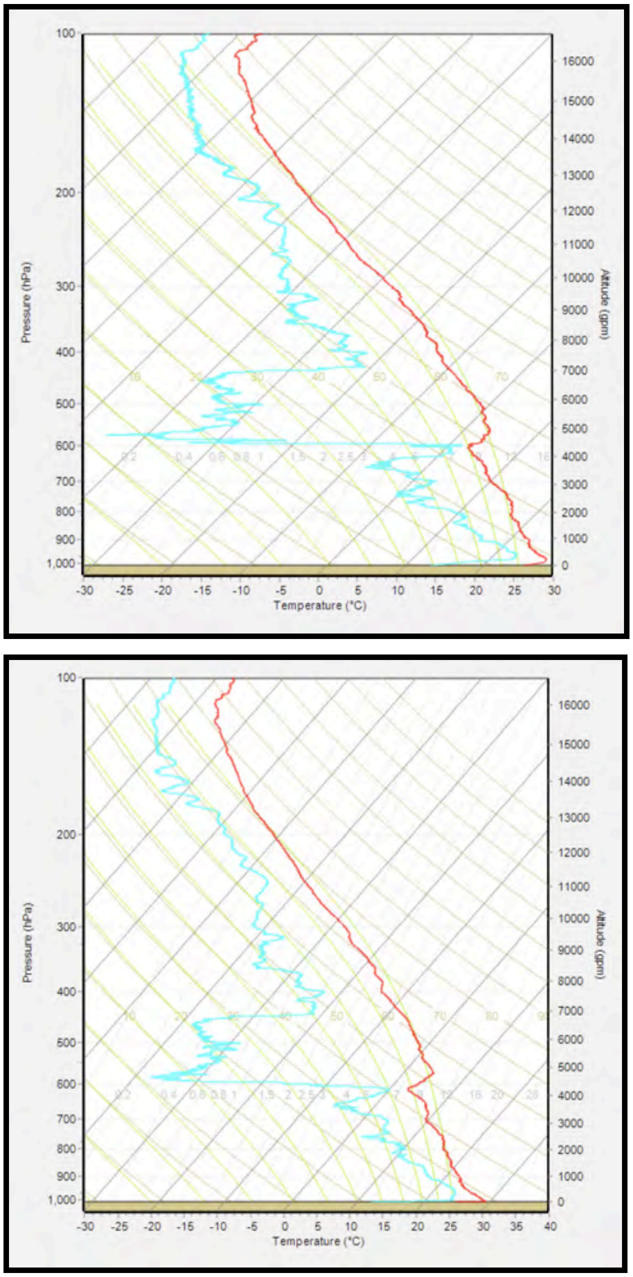

Ship Radiosonde: 12 and 15 UTC (15:30 and 20:30 IST)

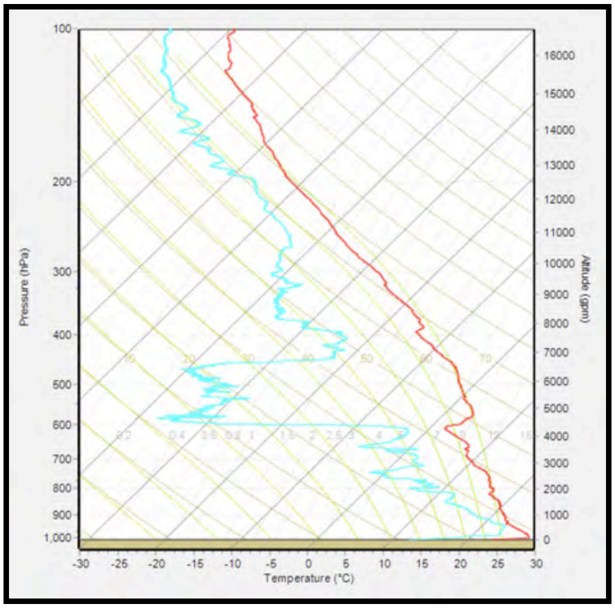

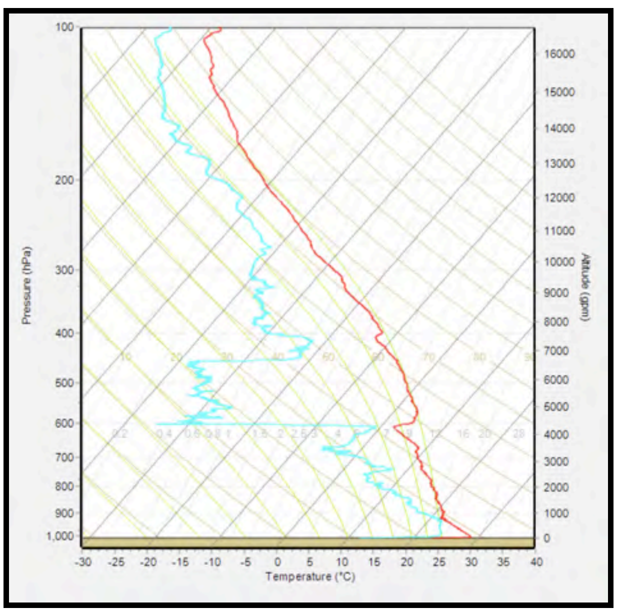

Ship Radiosonde: 18 and 21 UTC (23:30 and 02:30 IST)

Briefing: Temperatures in the low-80s (83). Winds 16–18 knots throughout the day. Sky coverage is mainly sunny with sparse clouds.

Special Note: GFS and ECMWF models predicted moist environment, therefore additional radiosondes were launched. Unfortunately, the region remained dry and no precipitation was observed.

23 June 2023

Captured: 13:38 IST

Briefing: Temperatures consistent in low-80s throughout the entirety of the day. Winds reach 22 knots early morning and average 19 knots throughout the day. Wind gusts up to 28 knots. Skies are mainly cloudy, mixed with mid-level clouds. Dry layer appears to have broken up due to moisture being advected from the Bay of Bengal. Ship's current coordinates are located in a dry slot, but potentially moving more north can improve chances of the ship meeting a more favorable environment for precipitation.

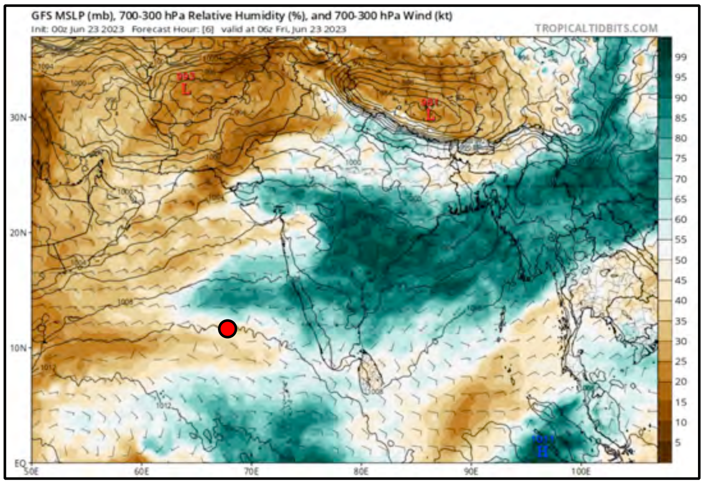

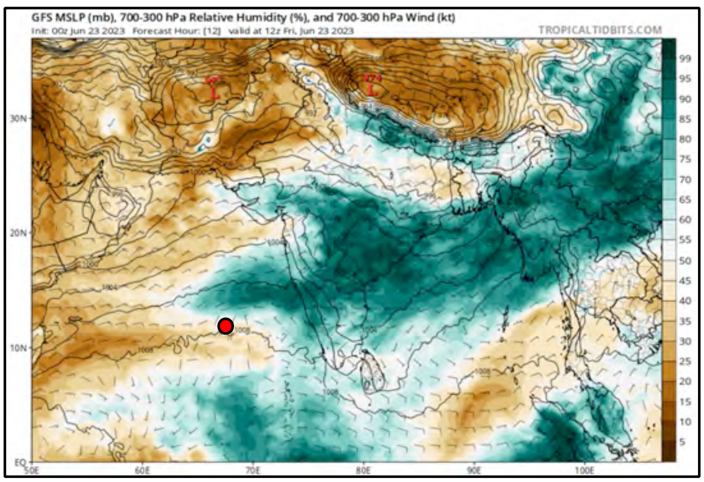

Relative Humidity GFS: June 23rd, 05:30 and 11:30 IST

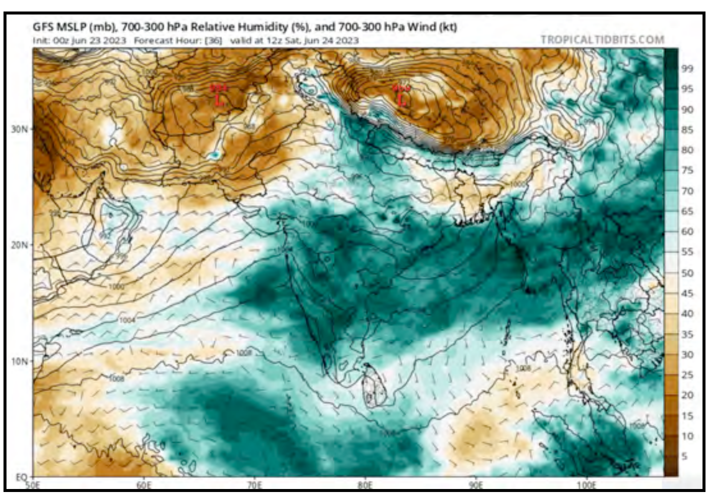

Relative Humidity GFS: June 23rd, 23:30 IST

Special Note: Increased moisture (humidity) north of ship's current coordinates (red circle [12.01N 67.44E]. Ship is located in a dry slot at 14:15 IST.

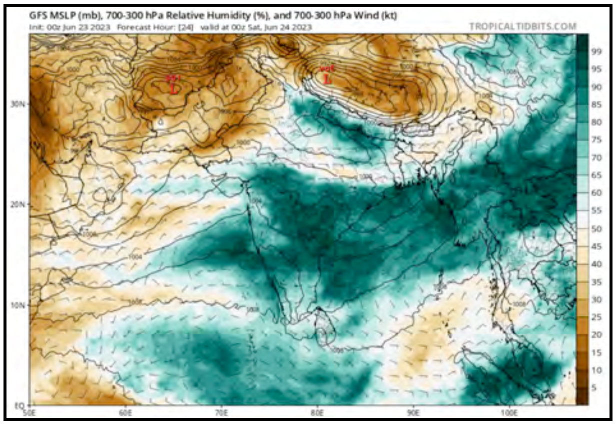

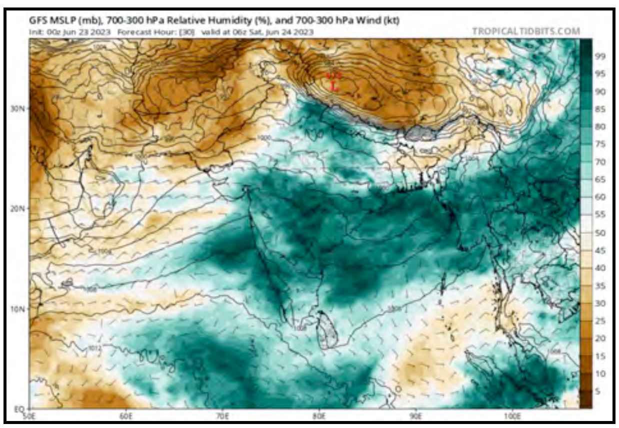

Relative Humidity GFS: June 24th, 05:30 and 11:30 IST

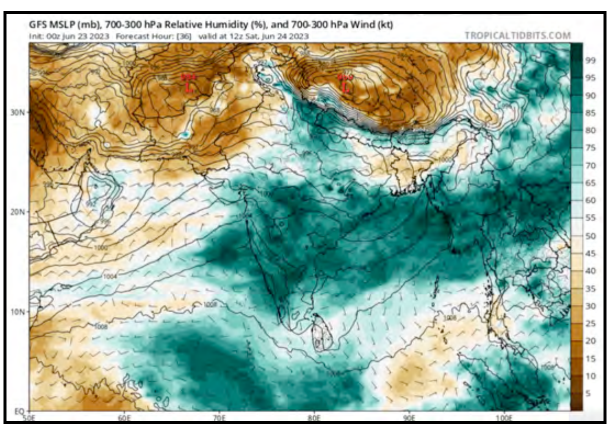

Relative Humidity GFS: June 24th, 15:30 IST

24 June 2023

Captured: 12:44 IST

Captured: 14:31 IST

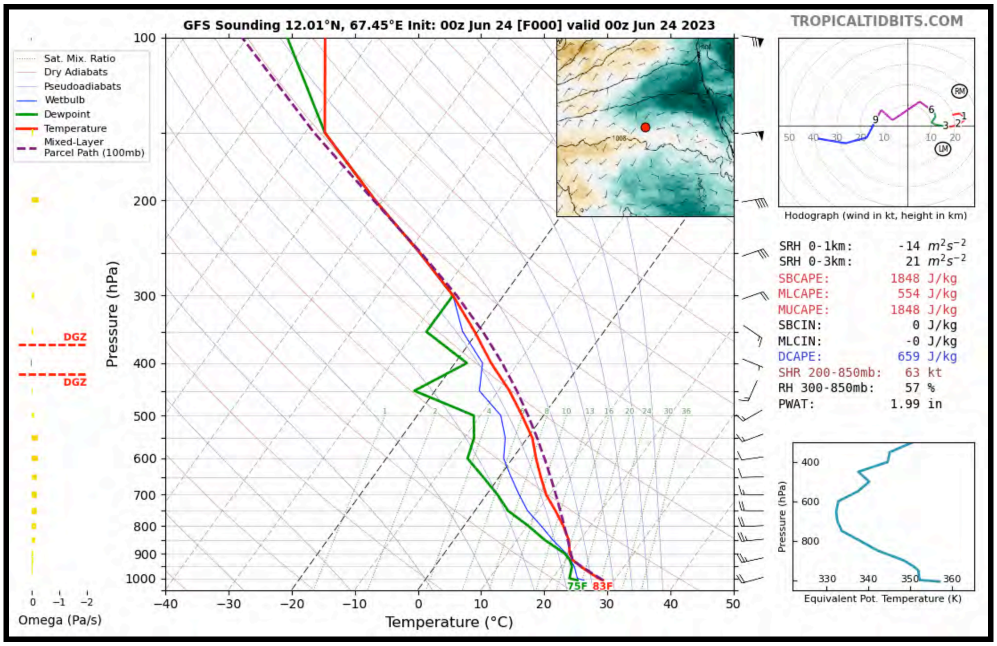

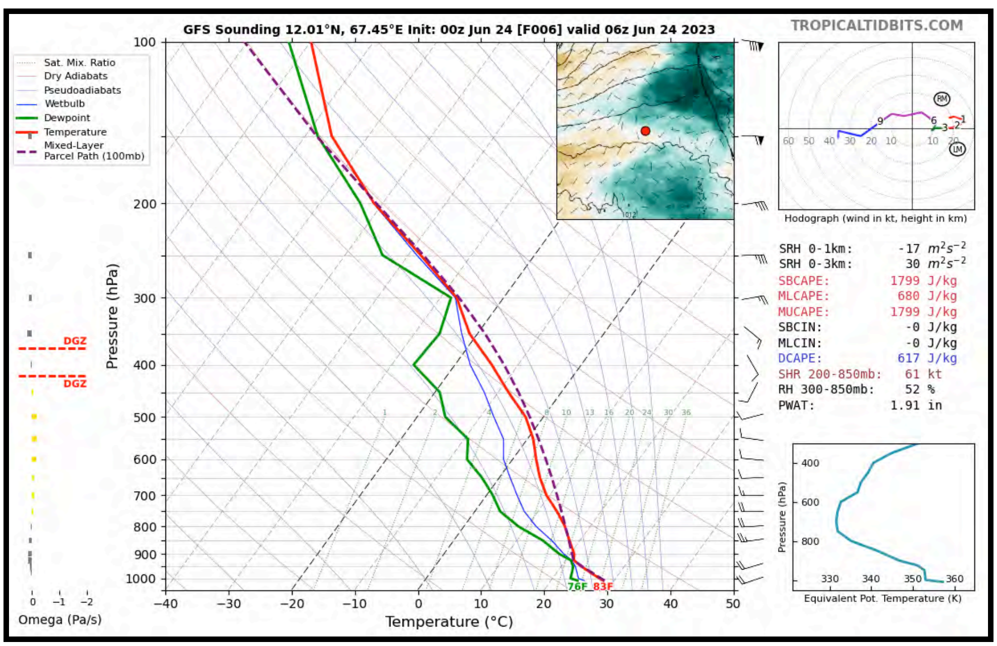

GFS Sounding: 0 UTC (05:30 IST) and 06 UTC (11:30 IST)

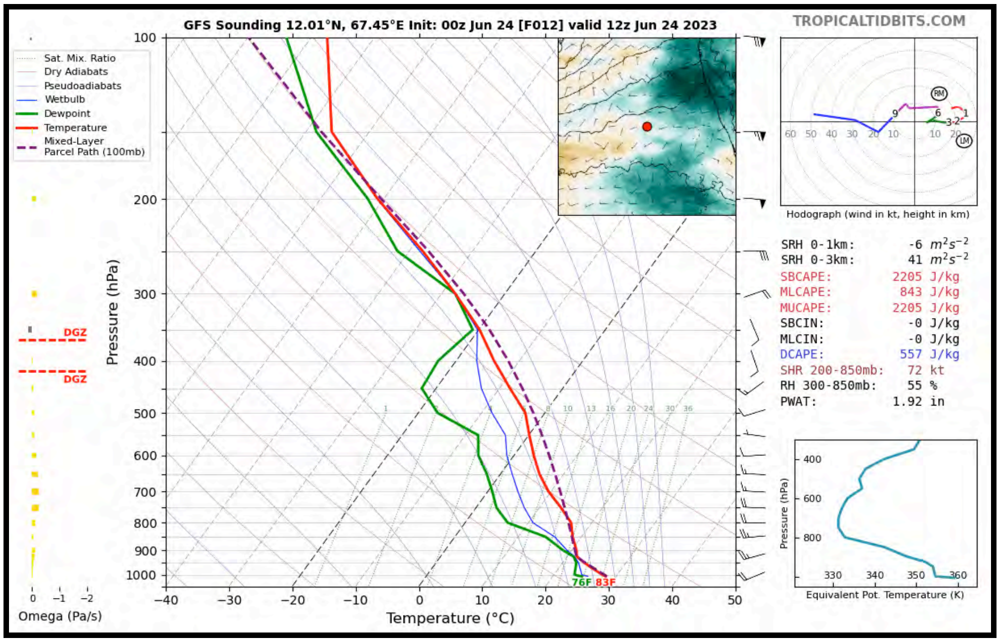

GFS Sounding: 12 UTC (15:30 IST)

Captured: 14:31 IST

Briefing: Winds 20–24 knots throughout the day. Wind gusts up to 30 knots. Temperatures remain consistent in the low-80s. Skies are partly sunny with haze. Sparse cloud coverage during the early hours. Cloud coverage increased throughout the day into the night. Increased moisture throughout the atmosphere as the ship moved slowly out of the dry slot.

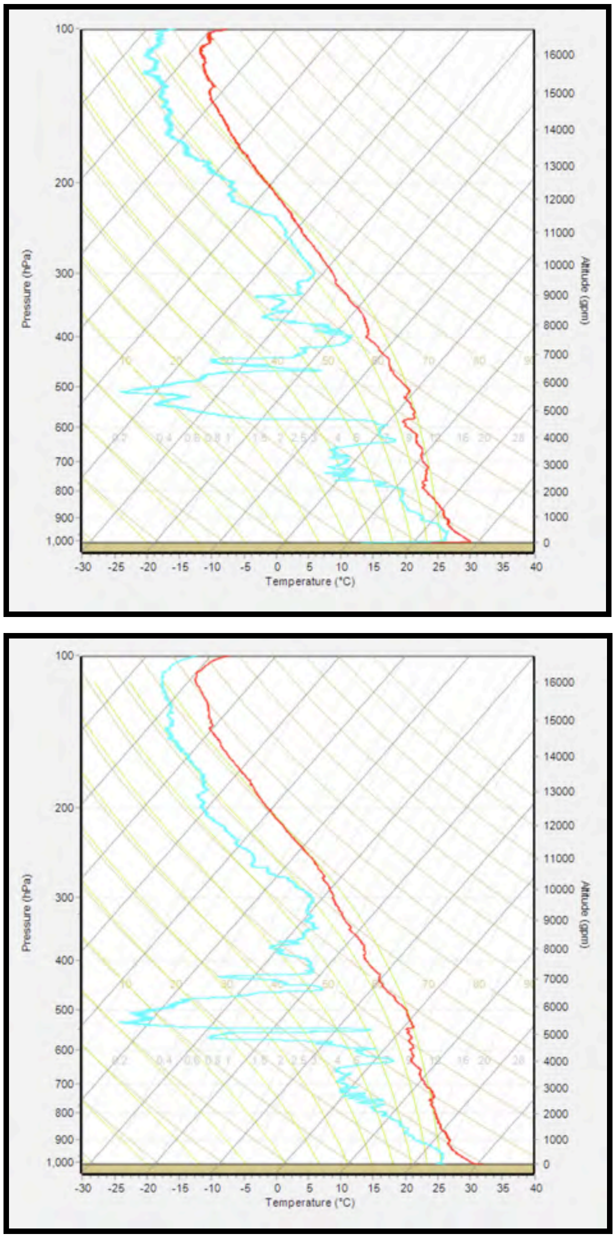

Ship Radiosonde: 0 and 06 UTC (05:30 and 11:30 IST)

25 June 2023

Captured: 13:32 IST

Captured: 16:01 IST

Captured: 16:02 IST

Briefing: Temperature in upper-80s (85–86) throughout the day. Wind 17–19 knots. Partly cloudy skies throughout the day and into the night. Ship returns to port in Goa by morning. Area of interest has increased in moisture and precipitation is expected as pilot cruise ends.

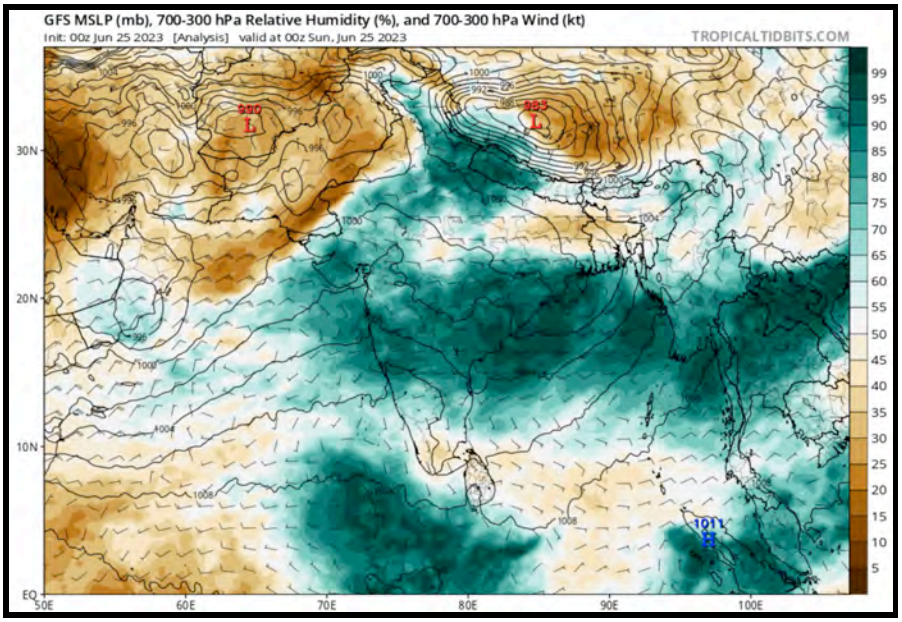

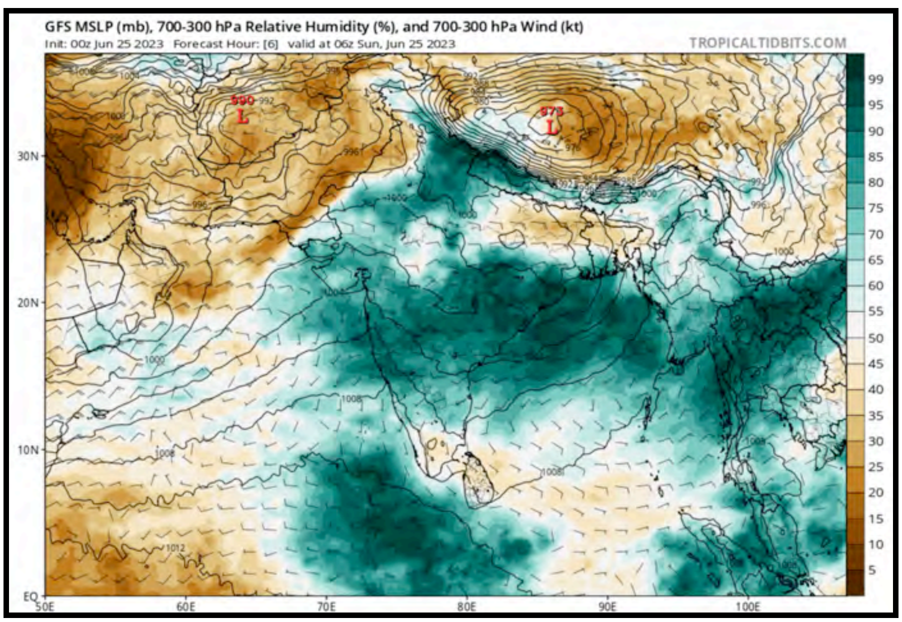

Relative Humidity GFS: 0 and 06 UTC (05:30 and 11:30 IST)

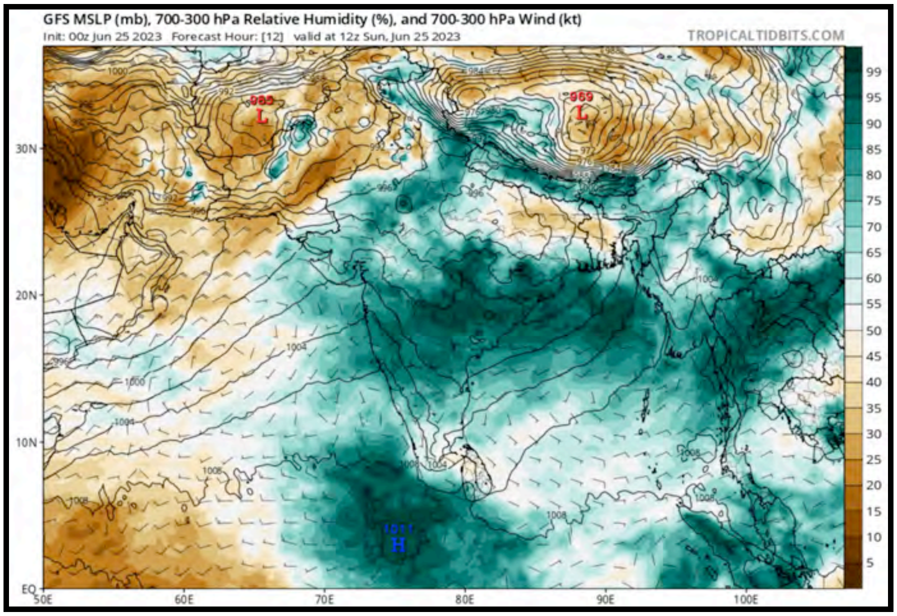

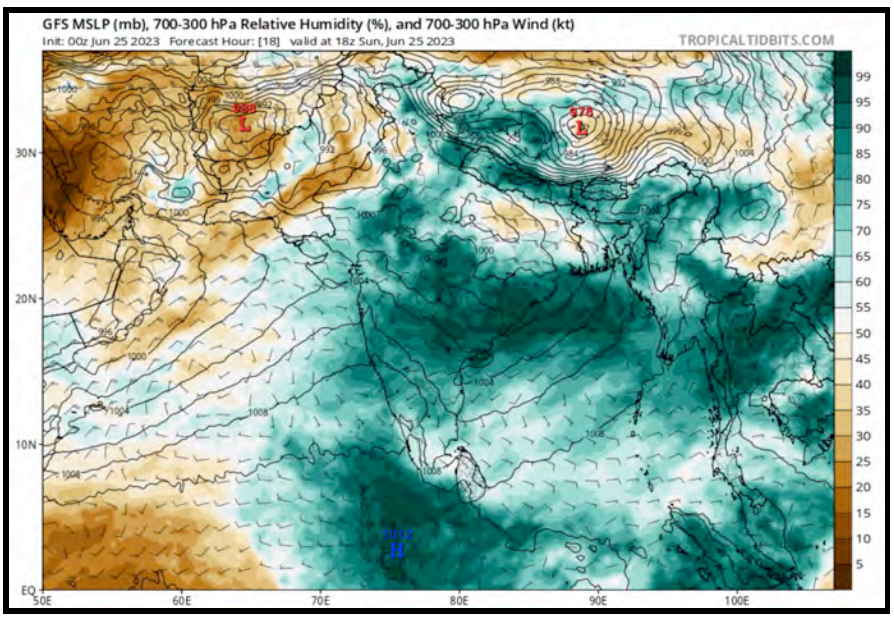

Relative Humidity GFS: 12 and 18 UTC (15:30 and 23:30 IST)